



# City Research Online

## City, University of London Institutional Repository

---

**Citation:** John, A. S, (2020). Psychophysical investigations of inverse cyclopean texture segmentation. (Unpublished Doctoral thesis, City, University of London)

This is the accepted version of the paper.

This version of the publication may differ from the final published version.

---

**Permanent repository link:** <https://openaccess.city.ac.uk/id/eprint/25469/>

**Link to published version:**

**Copyright and reuse:** City Research Online aims to make research outputs of City, University of London available to a wider audience. Copyright and Moral Rights remain with the author(s) and/or copyright holders. URLs from City Research Online may be freely distributed and linked to.

---

City Research Online:

<http://openaccess.city.ac.uk/>

[publications@city.ac.uk](mailto:publications@city.ac.uk)

---

Psychophysical investigations of  
inverse cyclopean texture segmentation

Adrian Simon John

Doctor of Philosophy

City, University of London  
Centre for Applied Vision Research  
Division of Optometry and Visual Sciences

April 2020



MAX-PLANCK-GESELLSCHAFT

## Contents

Figures	6
Tables	12
Acknowledgements	14
Declaration	15
Abstract	16
Chapter 1 General Introduction	17
1.1 Introduction	18
1.2 What does the visual system use texture for?	19
1.3 The phenomenology and mechanisms of texture segmentation	21
1.3.1 Explaining texture perception with image statistics	22
1.3.2 Texton theory	23
1.3.3 Computational models	25
1.3.4 The filter-based model of texture segmentation	26
1.3.4.1 Non-linear stage	27
1.3.4.2 Texture segmentation	27
1.3.4.3 The scale of linear filters	28
1.3.4.4 Modifications to the model	29
1.3.5 Feature integration theory for visual search & texture segmentation	29
1.3.5.1 What and where	31
1.3.5.2 The filter-based model for texture segmentation and visual search share a common foundation	31
1.3.5.3 Inconsistencies for the feature integration model	31
1.3.5.4 Modifications to the model	32
1.3.6 Saliency models for texture segmentation or pop-out	33
1.3.6.1 V1 saliency hypothesis	33
1.3.6.2 V1 saliency model	34
1.3.6.3 Lateral interactions	34
1.4 Review of the research for inverse cyclopean texture segmentation on which the research question is based	36
1.4.1 Introduction	36

1.4.2 Psychophysical investigations of inverse cyclopean texture segmentation	37
1.4.3 Inverse cyclopean texture segmentation occurs in brief dichoptic presentations (Kolb & Braun, 1995)	38
1.4.3.1 'Blindsight'?	38
1.4.4 Orientation-defined, inverse cyclopean visual search is impossible (Wolfe & Franzel, 1988)	39
1.4.5 Monocular visual processing can be investigated with the inverse cyclopean paradigm	40
1.5 Prior to recent evidence from Kolb and Braun, perceptual fusion was reported for brief exposures of orthogonal dichoptic stimuli	41
Chapter 2 General Methods	44
2.1 The method for presenting stimuli	44
2.1.1 Experimental procedure and stimuli	44
2.2 Psychometric functions	46
2.2.1 Parameter estimates for the following experiments	48
2.2.2 The generalised likelihood ratio	49
2.2.3 Model variants	50
2.3 Participants	51
2.4 Latin square	52
2.5 Task practice	53
2.6 Feedback	54
2.7 Nonius procedure and fixation point	54
2.8 Dropped or extra stimulus frames	55
2.9 Stimulus display	55
Chapter 3 Experiment 1	57
Is orientation-defined, inverse cyclopean texture segmentation dependent on texture density?	
3.1 Introduction	57
3.2 Methods	59
3.2.1 Methods: Experiment 1.1	61
3.2.2 Methods: Experiment 1.2	62
3.3 Results of Experiment 1.1	63

3.3.1 Results of Experiment 1.2	67
3.3.2 The effect of texture density on texture segmentation	67
3.4 Discussion	70
 Chapter 4 Experiment 2	 73
Is orientation-defined, inverse cyclopean texture segmentation affected by an effective contrast imbalance?	
4.1 Introduction	73
4.2 Methods: Experiment 2	73
4.2.1 Determining the balance-point	75
4.2.2 Dichoptic nonius procedure: Experiment 2	75
4.3 Results of Experiment 2	76
4.4 Discussion	79
 Chapter 5 Experiment 3	 81
The effect of texture density on inverse cyclopean texture segmentation	
5.1 Introduction	81
5.2 Methods: Experiment 3	81
5.2.1 Nonius procedure: Experiment 3	82
5.3 Results of Experiment 3	83
5.4 Discussion	86
 Chapter 6 Experiment 4	 87
Does a smaller inter-element space affect orientation-defined, inverse cyclopean texture segmentation?	
6.1 Introduction	87
6.2 Methods: Experiment 4	88
6.3 Results of Experiment 4	91
6.4 Discussion	95
 Chapter 7 Experiment 5	 97
Does inverse cyclopean texture segmentation vary with spatial scale?	
7.1 Introduction	97

7.2 Methods: Experiment 5	97
7.3 Results of Experiment 5	99
7.4 Discussion	102
Chapter 8 Experiment 6	103
Is inverse cyclopean texture segmentation dependent on stereoscopic vision?	
8.1 Introduction	103
8.2 Methods: Experiment 6	104
8.3 Results of Experiment 6	106
8.4 Discussion	110
Chapter 9 Experiment 7	111
Is effective contrast imbalance the mechanism for the dichoptic advantage for texture segmentation in brief durations?	
9.1 Introduction	111
9.2 Methods	113
9.2.1 Methods: Experiment 7.1	114
9.2.2 Methods: Experiment 7.2	115
9.3 Results of Experiment 7.1	118
9.3.1 Results of Experiment 7.2	119
9.4 Discussion	123
Chapter 10 General discussion	125
10.1 Conclusion	133
References	134

## Figures

- 1.1 Examples of visual texture: a view of Jupiter's bands and storms from the Juno space probe (top row; source: NASA), lichen growths on the trunk of a tree (second row; left panel) and black and white tiles (second row; right panel). 19
- 1.2 This image demonstrates pre-attentive segmentation of a region of x-shaped texture elements amongst L-shaped elements. Conversely, segmentation of a region of T-shaped texture elements in the right half of this image is possible, but requires attentive scrutiny. 20
- 1.3 Examples of cosine-phase (left panel) and sine-phase (right panel) Gabor textures. These textures represent some of the receptive fields in V1. The receptive field of a simple cell in V1 responds to a point of light in each portion of its RF as either excitatory (white) or inhibitory (black). The linearly weighted sum of these responses is the cells response to a pattern. 21
- 1.4 A texture region, shown in Cartesian quadrant IV, with identical 2<sup>nd</sup> order statistics to the background. 22
- 1.5 Textures with identical 2<sup>nd</sup> (and 3<sup>rd</sup>) order statistics that are easily differentiated. 23
- 1.6 Pre-attentive search for a cross (left panel) and serial search for a T among L's (right panel). 24
- 1.7 Einstein is visible at most reading distances, however, squinting, removal of corrective spectacles or viewing at a larger viewing distance reveals Ms Monroe. 26
- 1.8 2<sup>nd</sup> order stimulus: a Gabor function multiplied by random visual noise (Sutter, Sperling & Chubb, 1995). 27
- 1.9 The architecture of the filter-based model (Landy, 2013). 28
- 1.10 An example of a feature search; a line texture oriented at 90 degrees amongst line textures oriented at 0 degrees (left panel). An example of the results for this task show that reaction time was independent of set-size (right panel). 30
- 1.11 An example of a conjunction search (left panel); there was a red letter L amongst a background of red letter T's and blue letter L's. An example of the results for this task shows RT increased proportionally per item added to the display (right panel). 31
- 1.12 An example of a conjunction search, left and right panels (Sagi, 1988). 32

1.13	Either stimulus dimension may produce salience - the orientation of the black line segments that represent the boundary, or, their Weber contrast which is lower than the grey segments (due to the white background).	33
1.14	A vertical boundary on the left between tilted line segments is salient. Image from Zhaoping & May (2007).	34
1.15	Input image - a salient orientation boundary (top row). The V1 salience model output for the boundary is higher with respect to other regions (second row). The neuronal responses, or saliency, for each column in the model output (third row).	35
1.16	An inverse cyclopean stimulus for each of the two eyes (left & centre panels). Within each inverse cyclopean stimulus, an orientation-defined target is orthogonal to the distractors. The sum of these two images is given in the right panel to show the optically fused percept.	37
1.17	Wolfe and Franzel's dichoptic-overlapping stimuli (left & centre panels); the optically fused percept is shown in the right panel. The fixation point (not shown) was in the centre of each image. In these images, texture elements are not contrast randomised.	40
1.18	Superimposing the images in the left and centre panels (by crossing the eyes to view a distant, or alternatively a near, point in space) produces a percept of rivalry for which an example is shown in the right panel.	42
1.19	Diaz-Caneja stimuli. Superimposing both of the images (by crossing the eyes to view a distant point in space and aligning the crosshairs) can show a percept of the individual forms (parallel red and black lines, or, circular green and black lines).	43
2.1	The luminance profile of a cosine-phase Gabor stimulus. The wavelength and standard deviation of the stimulus are also shown.	45
2.2	Psychometric function for which observer data were Maximum likelihood fit (Wichmann & Hill, 2001a). The PMF was a Weibull function. The black solid line shows the original fit to observer data. The grey solid line shows a fit for which there was an error shown by the grey triangle and delta was fixed. The gray dashed line shows a fit for which delta varied freely.	48



2.3	Randot Stereo test and the polarising filters through which each of the random dot stereograms in the right-hand plate were viewed. Observers reported the shape perceived in depth. In the left-hand plate animals or Wirt circles were at different disparities to indicate stereoacuity.	52
2.4	Latin square order of 8 conditions for which inverse cyclopean texture segmentation was tested in sequence for each observer.	53
2.5	Dichoptic nonius procedure showing a dot and a line per eye as horizontally aligned.	55
3.1	8 x 8, 10 x 10 or 12 x 12 grids of dichoptic-overlapping Gabor stimuli (top, third and fifth rows respectively, left & centre panels) and 8 x 8, 10 x 10 or 12 x 12 grids of dichoptic-nonoverlapping Gabor stimuli (second, fourth and sixth rows respectively, left & centre panels). A binocular-overlapping stimulus is shown in the top, third and fifth rows, right panel, for which the two images in dichoptic-overlapping stimuli were optically fused. A binocular-nonoverlapping stimulus is shown in the second, fourth and sixth rows, right panel, for which the two images in dichoptic-nonoverlapping stimuli were optically fused. Each grid covered an equal unit area.	61
3.2	The dichoptic-overlapping (top and second rows) and dichoptic-nonoverlapping (third and fourth rows) tasks. For each task, the best-fitting values for threshold exposure duration and delta are shown for each texture density and each observer. For the dichoptic-overlapping task (second row), the gray line corresponds to a threshold exposure duration of 250 ms (2.4 log <sub>10</sub> ms). Error bars show the standard error of the best-fitting parameter values and were determined with a non-parametric bootstrap. Linear fits of alpha and delta to each observer's data for increasing texture density are shown by the coloured lines.	65
3.3	The binocular-nonoverlapping task: the best-fitting values for delta and threshold exposure duration are shown for each texture density (i.e. the texture density of a dichoptic-nonoverlapping stimulus) and each observer. Error bars show the standard error of the best-fitting parameter values and were determined with a non-parametric bootstrap.	66
3.4	Binocular noise-masked orientation-defined texture segmentation: the best-fitting values of threshold exposure duration for each texture	67

density are shown for observers MM, FV and JAS. Error bars show the standard error of the best-fitting parameter values and were determined with a parametric bootstrap. Delta was 2%. Linear fits of alpha to each observer's data for increasing texture density are shown by the dotted lines.




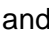

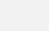
4.1	Example stimuli: an 8 x 8 grid of Gabor stimuli for each of the two eyes showing an orientation-defined target viewed with central fixation (top row, left and right panels) from a distance of 3m. The other interval of a two alternative forced choice procedure (2-AFC) contained distractors only (second row, left and right panels). The luminance contrast of each image is equal for illustration.	74
4.2	Dichoptic nonius procedure showing a dot and a line per eye as horizontally aligned. The location of aligned nonius dots served as the fixation point for a target viewed with central fixation.	76
4.3	Results for observers AJ, KM and JM show the probability of correctly identifying the target with each ratio of interocular luminance contrast when the contralateral eyes image was fixed at 100% luminance contrast. Error bars show 95% confidence intervals.	78
5.1	12 x 12 (first row) and 8 x 8 (second row) Gabor textures covered an equal unit area in dense and sparse textures respectively. Each image for the two eyes (left and right panels) is 100% luminance contrast for illustration.	82
5.2	Dichoptic nonius procedure for the 8x8 grid showing a dot and a line per eye as horizontally aligned.	83
5.3	Psychometric functions for observers AJ (top row), KM (second row) and JM (third row) show the probability of a correct response at logarithmically spaced exposure durations. The density of texture elements was 8 x 8 (all left panels) and 12 x 12 (all right panels).	84
5.4	The best-fitting values for delta and threshold exposure duration for each texture density and each observer. Error bars show the standard error of the best-fitting parameter values determined with a non-parametric bootstrap.	85
6.1	A grid of 8 x 8 Gabor textures within each image for the two eyes (left and right panels). Exp. 3's Gabor textures are shown in row	90

	1; four equal increases in sigma and wavelength for those Gabor textures are shown in rows 2 to 5.	
6.2	The best-fitting values for delta and threshold exposure duration for each value of sigma are shown for each observer. The dotted line is a linear fit of delta and alpha to each observer's data. Error bars show the standard error of the best-fitting parameter values determined with a non-parametric bootstrap.	92
6.3	The results for the sparse (8 x 8) Gabor textures when sigma was 0.31 degrees and the results for the dense (12 x 12) Gabor textures from Exp. 3. The best-fitting values for delta and threshold exposure duration are shown for each observer. Error bars show the standard error of the best-fitting parameter values determined with a non-parametric bootstrap.	94
7.1	The sparse 8 x 8 grid is shown in an image for each of the two eyes (left and right panels). These images show the fixation dot when the viewing distance was 3 m.	98
7.2	Psychometric functions for each observer show the probability of a correct response at logarithmically spaced exposure durations for 3 m (left panels) and 1 m (right panels) viewing distances.	100
7.3	The best-fitting values for delta and threshold exposure duration for 3 m and 1 m viewing distances for each observer. Error bars show the standard error of the best-fitting parameter values determined with a non-parametric bootstrap.	101
8.1	The stereo-matching hypothesis. Two matches with a stimulus in the contralateral eye are shown. A 90 degree oriented target presented to the left eye (red circle, left panel) is matched with either of the 90 degree oriented distractors presented to the right eye (red circles, right panel). A 0 degree oriented target presented to the right eye (green circle, right panel) is matched with either of the 0 degree oriented distractors presented to the left eye (green circles, left panel). The fixation point is in the centre of the display.	104
8.2	A column of Gabor textures with randomised luminance contrast within each image for the two eyes (left and right panels). The target interval is shown; the other interval of a two alternative forced choice procedure (2-AFC) contained distractors.	104

8.3	A row of Gabor textures within each image for the two eyes (left and right panels). Luminance contrast is randomised. The fixation point is shown in the centre of the display. The target interval is shown; the other interval of a two alternative forced choice procedure (2-AFC) contained distractors.	105
8.4	Results for observer AJ showing the probability of identifying the target in a row, column or grid. Error bars show 95% confidence intervals.	107
8.5	Results for observers JAS and BF showing the probability of identifying the target in a row or column. Error bars show 95% confidence intervals.	108
8.6	Results for observers KM and LE showing the probability of identifying the target in a row or column. Error bars show 95% confidence intervals.	109
9.1	A 6 x 6 grid of dichoptic-nonoverlapping Gabor stimuli. In this example, luminance contrast is 80% for -45 degree texture elements (left panel) and is 30% for 45 degree texture elements (right panel).	114
9.2	12 x 12 grids of dichoptic-overlapping (top row, left & centre panels) and dichoptic-nonoverlapping Gabor stimuli (second row, left & centre panels). In this example, the contrast of texture elements within the left eye's stimulus was reduced (left panels; the ratio was 1.22). A binocular-overlapping stimulus and a binocular-nonoverlapping stimulus are shown in the right panels of the top and second rows respectively; the maximum randomised contrast was 50%. A binocular-nonoverlapping stimulus for which the maximum randomised contrast was 100% is shown in the right panel, third row. 'Jitter' was added to the contrast of the texture elements by drawing them from a uniform distribution of log contrasts that was 9.5 dB wide (all left, all centre panels & third row, right panel) and 3.5 dB wide (top & second rows, right panels). Each stimulus covered an equal unit area. Texture elements were separated by 0.86 degrees within the 12 x 12 grid. The target interval is shown; the other interval of a two alternative forced choice procedure (2-AFC) contained distractors.	117
9.3	Results show the probability of a correct response to the interval containing an orientation-defined texture boundary for the two dichoptic tasks (shown in magenta) and the three dioptic tasks	121

(shown in cyan) for each observer. Error bars show 95% confidence intervals.

## **Tables**

- 3.1 Statistics. The generalised likelihood ratio,  $2(\ln l - \ln l_0)$ , shown as LL ratio, tested the null hypothesis where  $\ln l$  and  $\ln l_0$  are the log-likelihoods (LL) for a maximum likelihood fit to observer data for the model for a linear fit of alpha, or delta, to all texture densities and the model for which alpha, or delta, is unchanged for all texture densities respectively.  $k$  is the number of free parameters for each model; models differ in 1 degree of freedom. The critical value from the chi-squared distribution for  $2(\ln l - \ln l_0)$  is 8.62 when the critical region of 0.05 is corrected for 15 applications ( $0.05/15 = 0.003$ ). P values (determined from the chi-squared distribution for LL ratio values) are also given and are shaded as  =  $p \leq .003$ , or, unshaded =  $p > .05$ . 69
- 5.1 Statistics. The critical value from the chi-squared distribution for  $2(\ln l - \ln l_0)$  is 6.96 when the critical region of 0.05 is corrected for 6 applications ( $0.05/6 = 0.008$ ). P values:  =  $p \leq .008$ , or, unshaded =  $p > .05$ . 86
- 6.1 The inter-element space for the sparse (8 x 8) and dense (12 x 12) Gabor textures that were used in each Experiment. The area covered by the 8 x 8 and 12 x 12 notional grids was the same; 291600 pixels. The area occupied by all of the texture elements within each grid is given for each value of sigma. 91
- 6.2 Statistics. The critical value from the chi-squared distribution for  $2(\ln l - \ln l_0)$  is 6.96 when the critical region of 0.05 is corrected for 6 applications ( $0.05/6 = 0.008$ ). P values:  =  $p \leq .008$  and  =  $p \leq .05$ . 93
- 7.1 Statistics. The critical value from the chi-squared distribution for  $2(\ln l - \ln l_0)$  is 6.96 when the critical region of 0.05 is corrected for 6 applications ( $0.05/6 = 0.008$ ). P values:  =  $p \leq .008$ ,  =  $p \leq .05$  and unshaded P values =  $p > .05$ . 102
- 8.1 The number of trials (N) and p value (unpaired t-test) for a row and column mean differing (i) or differing to chance (ii). P values: 107

■ =  $p \leq .05$  and unshaded P values =  $p > .05$ .

- 9.1 The mean contrast (%) for dichoptic texture elements to appear uniform in contrast, the standard deviation (SD) for each mean and the ratio are given for each observer. Observers adjusted the contrast of texture elements within the left or the right eye's stimulus when orientation was – or + 45 degrees from vertical; the contrast of the contralateral eye's stimulus was fixed (30%). 118
- 9.2 Statistics. The null hypothesis was tested with the dichoptic-nonoverlapping (Figure 9.3; \*) and binocular-nonoverlapping (Figure 9.3; x, the maximum contrast was 100%) tasks. The number of trials for each task and p values for the chi-square statistic are given for each observer. The critical value for the chi-square distribution is 6.63, where the critical region = .01, with one degree of freedom. P values: ■ =  $p \leq .01$ . 122

## **Acknowledgements**

I wish to express my utmost appreciation to both supervisors, Michael and Josh, for their insightful input, intuitive guidance and unwavering support and also for the opportunity to develop my experience of scientific research. Thank you. I am also very grateful for the support given by Max Planck Institute.

I wish to give special thanks to the examiners; Professor Meese and Professor Tyler. Thank you for encouraging me to be a good scientist and also for your guidance and perceptiveness.

I would like to thank Michael for writing the program for Experiment 1, Josh for writing a program for a Gabor function, the developers of Psychtoolbox-3 and the developers of Palmedes. I would also like to thank John, Ron, Simon and Tracy in the department of Optometry and Visual Science for their advice and assistance during the PhD research degree. Thanks are also given to all of the Journal Club members for broadening both an experience of science and a way of thinking. Many thanks to the observers for their participation in the experiments.

Wholeheartedly dedicated to my family

## **Declaration**

I hereby declare this thesis is the result of my own work. The published or unpublished work of others is referenced to the respective authors.

I grant powers of discretion to the University Librarian to allow this project to be copied in whole or in part without further reference to me. This permission covers only single copies made for study purposes, subject to the normal consideration of acknowledgement.



## Abstract

Inverse cyclopean texture segmentation is segmentation based on monocular boundaries which are absent in the binocularly fused percept. Texture segmentation based on the monocular image does occur, even though texture segmentation is impossible in the optically fused image (Kolb & Braun, 1995). On the other hand, orientation-defined, inverse cyclopean visual search is impossible (Wolfe & Franzel, 1988). The purpose of the present study was therefore to investigate these apparent contradictions in the literature.

Orientation-defined texture elements within Kolb and Braun's stimulus occupied positions on a 20 x 20 notional grid. For Wolfe and Franzel's stimulus, 8 texture elements were spaced evenly on a circle. The purpose of Experiments 1.1 and 3 was to determine whether the critical variable for the difference between Kolb and Braun's and Wolfe and Franzel's results was texture density i.e. the number of elements within the display area. We found that orientation-defined, inverse cyclopean texture segmentation was better when texture elements were dense (12 x 12) than when those elements were sparse (8 x 8) and covered the same area (Exp. 1.1 & 3). The purpose of Experiment 4 was to determine whether texture segmentation depended on orientation-defined texture boundaries that were closer together. Texture segmentation improved when the number of texture elements within the sparse grid (8 x 8) used in Experiment 3 was held constant and texture boundaries were closer together (Exp. 4). This implies that the critical difference between Kolb and Braun's and Wolfe and Franzel's experiments is the proximity of orientation-defined, texture boundaries.

The purpose of Experiment 2 was to investigate the possibility that, if there were an effective contrast imbalance between the two eyes, the texture boundary within an inverse cyclopean stimulus might be visible in the optically fused percept and be detected by mechanisms at a binocular stage of processing. An imbalance in sensory input from the two eyes does affect orientation-defined, inverse cyclopean texture segmentation (Exp. 2). Therefore, the purpose of Experiment 7 was to determine whether effective contrast imbalance between the two eyes was responsible for high performances for texture segmentation when texture elements were dense (Exp. 1.1 & 3) and when texture boundaries were closer together (Exp. 4). Performances for orientation-defined, inverse cyclopean texture segmentation were >80% when the balance-point was used to equalise a difference in effective contrast between the two eyes (Exp. 7.2). This implies that monocular input is available to texture segmentation mechanisms.

## **General Introduction**

This dissertation reports experiments which investigate the phenomenology and mechanisms of inverse cyclopean texture segmentation. Accordingly, I shall first review what is known about the phenomenology and mechanisms of texture segmentation. Next, I shall report research for texture segmentation with inverse cyclopean stimuli on which the research question is based. This reveals apparent contradictions in the literature for which it is the purpose of the experiments reported in this thesis to investigate. The research question is conveyed on page 37; Psychophysical investigations of inverse cyclopean texture segmentation. This is followed by a review of the relevant facts regarding binocular rivalry and fusion. The experiments are then conveyed, followed by a General Discussion and Conclusion.

## 1.1 Introduction

The human visual system has an innate capability for perceiving texture. Although there are many types of texture in nature, textures might also be man-made. Some of the textures that exist in nature are Jupiter's bands and storms (Figure 1.1; top row) and lichen growths on the trunk of a tree (Figure 1.1; second row, left panel). Other examples of texture in nature are the wing patterns of butterflies, the markings on a tiger's or cloud leopard's fur and the markings of some bird's eggs. Man-made examples of texture are tiles (Figure 1.1; second row, right panel) or a polished granite worktop. The light reflected from a texture produces variations in light across the retina which the visual system uses to create a percept of visual texture. Visual texture might also be correlated with a tactile texture component. For example, lichen growths can be distinguished from the trunk of a tree by both their visual and tactile texture components. However, the other examples given are visual textures that do not have a corresponding tactile texture component. A compelling percept of visual texture can be created even without a correlated tactile component.

A texture is formed from individual texture elements. A line segment, a dot or an x-shaped figure are examples of texture elements that were used to investigate the visual perception of texture. Texture elements form a textured region or pattern due to their similarity and their proximity to one another. Specifically, visual texture is defined statistically. Texture is defined as a pattern with self-similar  $n$ th-order statistics at some scale of sampling (Tyler, 2004). That is, self-similarity at a given scale of sampling, rather than across scale which is used for some fractal patterns.  $N$ th-order statistics are defined as the probability that the vertices of a polygon with  $n$  sides falls on  $n$  colours of a texture when thrown randomly onto the texture (Julesz, 1995). Further details for  $n$ th-order statistics are given in section 1.3.1 (Explaining texture perception with image statistics).

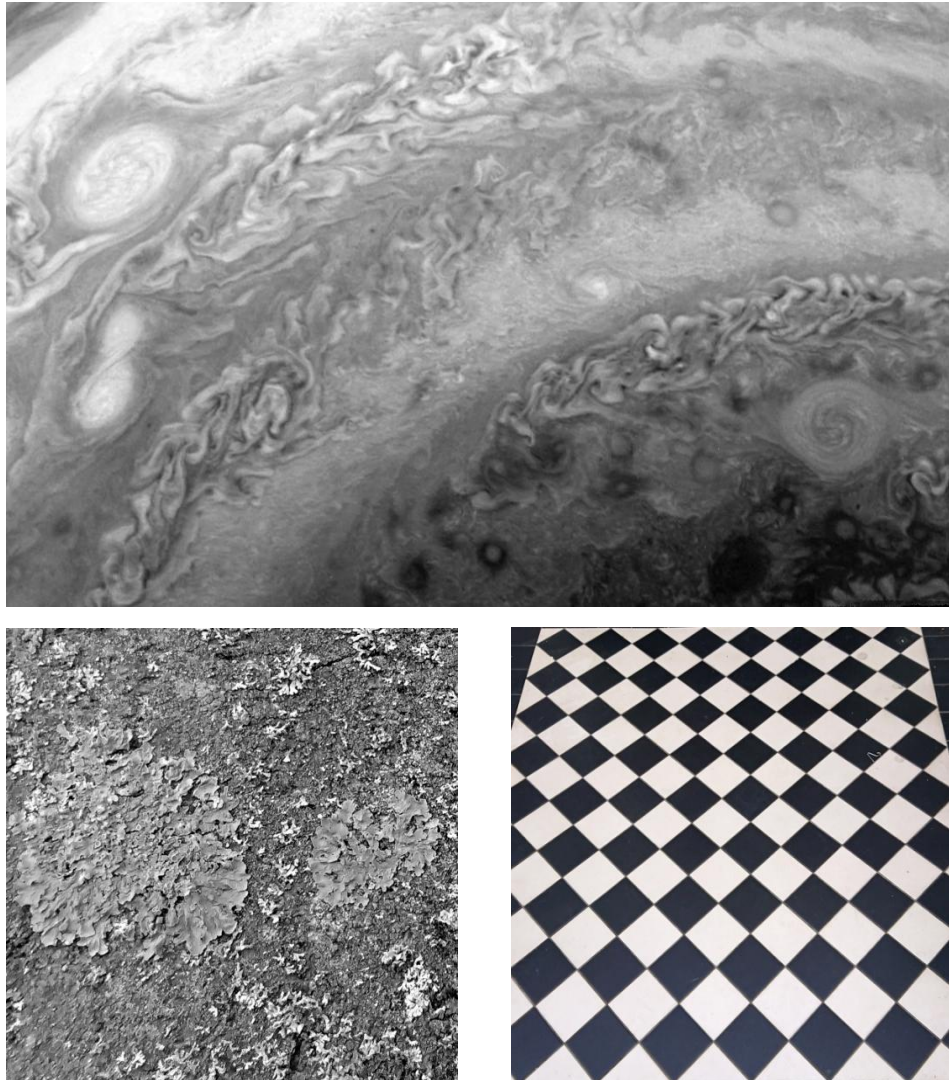


Figure 1.1. Examples of visual texture: a view of Jupiter's bands and storms from the Juno space probe (top row; source: NASA), lichen growths on the trunk of a tree (second row; left panel) and black and white tiles (second row; right panel).

## 1.2 What does the visual system use texture for?

Texture is fundamental for perceiving the visual world. The visual system uses texture as a cue to segment an image into regions which represent objects and surfaces. Texture is also useful for determining the shape of a surface. Texture can also be used for the identification of extensive surfaces, the waves of an ocean for example.

One purpose of texture perception is enhancing segmentation. Texture segmentation is a process that differentiates one texture from another. An example of texture segmentation is shown in Figure 1.2 (Julesz, 1984). In this example, texture segmentation for the region of x-shaped texture elements amongst L-shaped elements occurs rapidly and unconsciously. Texture segmentation that is 'effortless' and occurs in parallel is termed pre-attentive texture segmentation. Models for texture segmentation typically have a first stage at which the statistical attributes of an image are extracted and a second stage at which segmentation occurs. For the filter-based model, texture segmentation is explained by the detection of texture-defined boundaries.

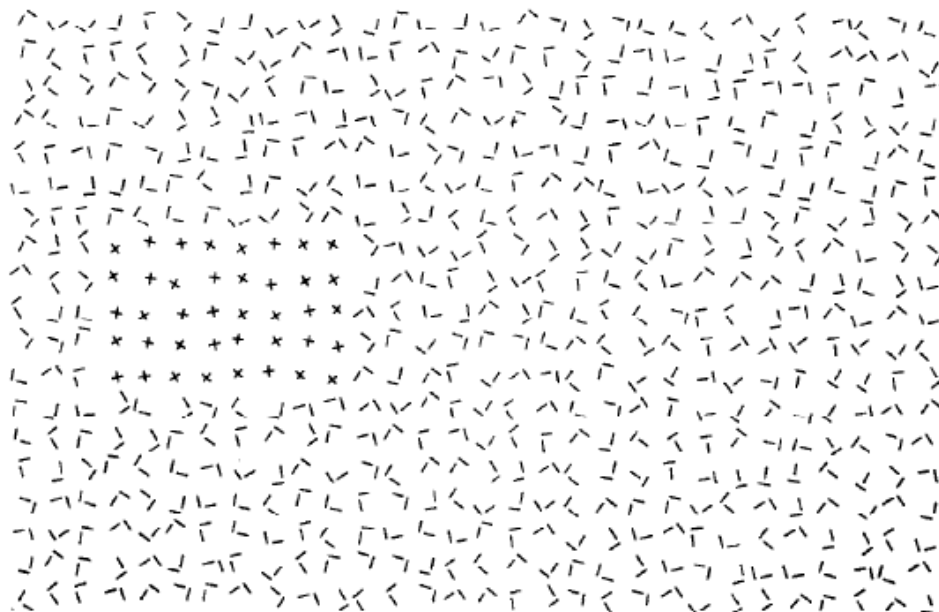


Figure 1.2. This image demonstrates pre-attentive segmentation of a region of x-shaped texture elements amongst L-shaped elements. Conversely, segmentation of a region of T-shaped texture elements in the right half of this image is possible, but requires attentive scrutiny.

Another purpose of texture perception is creating an impression of depth. For example, the texture elements in Figure 1.1 (second row, right panel) are black and white tiles that decrease in size from the bottom to the top of the image. The visual system uses the systematic variation in elements to infer depth from a texture gradient. Depth can be inferred from the size of images on the retina; nearer objects cast larger images than objects that are further away. This image

demonstrates that two eyes are not required to perceive depth; a texture gradient is a monocular cue to depth. This image also demonstrates that texture is used to perceive a slanted surface.

The uses of visual texture are investigated by creating textures that stimulate neurons within the visual pathways of the brain. For example, Gabor textures (Figure 1.3). A Gabor stimulus is a Gaussian carrier multiplied by a sine wave modulation. The Gaussian carrier is a mathematical function, e.g. a normal distribution or 'bell-shaped' curve, and the standard deviation describes the width of the stimulus. Gabor textures are akin to some receptive fields in area V1 of the visual cortex. The receptive field (RF) of simple cells in V1 were conceptualised and modeled as linear filters. An RF is linear if the points of light that stimulate the whole of the receptive field of the neuron elicit a linearly weighted response of their intensities.

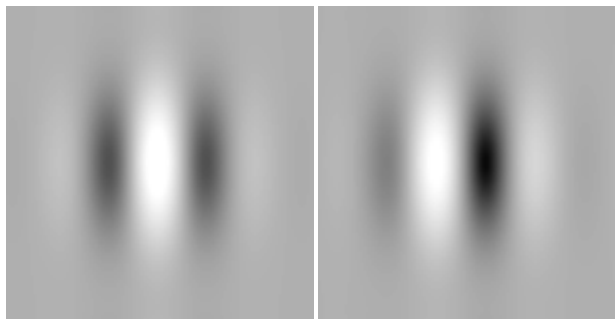


Figure 1.3. Examples of cosine-phase (left panel) and sine-phase (right panel) Gabor textures. These textures represent some of the receptive fields in V1. The receptive field of a simple cell in V1 responds to a point of light in each portion of its RF as either excitatory (white) or inhibitory (black). The linearly weighted sum of these responses is the cells response to a pattern.

### 1.3 The phenomenology and mechanisms of texture segmentation

The experiments reported in this thesis investigate the phenomenology and mechanisms of texture segmentation. In this section (section 1.3), the phenomenology and mechanisms of texture segmentation are reviewed. First, the statistical approach to texture segmentation is reviewed. The computational models for texture segmentation are then reviewed. This is followed by a review of a behavioural paradigm for texture segmentation; visual search.

### 1.3.1 Explaining texture perception with image statistics

Julesz theorised that the visual system utilised second-order image statistics for texture perception (Julesz et al, 1973). The initial approach was to represent texture as dipole statistics to describe the power, or amplitude, spectrum. The power spectrum is derived from the Fourier transform to represent the absolute values for the power, i.e. luminance and frequency, for texture. Differences in second-order statistics determined segmentation. Julesz showed that a pair of dipole textures that contained identical and homogenous 2<sup>nd</sup> order statistics, with equal power spectra, was impossible to differentiate pre-attentively (Julesz et al, 1973). An example of a texture pair with identical 2<sup>nd</sup> order statistics is shown in Figure 1.4 (Julesz, Gilbert & Victor, 1978). In this example, mirror image textures are impossible to differentiate from non-mirror image textures; attentive scrutiny is required.

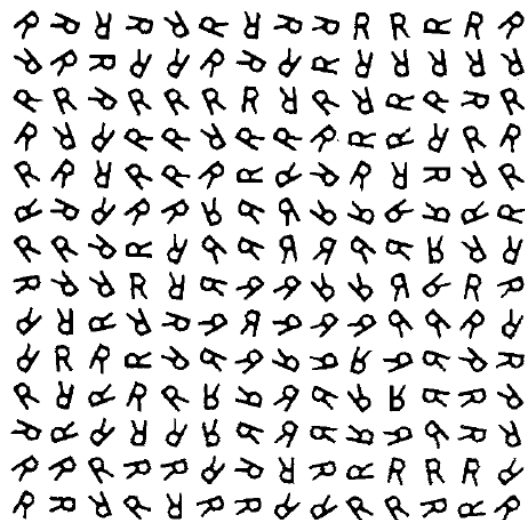


Figure 1.4. A texture region, shown in Cartesian quadrant IV, with identical 2<sup>nd</sup> order statistics to the background.

This conjecture implies that the mechanisms that represent texture are sensitive to the local spatial structure within an image but are also insensitive to the global phase, or spatial location, spectra. Indeed, images containing small patches with amplitude spectra from one image, such as a face, and phase spectra from another image, such as a car, were recognised by their amplitude rather than their phase spectra (Morgan, Ross & Hayes, 1991). This finding supports Julesz's conjecture in that the local spatial structure of texture is represented as amplitude spectra; this is intrinsic to determining 1<sup>st</sup> and 2<sup>nd</sup>-order image statistics. Collectively, these findings

also suggest that 3<sup>rd</sup> or higher-order statistics are required for texture borders to 'pop-out' in pre-attentive vision.

Julesz actually found his theory insufficient to explain the apparent visual difference between certain texture pairs containing identical 2<sup>nd</sup> order statistics (Julesz et al, 1973). This was also true for images containing 3<sup>rd</sup>-order, or iso-trigon, statistics (Julesz, Gilbert & Victor, 1978). An example of textures with identical 2<sup>nd</sup> (and 3<sup>rd</sup>) order statistics that are easily differentiated are shown in Figure 1.5 (Julesz & Schumer, 1981).

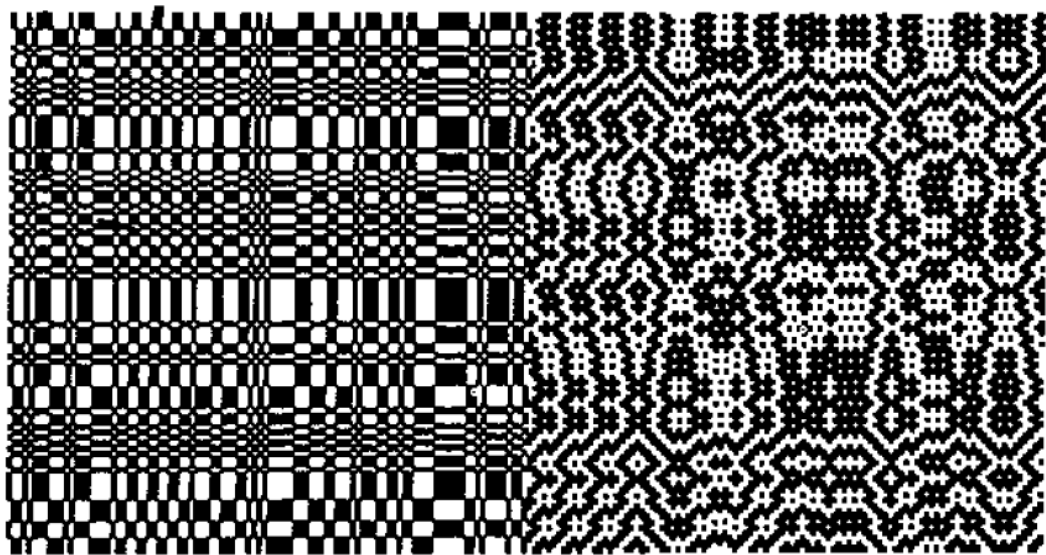


Figure 1.5. Textures with identical 2<sup>nd</sup> (and 3<sup>rd</sup>) order statistics that are easily differentiated.

However, explaining the apparent difference between these textures led Julesz (1984) to link the statistical approach, in terms of a modified form of the conjecture that applied 1<sup>st</sup> order statistics, with the local features within images, i.e. textons. Julesz also explained texture segmentation in terms of differences in responses of cells in the visual system, acting as linear filters, to differences in textons as local features (Julesz & Schumer, 1981).

### 1.3.2 Texton theory

All textures and patterns could theoretically be reduced to three local conspicuous features which were termed textons (Julesz, 1984). The three types of texton as described by Julesz are:



1. Elongated blobs e.g. rectangles, ellipses or line segments which may or may not have additional attributes of colour, binocularity, movement, flicker rate, a certain orientation or proportional size such as width and length.
2. Terminators e.g. the ends of line segments or edges.
3. Crossings of line segments e.g. a cross or corners.

The combination of textons as conspicuous features was proposed to form all textures and patterns. 'Easy' texton segmentation was shown by 'effortless', unconscious or pre-attentive segmentation that occurred quickly and in parallel. Conversely, 'hard' segmentation was delineated by a difficult or effortful task which required a serial search. The delineation was attributed to the locus of attention which was understood to be limited in the sense of requiring 50 ms increments per texton difference (Julesz, 1984). Thus the time required for a serial search increased linearly with the number of textons, or items. This locus, or 'where', was spatially restricted such that Julesz and Bergen (1983) coined the term focal attention for a serial texton search, i.e. 'what'. Conversely, pre-attentive segmentation depended on texton grouping in terms of density or number, rather than differences in neighbouring textons, but was independent of focal attention. As an example, let the eyes roam the left panel of Figure 1.6 (Julesz & Bergen, 1983) to note which texton(s) are apparent. An illustration of the texton differences requiring either a pre-attentive search that directs attention rapidly to the cross or a serial search for the T among L's is given in the right panel of Figure 1.6.

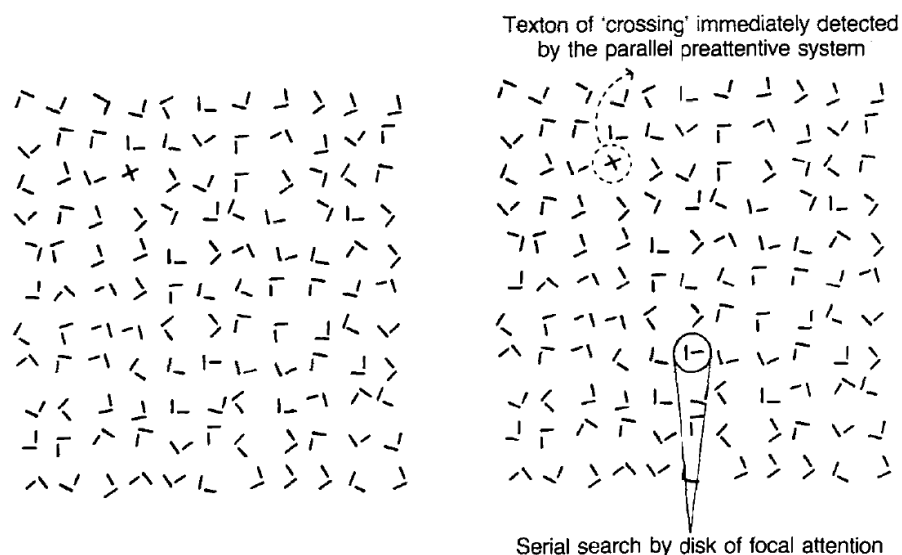


Figure 1.6. Pre-attentive search for a cross (left panel) and serial search for a T among L's (right panel).

This ease or difficulty of segmentation was mirrored by Treisman's work on pre-attentive, or parallel, search and conjunction, or serial, search (Treisman & Gelade, 1980). However, contrary to the finding of Julesz and Bergen (1983), the discriminability of a region of X's from a region of surrounding L's, for which X's and L's were the same size and randomly oriented, was difficult but improved by increasing the size of L's when the number of X's and L's is unchanged (Bergen & Adelson, 1988). Thus, segmentation could be explained by a mechanism tuned to texture size rather than density.

### 1.3.3 Computational models

In the late 1980's and early 1990's and following the statistical conjecture of Julesz, the computational models of texture segmentation converged into a simple linear analyser model involving filters tuned in the domains of orientation and spatial frequency.

The channels that comprise texture are postulated to be low-level visual processes in that they occur early in the visual system following retinal input and carry signals in parallel to areas V1 and V2 in the visual cortex. Parallel channels define the perception of texture segmentation. A texture, or rather, the principal components of a texture are spatial frequency and orientation and these were the components that determined easy vs. hard segmentation (Graham, 1991). The characteristic of each spatial frequency channel is assumed to be a linear, translation invariant filter.

A compelling demonstration of the parallel channels for spatial frequency is shown in Figure 1.7 (with permission from Professor Aude Oliva, MIT). This hybrid image is a combination of the high spatial frequencies of an image of Prof Einstein and the low spatial frequencies of an image of Ms Monroe. This demonstration also reveals oriented filter outputs at different spatial scales e.g. the oriented filters for the perception of Einstein's eyebrows differ in scale to those for Ms Monroe.

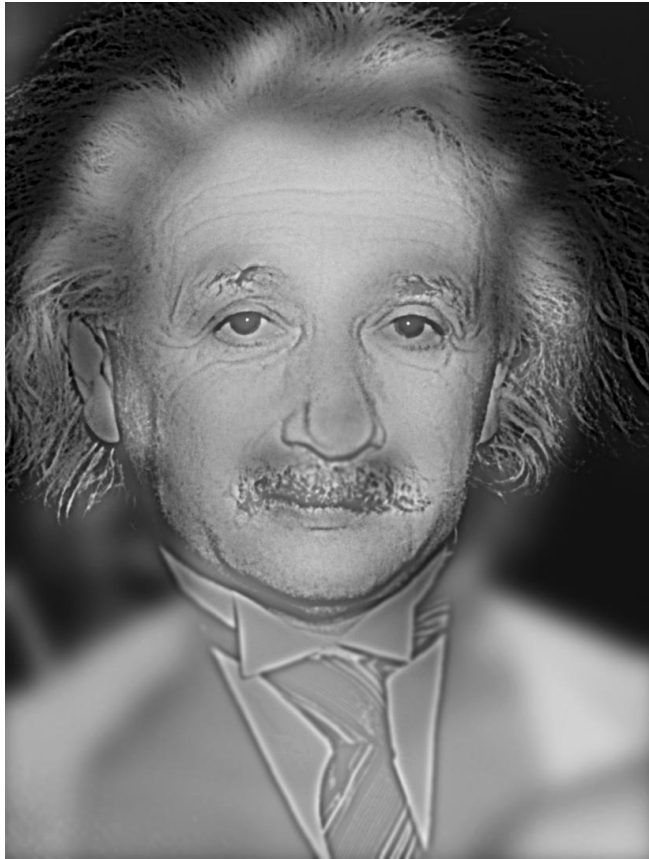


Figure 1.7. Einstein is visible at most reading distances, however, squinting, removal of corrective spectacles or viewing at a larger viewing distance reveals Ms Monroe.



#### 1.3.4 The filter-based model of texture segmentation

The filter-based model is a computational model for texture segmentation that operates in a similar manner to the linear responses of simple cells and the non-linear responses of complex cells within the visual cortex in their processing of the visual field for texture segmentation.

The filter-based model has three sequential feed-forward stages. In this model, the outputs of a bank of 1<sup>st</sup> stage linear filters are transformed by a non-linear process prior to segmentation at the 2<sup>nd</sup> stage of linear filtering, which is followed by an observer's decision (Chubb & Landy, 1991). The structure of an additional stage of linear filtering that followed the non-linear stage explained texture segmentation by a size-tuned mechanism (Bergen & Adelson, 1988). The model is either referred to in terms of the sequential response characteristics of each stage, i.e. LNL which denotes the linear, nonlinear and linear stages, or alternatively as filter-rectify-filter (FRF) notation. The model is informally referred to as the back pocket model of texture segmentation.

At the 1<sup>st</sup> stage of linear filtering, local orientation selective filters represent all of the spatial locations in the visual field. There are a large number of 1<sup>st</sup> stage linear spatial filters and these are sensitive to luminance variation (Chubb & Landy, 1991). That is, 1<sup>st</sup> stage filters extract second-order statistics. The two-stage filter architecture explains segmentation of second-order texture patterns. An example of a 2<sup>nd</sup> order stimulus is shown in Figure 1.8. 2<sup>nd</sup> order filters were selective to spatial frequency (Sutter, Sperling & Chubb, 1995) and responded to contrast modulation (Chubb & Landy, 1991; Sutter, Sperling & Chubb, 1995; Landy & Oruç, 2002).

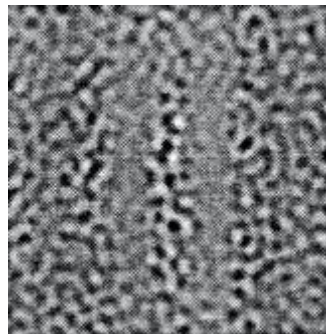


Figure 1.8. 2<sup>nd</sup> order stimulus: a Gabor function multiplied by random visual noise (Sutter, Sperling & Chubb, 1995).

#### 1.3.4.1 Non-linear stage

Chubb and Landy (1991) found a non-linear characteristic for the segmentation of two texture borders that were constructed from 1<sup>st</sup> order statistics, or luminance. They concluded that, since this effect was unrelated to 2<sup>nd</sup> order statistics, the pointwise non-linearity is applied at the 2<sup>nd</sup> stage of the model. Similarly, the value of every spatial point in the filters that form the outputs from the 1<sup>st</sup> stage linear filters is transformed (Sutter, Beck & Graham 1989; Graham, 1991). The transformation is non-linear and could be e.g. full wave rectification (i.e. an absolute positive value for all of the points), half-wave rectification (i.e. only the points with positive values form an output) or the squaring of every point (Graham, 1991). Weighting the outputs of filters in this way computes the local structure for texture which directly contributes to the segmentation of a textured region at the 3<sup>rd</sup> stage of filtering.

#### 1.3.4.2 Texture segmentation

For the filter-based model, texture segmentation is the creation of a texture boundary between different regions of texture. Differences between the spatial

outputs from the non-linear stage determine the segmentation of these regions (Chubb & Landy, 1991; Graham, 1991; Bergen & Landy, 1991) at the 2<sup>nd</sup> stage of linear filtering or the third stage of the model (Chubb & Landy, 1991). The architecture of the model is shown in Figure 1.9 (Landy, 2013) along with additional pooling that, depending on the segmentation task, may or may not follow the 2<sup>nd</sup> stage of linear filtering.

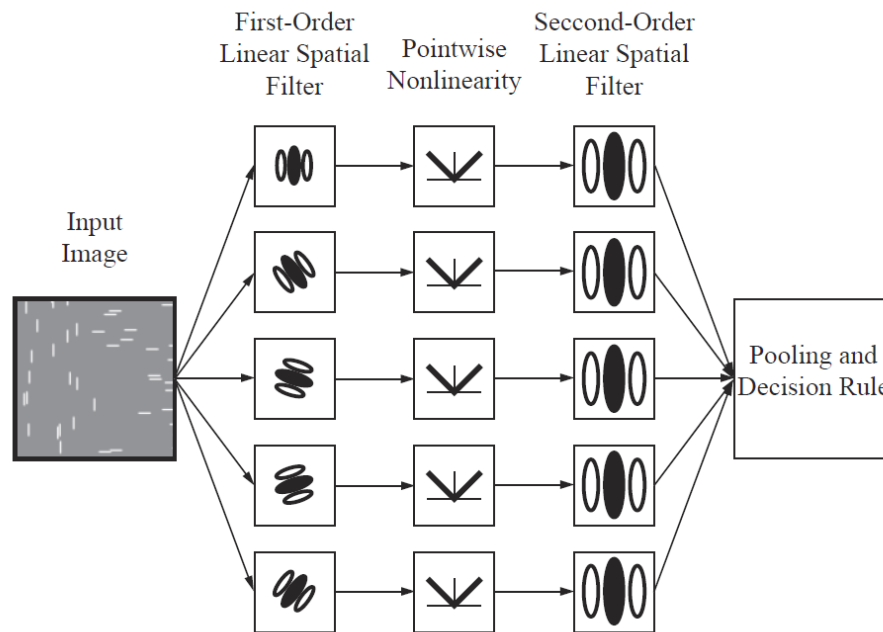


Figure x.2. The back-pocket model of texture segregation, consisting of a linear filter, a point-wise nonlinearity, and a second-order linear filter at a coarser scale.

Figure 1.9. The architecture of the filter-based model (Landy, 2013).

#### 1.3.4.3 The scale of linear filters

Texture segmentation may depend, at least computationally, on the scale of the 1<sup>st</sup> and 2<sup>nd</sup> stage linear filters. The 1<sup>st</sup> stage of filtering is selective to operating on a fine spatial scale while the 2<sup>nd</sup> stage of filtering operates on a coarser spatial scale (Sutter, Sperling & Chubb, 1995). Equally, studies have shown that the 1<sup>st</sup> and 2<sup>nd</sup> stage linear filters are bound in spatial scale in that segmentation of textures is scale invariant (Sutter, Sperling & Chubb, 1995; Kingdom & Keeble 1999; Dakin & Mareschal, 2000). In addition, the density of high and low spatial frequency textures can influence the selection of the appropriately sized, and spatially scaled, 2<sup>nd</sup> stage linear filters for segmentation (Rainville & Kingdom, 2002). Moreover, using gratings defined by a sinusoidal variation in texture orientation a low-pass characteristic was found for 2<sup>nd</sup> order orientation filtering (Keeble, Kingdom, Moulden & Morgan, 1995).

#### 1.3.4.4 Modifications to the model

There are several or more forms of the model which depend on the observer's task, the stimuli used and the resulting computations performed for texture perception, for example additional pooling and decision stages are shown in Figure 1.9.

#### 1.3.5 Feature integration theory for visual search and texture segmentation

The segmentation of texture may be also explained in terms of the difference in one or more basic features such as colour and shape (Treisman & Gelade, 1980).

Evolution is likely to have equipped human beings with an ability to rapidly find and identify features of interest, salience or difference and to also search in a serial manner for such features within the visual environment. A model for explaining this ability in terms of both paradigms of visual search and texture segmentation, feature integration theory, is a two stage process where features are either found pre-attentively or are bound by focused attention (Treisman & Gelade, 1980). In this context features are, for example, orientation, luminance, spatial frequency, shape, colour, near or far depth or motion and are described as the definitive features that are processed separately by the visual system (Treisman & Gormican, 1988).

The first stage of the feature integration model is termed a feature search. That is, pre-attentive *pop-out* occurred in parallel such that the reaction time to find a target feature was independent of the number of background, or distractor, items (Treisman & Gelade, 1980). Pop-out denotes the almost instantaneous 'pop' of a feature 'out' from the background, e.g. a line texture oriented at 90 degrees amongst line textures oriented at 0 degrees respectively (Figure 1.10; left panel), irrespective of the number of items, or set-size. The time to react to pop-out, the reaction time (RT), was independent of set-size producing a flat plot for RT as the number of items increased, i.e. the slope was 0 ms per item (Figure 1.10; right panel).

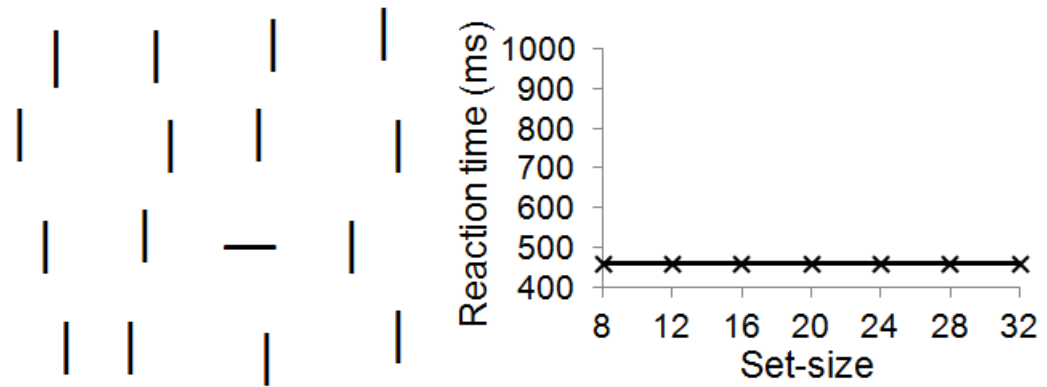


Figure 1.10. An example of a feature search; a line texture oriented at 90 degrees amongst line textures oriented at 0 degrees (left panel). An example of the results for this task show that reaction time was independent of set-size (right panel).

Attention is called in a bottom-up direction that is driven by the stimulus feature. Bottom-up can be defined as attention operating from the bottom, or the first stage, of the model up to second stage. Further to individual features, their size also readily guided attention (Treisman & Gormican, 1988; Wolfe & Horowitz, 2004).

The second stage of the feature integration model is termed a conjunctive search. That is, pop-out did not occur in parallel as combinations of more than one feature required serial processing. This latter stage requires focal attention to process features in serial and also describes the limits of distributing attention across multiple feature dimensions (Treisman & Gormican, 1988). An example of a conjunction search is finding a red letter L amongst a background of red letter T's and blue letter L's (Figure 1.11; left panel). An example of the results for this task are shown in Figure 1.11 (right panel) where the steep slope of the plot represents a proportional increase in RT per item added to the set-size, or ms/item.

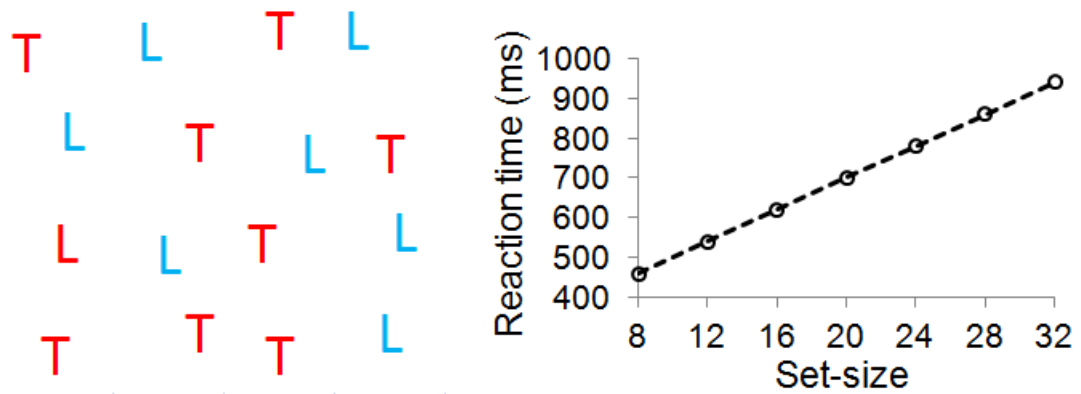


Figure 1.11. An example of a conjunction search (left panel); there was a red letter L amongst a background of red letter T's and blue letter L's. An example of the results for this task shows RT increased proportionally per item added to the display (right panel).

#### 1.3.5.1 What and where

Individual maps initially represent each feature, i.e. 'what', and the features themselves determine pop-out in parallel at the first stage. An individual 'master map' is formed from the spatial locations of features, i.e. 'where', for attention to peruse and locate features in a serial manner at a later stage (Treisman & Gormican, 1988). The binding, or 'gluing', of individual features and the subsequent recognition of an object also require focal attention (Treisman & Gelade, 1980).

#### 1.3.5.2 The filter-based model for texture segmentation and visual search share a common foundation

The foundation for the 1<sup>st</sup> stage of linear filtering in the filter-based model (Chubb & Landy, 1991) and feature maps in feature integration theory (Treisman & Gelade, 1980) is input from spatial frequency-tuned and oriented channels (Sutter, Beck & Graham 1989; Graham, 1991). 2<sup>nd</sup> order (dipole) statistics can be extracted in both models (Caelli & Julesz, 1978). However, the functionality of each model differs. The filter-based model grades spatially local regions of texture for segmentation. For visual search, a feature either forms a feature map or none is produced.

#### 1.3.5.3 Inconsistencies for the feature integration model

Explaining pop-out as the parallel processing of any individual feature is consistent with the functional specialisation of brain regions that subserve individual processes



such as the processing of orientation in V1 (Livingstone & Hubel, 1984) and motion in V5 (Zeki et al, 1991). However, the theory is inconsistent with the findings that showed some 'double duty' neurons in V1, although rare, were tuned to more than one individual feature, for example, a horizontal orientation and a green colour (Livingstone & Hubel, 1984). Although feature integration theory predicts that a target stimulus differing in both spatial frequency and orientation to distractors (Fig. 1.12, left panel) is difficult to discriminate, discrimination was easy when the boundaries between all of the stimuli were manipulated by reproducing the stimuli as a sum of both spatial frequencies, high and low, and both orientations, horizontal and vertical, Fig. 1.12, right panel (Sagi, 1988).

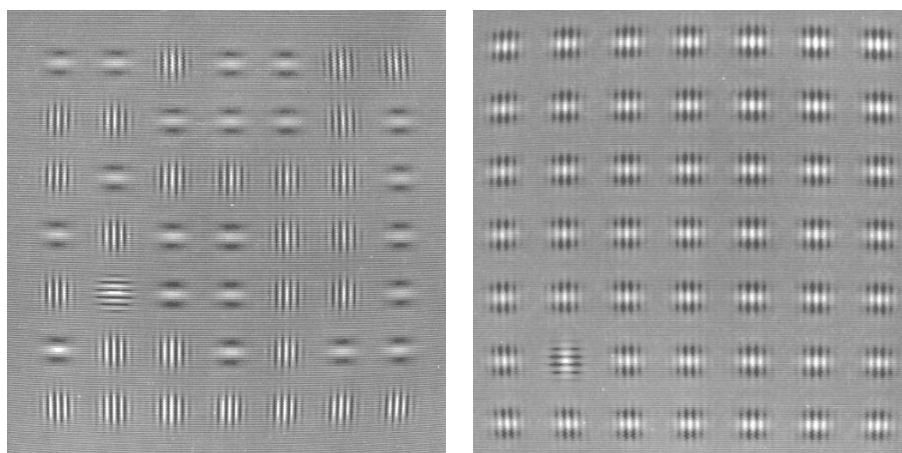


Figure 1.12. An example of a conjunction search, left and right panels (Sagi, 1988).

#### 1.3.5.4 Modifications to the model

Feature integration theory was modified in order to explain parallel, or pre-attentive, search for some combinations of features such as colour and orientation, for example a red bar with vertical orientation. Features were still theorised as being processed in individual channels but the difference to the original model was some combinations of features in the first stage could guide attention in a top-down direction to initiate pop-out (Wolfe, Cave & Franzel, 1989). Top-down denotes attention being driven cognitively from the top, or the second stage, of the model down to the first stage. However, the guided search model (Wolfe, Cave & Franzel, 1989) does not explicitly examine texture segmentation.

To conclude, feature integration theory has remained as one of the main theories with which search asymmetries are explained, i.e. pop-out occurs for a stimulus with feature x amongst a set of stimuli with feature y, but not vice versa.

### 1.3.6 Saliency models for texture segmentation or pop-out

In this report, saliency denotes segmentation, or pop-out, as a function of visual processing for perception. Saliency has been proposed to fulfil a role of directing attention, guiding eye movements and selecting features for additional processing by attention. An orientation boundary between line segments oriented at 45 and 135 degrees can be described as salient (Figure 1.13):



Figure 1.13. Either stimulus dimension may produce saliency - the orientation of the black line segments that represent the boundary, or, their Weber contrast which is lower than the grey segments (due to the white background).

Figure 1.13 illustrates only one of a variety of feature dimensions produces saliency. Saliency is determined in a bottom-up direction from the responses of V1 cells (Li, 1999). The V1 saliency hypothesis and model explains the neural mechanism for texture segmentation in addition to saliency and is consistent with the physiological findings (Li, 1999).

#### 1.3.6.1 V1 saliency hypothesis

In one model, saliency is determined in a bottom-up manner by the neurons within V1 that have the maximum response to stimulation in their RF (Li, 1999; Zhaoping & May, 2007; Zhaoping, 2008). The responses of neurons, rather than their selectivity e.g. to orientation or colour, determines saliency. The spatial location of the visual

scene that corresponds to the receptive fields of the neurons in V1 with the highest firing rate is used for the creation of a salience map for further processing by attention (Zhaoping & May, 2007; Zhaoping, 2008). The maximum firing rate of V1 neurons can be determined physiologically by recording the number of spikes/second with electrodes. Alternatively, salience can be determined psychophysically by measuring the reaction time to find a boundary such as the vertical boundary on the left between tilted line segments shown in Figure 1.14.

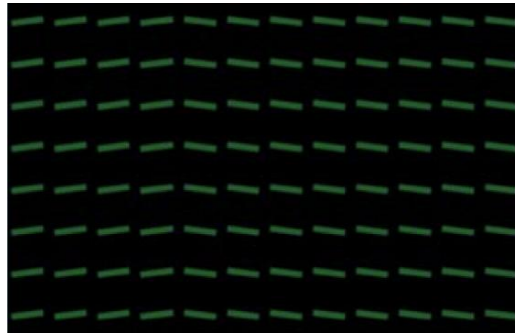


Figure 1.14. A vertical boundary on the left between tilted line segments is salient. Image from Zhaoping and May (2007).

#### 1.3.6.2 V1 salience model

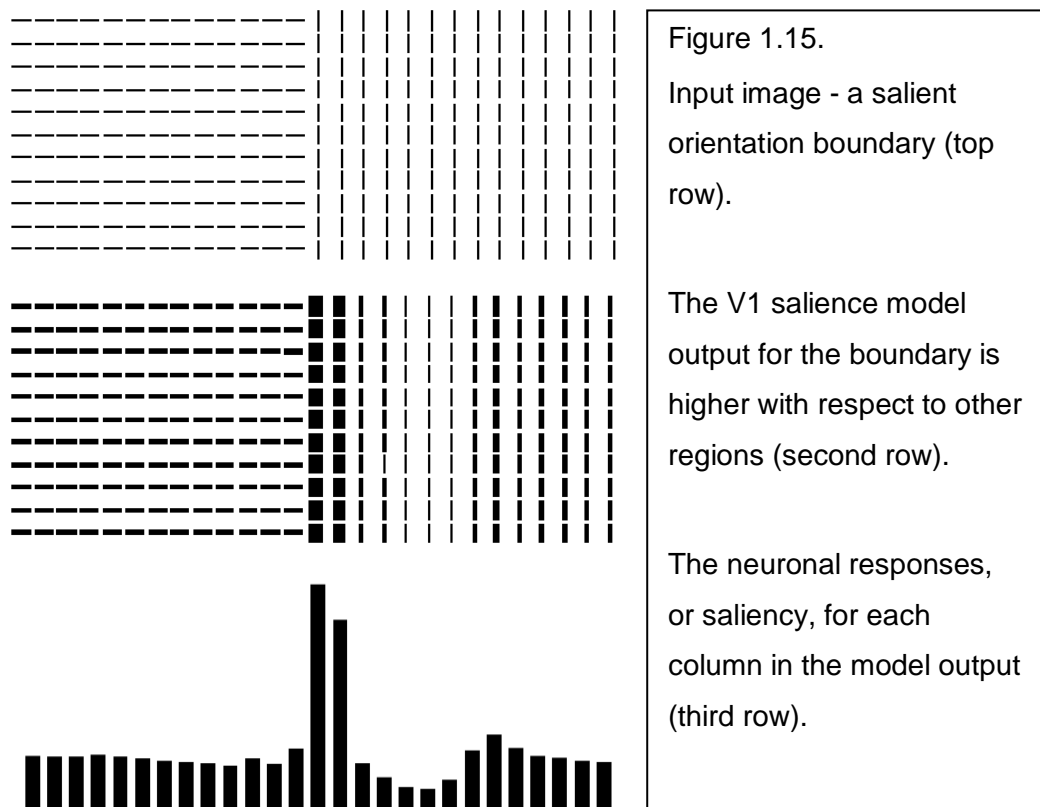
Rather than the separate feature maps for each feature which comprise feature integration theory, one salience map is formed from the maximum response of V1 neurons (Zhaoping & May 2007; Zhaoping, 2008). Therefore, the Max rule governs the formation of the salience map and pop-out or segmentation. The most salient location is determined by a winner-takes-all strategy (Zhaoping & May 2007).

#### 1.3.6.3 Lateral interactions

In the model the responses of V1 neurons to an optimal stimulus can be suppressed by other neurons outside the classical RF. An example is iso-orientation suppression (Knierim & van Essen, 1992; Levitt & Lund, 1997; Zipser, Lamme & Schiller, 1996). Inhibition is maximal from neurons with the same tuning characteristics. These neuronal responses may be mediated by long range horizontal projections of neuronal axons up to cortical distances of 4 mm within V1 (Gilbert & Wiesel, 1983). The function of connections between non-overlapping receptive fields was proposed to be either inhibitory, or, to produce an RF with a larger size. Since this finding, the precise function for lateral intra-cortical connections within V1 has attracted much speculation. The V1 salience model

shows these connections to modulate neuronal responses for segmentation (Li, 1999).

An example of a salient orientation boundary, the output produced by the V1 salience model for this orientation boundary and the neuronal responses which produce saliency are shown in Figure 1.15 (Li, 1999). Saliency results from the maximum responses of V1 neurons to vertical elements at the location of the orientation boundary i.e. the figure. These responses are not suppressed by neurons responding to orthogonal horizontal bars outside the classical RF. Moreover, iso-orientation suppression is greatest for background elements with equal orientation. Thus, texture segmentation results from the neuronal responses to the figure and the suppression of responses to the ground.



## **1.4 Review of the research for inverse cyclopean texture segmentation on which the research question is based**

This section (section 1.4) introduces the inverse cyclopean paradigm and conveys the research question for the experiments reported in this thesis. The research for inverse cyclopean texture segmentation on which the research question is based is then reviewed. This reveals apparent contradictions in the literature for which it is the purpose of the experiments reported in this thesis to investigate. In the following section (section 1.5), the relevant facts regarding binocular rivalry and fusion are reviewed.

### **1.4.1 Introduction**

The two frontal eyes in humans and primates allow for a large region of binocular overlap and perception in three dimensions, or stereoscopic vision. This percept can be inferred from disparate images falling on each retina because of the horizontal separation of the eyes, i.e. disparity. Normally, the world is not perceived as disparate images but as a single fused image. Binocular fusion of the images in the two eyes occurs when the light from an object produces similar images that fall within Panum's fusional area, wherein the fusion range is greater for horizontal than for vertical separations of retinal disparities (Howard, 2002; Panum, 1858). The percept of fusion that is formed from the disparity range can occur in parallel with, or without, the percept of stereo vision, and vice versa as these are distinct processes that arise from binocular visual processing (Julesz & Miller, 1975; Marr & Poggio, 1979; Georgeson & Wallis, 2014).

An inverse cyclopean stimulus is a stimulus in which a monocularly visible pattern is invisible upon optical fusion of both eyes' images (Julesz, 1971). Monocular is derived from the Greek *mono* meaning 'one' and the Latin *oculus* meaning 'eye'. An inverse cyclopean stimulus is shown in Figure 1.16 (left & centre panels). The texture elements within each inverse cyclopean stimulus are orientation-defined; the left eye's target is the right eye's distractor, and vice versa. The inverse cyclopean stimuli shown in Figure 1.16 are dichoptic. For dichoptic stimuli, one of the two eyes views texture elements within a stimulus that are different from the texture elements within the other stimulus that the other eye views. Whilst texture elements within a dichoptic stimulus might be visible in the optically fused percept, an orientation-

defined, dichoptic-overlapping (inverse cyclopean) target is invisible in the optically fused percept (Figure 1.16; right panel). Conversely, for a binocular stimulus, the two eyes view the same texture elements within the stimulus.

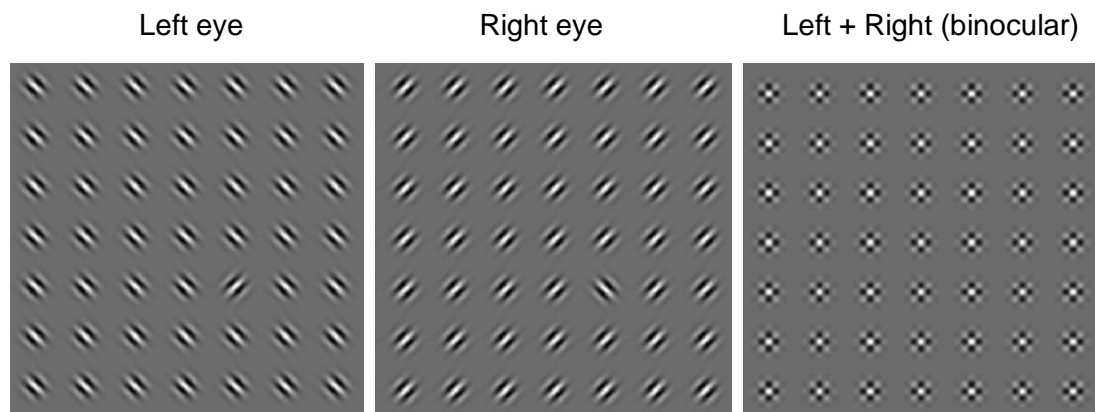


Figure 1.16. An inverse cyclopean stimulus for each of the two eyes (left & centre panels). Within each inverse cyclopean stimulus, an orientation-defined target is orthogonal to the distractors. The sum of these two images is given in the right panel to show the optically fused percept.

#### 1.4.2 Psychophysical investigations of inverse cyclopean texture segmentation

Kolb and Braun (1995) showed orientation-defined, inverse cyclopean texture segmentation occurs even when segmentation is impossible in the fused image. On the other hand, orientation-defined, inverse cyclopean visual search is impossible (Wolfe & Franzel, 1988). Therefore, the research question for the experiments reported in this thesis is: what difference in experimental procedures is responsible for these different results? Although Kolb and Braun's and Wolfe and Franzel's results were in the texture segmentation and visual search paradigms respectively, the different paradigms for these researchers is incidental to the research question. The purpose of the experiments reported in this thesis is to investigate the difference in Kolb and Braun's and Wolfe and Franzel's orientation-defined, dichoptic-overlapping (inverse cyclopean) displays that is responsible for their different results.

### 1.4.3 Inverse cyclopean texture segmentation occurs in brief dichoptic presentations (Kolb & Braun, 1995)

Kolb and Braun (1995) showed that texture segmentation based on the monocular image could occur even when it was impossible in the fused image. Their dichoptic-overlapping (inverse cyclopean) stimulus is shown in Figure 1.16; however, the target was four Gabor stimuli. 20 x 20 Gabor stimuli covered the same unit area on a notional grid within each dichoptic-overlapping stimulus. Texture density is defined as the number of texture elements within an area of the display. The area of the display for Kolb and Braun's stimulus was the area covered by the 20 x 20 notional grid. Texture elements were separated by 1 degree. The density of texture elements within Kolb and Braun's dichoptic-overlapping stimulus is termed dense. The control condition was binocular for which either stimulus shown in Figure 1.16 (left or centre panel) was presented to both eyes. Exposure duration was 250 ms. For both conditions, observers reported one of the four potential quadrants to contain the target in a 4-alternative forced choice procedure (4-AFC) for which chance performance was 25%. Performance was  $83.3 \pm 1.8\%$  for binocular orientation-defined stimuli which suggests efficient texture segmentation. However, although performance for dichoptic-overlapping stimuli was poorer ( $75.2 \pm 1.1\%$ ) the difference from chance was significant. This result shows texture segmentation based on monocular boundaries in dichoptic-overlapping (inverse cyclopean) stimuli is visible in brief 250 ms presentations.

#### 1.4.3.1 'Blindsight'?

The three observers in Kolb and Braun's experiment also rated their confidence, on a scale of 1 to 10, that their response was correct. The confidence ratings correlated with performance in the binocular condition; however, for the dichoptic-overlapping condition confidence ratings did not correlate with performance which led Kolb and Braun to interpret this result as 'blindsight'. Blindsight is a condition that is caused by a lesion in visual area V1 and is characterised by performing visual tasks without subjective visual awareness (Weiskrantz, Barbur & Sahraie, 1995). Visual awareness denotes a subjective description of seeing or being aware of the visibility of a stimulus in a task. The 'blindsight' interpretation was challenged by Morgan, Mason and Solomon (1997). Morgan, Mason and Solomon replicated Kolb and Braun's experiment using dichoptic-overlapping and monocular, for which either

dichoptic-overlapping stimulus was viewed by one eye, conditions. The three observers in Morgan, Mason and Solomon's experiment rated their confidence that their response was correct. There were also 10 possible responses for their rating; however, on a scale of 0 to 9. Observers were instructed to use the full range of the rating scale. However, observers rated their absolute confidence for performances with the dichoptic-overlapping task, independently of their confidence for performances with the monocular task. Exposure duration was 250 ms. Contrary to Kolb and Braun's finding, the observer's confidence ratings correlated with high performance in both dichoptic-overlapping and monocular conditions. Kolb and Braun instructed observers to use the full range of the rating scale (1-10) in both conditions which encouraged observers to rate their relative, but not absolute, confidence for locating vaguely visible cues for the dichoptic-overlapping condition. Rather than responding with consistently low confidence ratings, observers may have chosen to respond with random ratings. This explained why ratings were not skewed towards low confidence and the reason for high confidence when errors in task performance were made; thus 'blindsight' was not evident.

#### 1.4.4 Orientation-defined, inverse cyclopean visual search is impossible (Wolfe & Franzel, 1988)

When the left eye's target is the right eye's distractor, and vice versa, orientation-defined visual search is impossible (Wolfe & Franzel, 1988). In Experiment 10, Wolfe and Franzel measured the reaction time to find an orientation-defined, dichoptic-overlapping (inverse cyclopean) target. There were either trials for which an orthogonal target was presented amongst distractors all sharing the same orientation, or, blank trials for which no target was presented and distractors shared the same orientation. Wolfe and Franzel's dichoptic-overlapping stimulus is shown in Figure 1.17. Texture elements were contrast randomised. Their contrasts were determined from one of four values; however, these values were not given. The purpose of contrast randomisation was to eliminate a difference in effective contrast between the two eyes. If there were a difference in effective contrast between the two eyes, an orientation-defined target in a dichoptic-overlapping stimulus might be visible in the optically fused percept and pop-out. Set-size was 2, 4 or 8 texture elements that were spaced evenly on a circle around fixation. Even though the largest set-size for Wolfe and Franzel's dichoptic-overlapping stimulus was 8 texture elements, these elements were separated by 1.9 degrees; thus, texture



elements were sparser than the texture elements within Kolb and Braun's dichoptic-overlapping stimulus. Wolfe and Franzel found orientation-defined, inverse cyclopean visual search was impossible.

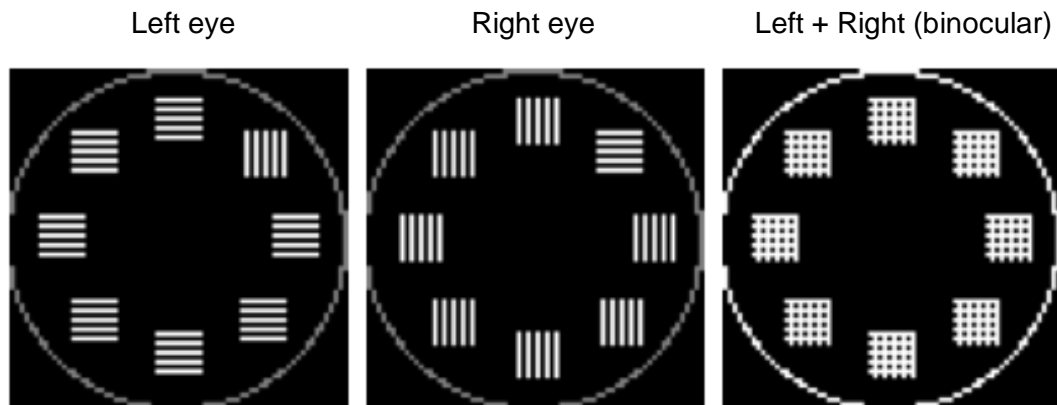


Figure 1.17. Wolfe and Franzel's dichoptic-overlapping stimuli (left & centre panels); the optically fused percept is shown in the right panel. The fixation point (not shown) was in the centre of each image. In these images, texture elements are not contrast randomised.

#### 1.4.5 Monocular visual processing can be investigated with the inverse cyclopean paradigm

The inverse cyclopean paradigm is an elegant paradigm for investigating the visual processing that occurs prior to integration of the inputs from the two eyes. This is because monocular texture boundaries within dichoptic-overlapping (inverse cyclopean) stimuli are invisible in the optically fused percept. It would be impossible for putative dichoptic-overlapping (inverse cyclopean) texture boundaries to be detected after the inputs from the two eyes are integrated. The experiments reported in this thesis investigate the phenomenology and mechanisms for texture segmentation that occur prior to integration of the inputs from the two eyes.

Whilst orientation-defined, binocular visual search is trivially easy (Treisman & Gelade, 1980; Wolfe & Horowitz, 2004), orientation-defined, inverse cyclopean visual search is impossible (Wolfe & Franzel, 1988). This led Wolfe and Franzel to conclude monocular input cannot be accessed for visual search. On the other hand, texture segmentation based on the monocular image does occur, even when texture segmentation is impossible in the optically fused image (Kolb & Braun,

1995). This implies that orientation-defined, dichoptic-overlapping (inverse cyclopean) texture boundaries are detected by a monocular process, prior to integration of the inputs from the two eyes. Thus, monocular input is available to texture segmentation mechanisms (Morgan, Mason & Solomon, 1997; Solomon & Morgan, 1999).

Attention can operate on and change the properties of 2<sup>nd</sup> stage linear spatial filters (Yeshurun & Carrasco, 2000). Yeshurun and Carrasco used an orientation-defined binocular target for their experiment. However, when stimuli are dichoptic-overlapping (inverse cyclopean), attention cannot be directed to a monocular stage of processing (Solomon & Morgan, 1999). This implies that, if orientation-defined, inverse cyclopean texture segmentation is consistent with the filter-based model of texture segmentation (Chubb & Landy, 1991), the properties of 2<sup>nd</sup> stage filters would be unchanged by attention.

The experiments reported in this thesis investigate orientation-defined, inverse cyclopean texture segmentation. However, for dichoptic-overlapping (inverse cyclopean) displays, an observer may simply close one of the two eyes to view an orientation-defined target monocularly. Whilst an orientation-defined, dichoptic-overlapping (inverse cyclopean) target can only be detected by a mechanism that exists at a monocular stage of processing, an orientation-defined target viewed by one of the two eyes could be detected by mechanisms that exist at both monocular and binocular stages of processing. Morgan, Mason and Solomon (1997) found that, for all three observers, texture segmentation in brief 250 ms durations was perfect for the monocular task. If performance was 100% for a dichoptic-overlapping (inverse cyclopean) task when exposure duration was 250 ms, this might imply that an observer has closed one of the two eyes. In the following experiments, performance that is consistent with an observer closing one of the two eyes is reported in the results section. Alternatively, performances consistent with the dichoptic-overlapping (inverse cyclopean) task are reported.

### 1.5 Prior to recent evidence from Kolb and Braun, perceptual fusion was reported for brief exposures of dichoptic-overlapping stimuli

Kolb and Braun (1995) found that performances for orientation-defined, inverse cyclopean texture segmentation were significantly above chance. This implies

dichoptic-overlapping stimuli are not optically fused in brief durations. Kolb and Braun's, Morgan, Mason and Solomon's (1997) and Solomon and Morgan's (1999) dichoptic-overlapping tasks would be impossible if their stimuli were optically fused in brief durations. Prior to these experiments, perceptual fusion was reported for brief exposures of dichoptic-overlapping stimuli.

Hering (1874) reported that brief exposures of orthogonal lines, e.g. lines drawn at 45 & 135 degrees, in corresponding retinal positions were seen as fused whereas binocular rivalry was seen for longer exposures. Binocular rivalry refers to perception alternating between e.g. oriented lines. What is perceived from moment to moment during binocular rivalry is a dynamically alternating pattern of both of the images where part of each image is visible while the other parts are not. Historically this phenomenon has attracted the attention of perceptual scientists like Helmholtz and Hering although its origins can be traced back to a translation of a report by Porta in 1593 (Wade, 1998). An example of binocular rivalry is shown in Figure 1.18 (Wilson, 2010).



Figure 1.18. Superimposing the images in the left and centre panels (by crossing the eyes to view a distant, or alternatively a near, point in space) produces a percept of rivalry for which an example is shown in the right panel.

Further reports supported fused percepts for brief exposures of dichoptic-overlapping stimuli (Wolfe 1983; Anderson et al, 1978). Wolfe (1983) reported that orthogonal gratings fuse into a tartan, or plaid, percept when presented in a dichoptic flash for durations less than 150 ms. This percept was independent of stimuli spatial frequency and luminance. However, rivalry was observed when successive presentations are 150 ms apart. In this study, observers rated their experience by responding on a scale from 0 (rivalry) to 4 (fusion). These subjective reports are an interpretation of the observer's percept rather than an implicit property of texture during the pre-rivalrous experience. Anderson (1978) reported

fusion for high-contrast dichoptic-overlapping stimuli for presentations less than 200 ms and rivalry for presentations more than 400 ms. Moreover, a percept of binocular rivalry required exposures longer than 200 ms (Dawson, 1913).

The periods of dominance and suppression are a critical property of rivalrous stimuli. Moreover, a 'patchy' percept has been described by observers during the period of perceptual dominance for which this percept is strong for rival stimuli viewed with central fixation (Blake, O'Shea & Mueller, 1992). Alternatively, perceptual dominance for a local patch may spread to a figural interpretation (Diaz-Caneja, 1928). Alternating rivalry may sometimes occur between alternative figural interpretations rather than between the eyes. An example by Diaz-Caneja is shown in Figure 1.19 (Alais, O'Shea, Mesana-Alais & Wilson, 2000). After fusion of the two images, perception alternates between that of continuous horizontal red lines versus continuous curved lines.

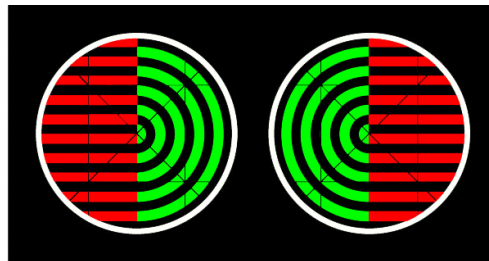


Figure 1.19. Diaz-Caneja stimuli. Superimposing both of the images (by crossing the eyes to view a distant point in space and aligning the crosshairs) can show a percept of the individual forms (parallel red and black lines, or, circular green and black lines).

## **General Methods**

The purpose of experiments reported in this thesis is to investigate inverse cyclopean texture segmentation. In each of the following experiments there is a methods section that conveys the methods that are specific to each experiment. General methods which apply to all of the experiments are conveyed in the following sections.

### **2.1 The method for presenting stimuli**

Shutter goggles presented dichoptic-overlapping stimuli in corresponding retinal locations in the two eyes. If the goggles were removed, the patterns were optically fused and would be invisible to the observer. Presentation of alternate video frames containing stimuli was achieved by a Cambridge Research Systems Bits# switching the shutter state of Cambridge Research Systems FE-1 goggles in synchrony with a Sony display. The FE-1 goggles were a requirement for dichoptic stimuli; however, the shutters reduced the luminance of the stimuli by 78%. Both shutters of the goggles were open on successive frames for optical fusion of the two images in dichoptic-overlapping stimuli to produce binocular stimuli. Although the goggles were not a requirement for a binocular stimulus, observers wore the goggles for both dichoptic and binocular viewing for the reduction in luminance to be equal.

#### **2.1.1 Experimental procedure and stimuli**

The experiments were conducted in a darkened room to prevent light reflections within the goggle apertures and variations in display luminance. The display had been adapted to measure precise viewing distances to the two eyes. Observers viewed the display from 1 m unless otherwise stated. Experiment sessions began after 5 minutes of dark adaptation and lasted no longer than two hours with breaks between consecutive blocks as measures to minimise the effect of tiredness or fatigue on results. After each session observers were asked to report their experience of the task.

Gabor stimuli were generated and presented using Psychtoolbox-3 (Kleiner, Brainard & Pelli, 2007) software running on a MacBook Pro computer. A Gabor stimulus is described on page 21. Stimuli were generated on-the-fly every trial using

the following method. Each Gabor texture was added within the pre-defined 600 x 600 pixel stimuli array via linear superposition, allowing for each Gaussian envelope extending to infinity; summation effectively prevented texture-boundary luminance artefacts. Gabor stimuli were cosine-phase. An equation for a Gabor stimulus is:

$$lum(loc_x, loc_y) = lum_0 \left( 1 \pm c \sin(2\pi f(loc_y \sin(ang) + loc_x \cos(ang)) + \phi) \exp \left[ \frac{loc_x^2 + loc_y^2}{2\sigma^2} \right] \right) \quad (1)$$

Where  $lum$  is the value for the luminance at location  $(loc_x, loc_y)$ ,  $lum_0$  is the mean luminance,  $c$  is the contrast of the stimulus,  $f$  is spatial frequency (the inverse of the wavelength  $\lambda$ ),  $ang$  is orientation,  $\phi$  is phase and  $\sigma$  is the standard deviation (the width of the spatial window of the stimulus). The luminance profile of a Gabor stimulus is shown in Figure 2.1.

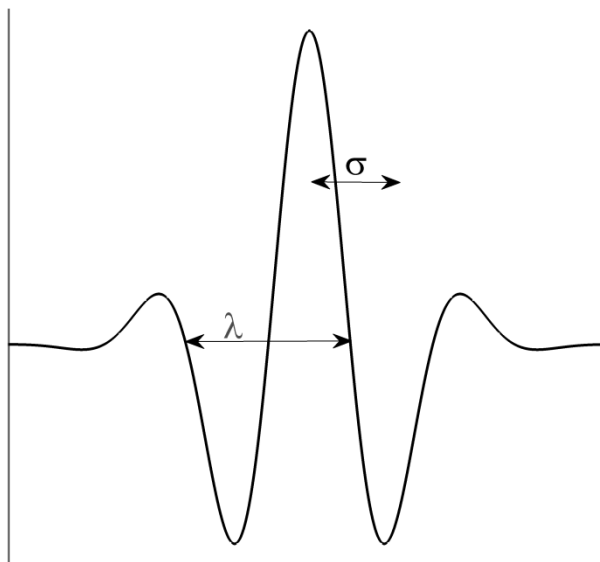


Figure 2.1. The luminance profile of a cosine-phase Gabor stimulus. The wavelength ( $\lambda$ ) and standard deviation ( $\sigma$ ) of the stimulus are also shown.

On every trial, randomisation was used to determine whether orientation was either 45 or -45 degrees with respect to vertical. Randomisation was used to determine whether orientation was either 0 or 90 degrees on every trial for Experiment 6 only. The target was orthogonal to the distractors. The orientation-defined target was 4.3 degrees of visual angle from fixation in Cartesian quadrant IV (CQ4) of the display in Experiments 3, 4 and 5 and was 4.7 degrees from fixation in CQ4 for Experiment 6.

In Experiment 7, the target was 4.3 degrees of visual angle from central fixation in Cartesian quadrant II of the display.

Blocked trials for each condition were also trials in which the retinal eccentricity of the target from fixation was unchanged. Blocked trials were used in Experiments 2, 3, 4, 5 and 6, but were not used in Experiment 1 or in Experiment 7. In Experiments 3, 4 and 5, rather than stimulus location, the observer's fixation was manipulated so that the target was 4.3 degrees of visual angle from fixation. The target was an equal visual angle from central fixation to prevent the results being affected by differences in sensitivity at different retinal eccentricities. Prior to every block observers were informed of the location of the target and the use of blocked trials also reduced location uncertainty.

On every trial observers signalled the interval containing an orientation-defined target in a two alternative forced choice procedure (2-AFC) while the other interval contained distractors only. In Experiment 1, further details are given for a forced choice task for which the number of alternatives ( $m$ ) was 2 or 4.

Exposure durations were 16, 50, 150, 450 and 1350 ms and were logarithmically spaced. For each block, trials were divided equally between the five durations. Alternatively, there was one exposure duration per block of trials for Experiments 2, 6 and 7. For each block, trial sequence was randomised with respect to the target interval to ensure the observer had no prior knowledge of the interval containing the target.

## 2.2 Psychometric functions

An observer's performance in the psychophysical task was measured using the method of constant stimuli for logarithmically spaced exposure durations. The range of stimulus levels included short durations, at which performance was at chance, through to long durations to represent obvious intensities for which task errors were assumed to be stimulus-independent (Wichmann & Hill, 2001a). Each trial within each condition was assumed independent and identically distributed over  $N$  total number of trials sufficient for the number of correct responses to be sampled from a binomial distribution. The total number of trials is  $N = \sum n_i$  where  $n_i$  is the number of

trials per block  $i$ . The proportion of correct responses  $y_i/n_i$ , where  $y_i$  is the number of correct responses, were assumed the sum of random sampling from a Bernoulli process for which  $p_i$  is the probability of a correct response.

Frequencies correct for each task and observer were maximum likelihood fit. The probability of a correct response as a function of the independent variable  $x$ , exposure duration, formed the psychometric function  $\Psi$

$$\Psi(x; \alpha, \beta, \gamma, \delta) = \gamma + (1 - \gamma - \delta)F(x; \alpha, \beta) \quad (2)$$

$\gamma$  was fixed equal to  $1/m$  as 0.5 or 0.25 to represent the lower bound in performance due to intrinsic noise as chance performance in 2-AFC and 4-AFC tasks respectively (Treutwein & Strasburger, 1999; Wichmann & Hill, 2001a).  $F(x; \alpha, \beta)$  is the critical term describing the abscissa parameter  $\alpha$  and the slope, or spread, parameter  $\beta$  of the function. Threshold ( $\alpha$ ) is the stimulus intensity at a level of performance on the abscissa, the inverse of  $F$ , and slope ( $\beta$ ) is the rate at which performance changes with stimulus intensity, the gradient of  $F$ . Delta ( $\delta$ ) represents the amount of reduction in an observer's performance at large stimulus intensities.

The upper bound of psychometric ceiling, asymptote, defined as  $1 - \delta$  reflects the observer's inability to respond to obvious stimuli (Wichmann & Hill, 2001a; Treutwein & Strasburger, 1999). Obvious stimulus intensities at which performance deviated from 100% were assumed to be due to effects which were independent of sensory processes. These effects may be fluctuations in attention, alertness, response errors, non-observed stimuli or mechanical failure of the apparatus. Wichmann and Hill (2001a) showed biased parameter estimates of  $\alpha$  and  $\beta$  unless an accurate value for  $\gamma$  and  $\delta$  are given, or  $\delta$  is allowed to vary as a free parameter, when observer data is Maximum likelihood fit. Therefore, an accurate estimate of an observer's performance for a task can only be determined when the estimate of  $\delta$  is accurate, or when  $\delta$  is allowed to vary freely. Furthermore, the results for a task are incorrect unless they are determined from accurate values of  $\alpha$  and  $\beta$ .

The bias in parameter estimates is illustrated in Figure 2.2, which shows the number of correct responses given by an observer in a 2-AFC detection task. The black solid line shows a PMF when observer data contained 49 trials fit with a Weibull



function for which the estimate of  $\alpha$  was 1.57 and  $\beta$  was 4.4. The grey solid line shows a Weibull fit to observer data containing an error on the 50<sup>th</sup> trial where a 2% error, shown as a grey triangle in the PMF, caused performance to be 98% for which the estimate of slope ( $\beta$ ) was severely affected (slope was shallower) and  $\alpha$  was affected; thus, estimates were biased. However, when  $\delta$  was an additional parameter allowed to vary freely, the grey dashed line shows a Weibull fit to observer data for which the best-fitting parameter estimates of  $\alpha$  and  $\beta$  were 1.54 and 4.4 respectively and  $\delta$  was estimated to be 0.14.

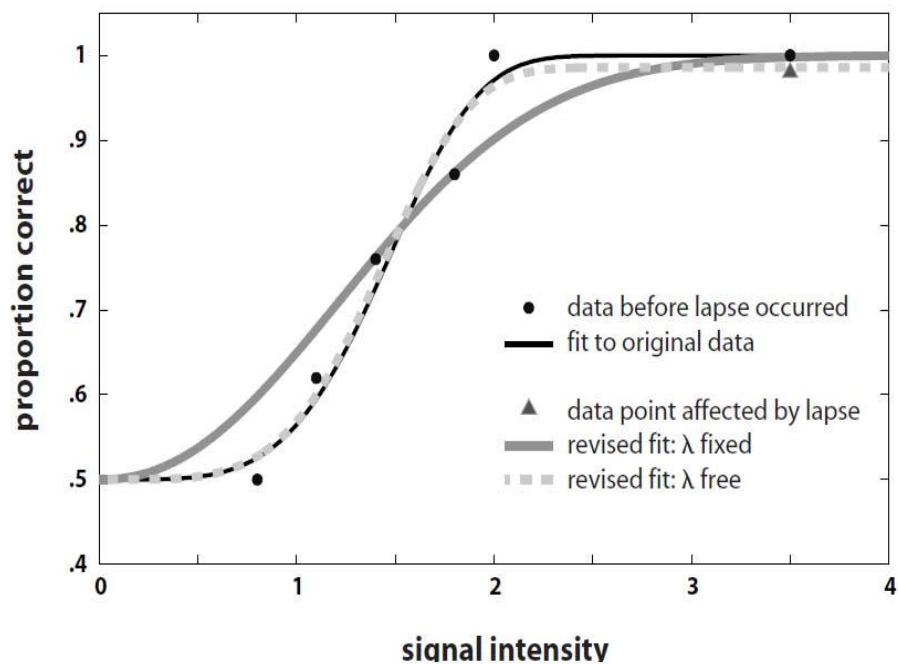


Figure 2.2. Psychometric function for which observer data were Maximum likelihood fit (Wichmann & Hill, 2001a). The PMF was a Weibull function. The black solid line shows the original fit to observer data. The grey solid line shows a fit for which there was an error shown by the grey triangle and  $\delta$  was fixed. The grey dashed line shows a fit for which  $\delta$  varied freely.

### 2.2.1 Parameter estimates for the following experiments

Under ordinary viewing conditions, i.e. binocular, stimulus-independent response errors were expected when prolonged inspection ensured an orientation-defined target was made obvious. For Experiment 1.2, the estimate of delta  $\delta$  was based on an estimate of the probability of a finger error: 0.02. However, an orientation-defined, dichoptic-overlapping (inverse cyclopean) may never become obvious with

prolonged viewing, e.g. 5 seconds; thus, threshold ( $\alpha$ ), slope ( $\beta$ ) and delta ( $\delta$ ) were parameters allowed to vary freely. Furthermore, the dichoptic and binocular orientation-defined targets that were used in Experiment 1.1, which were nonoverlapping, might not become obvious with prolonged viewing; therefore, delta was allowed to vary freely.

The best-fitting values for  $\alpha$ ,  $\beta$  and  $\delta$  were determined by the Palmedes toolbox (Prins & Kingdom, 2009) and the standard error in these best-fitting values were determined from a parametric or non-parametric bootstrap. The former method for optimising parameter estimates based on an assumed PMF shape and the latter for estimates based on actual values of proportion correct for the independent variable exposure duration  $x$  which forms the PMF  $\Psi$ . The psychometric function  $\Psi$  was a Cumulative normal.

### 2.2.2 The generalised likelihood ratio

The purpose for each experiment is described in each chapter in which hypotheses are defined. Further to obtaining an observer's proportion of correct responses given as a function of the independent variable  $x$ , inversion of the probability distribution to a function of parameters given an observer's responses obtained Maximum likelihood estimates of parameters and the log-likelihood  $\ln l$ .

The generalised likelihood ratio,  $2(\ln l - \ln l_0)$ , or LL ratio, tested the null hypothesis where  $\ln l$  and  $\ln l_0$  are log-likelihoods for models which correspond to the alternative and null hypotheses respectively. The null hypothesis is the nested model in which the best-fitting parameter values were equal and unchanged for every condition. An example is testing the effect of texture density on inverse cyclopean texture segmentation (Experiments 1 & 3). The null hypothesis is the nested model in which the best-fitting parameter values for  $\alpha$ , or  $\delta$ , were equal and unchanged for all texture densities with log-likelihood values  $\ln l_0$  for each observer. The alternative hypothesis is texture density affected  $\alpha$ , or  $\delta$ , with log-likelihood values  $\ln l$  for each observer. Another example is testing the effect of a smaller inter-element space on inverse cyclopean texture segmentation. In Experiment 4, the inter-element space was manipulated by increasing sigma ( $\sigma$ ) in linear increments. The null hypothesis is the nested model in which the best-fitting parameter values for  $\alpha$ , or  $\delta$ , were equal and unchanged with a smaller inter-element space with log-likelihood values  $\ln l_0$  for

each observer. The alternative hypothesis is a smaller inter-element space affected  $\alpha$ , or  $\delta$ , with log-likelihood values  $\ln l$  for each observer.

### 2.2.3 Model variants

Where there were different models, the model with the best-fit to observer data was assessed. However, the model with the best-fit to observer data was not a model for texture segmentation. The Bayesian Information Criterion (Schwarz, 1978) or BIC was used as this method is not dependent on an evaluation or assumption of the prior distribution. For model (M), containing  $\hat{\theta}$  parameter values obtained by maximising the likelihood function ( $\hat{L}$ ) for observer data  $x$ , the BIC is:

$$\text{BIC} = -2 \cdot \ln \hat{L} + k \cdot (\ln(N) - \ln(2\pi)) \quad (3)$$

Where  $\hat{L} = p(x | \hat{\theta}, M)$  is the likelihood function. Inference of the BIC accounts for uncertainty in both parameters and models  $m_j \dots M$ . BIC is appropriate for selecting the best-fitting model since the number of trials ( $N$ ) for  $x$  was greater than 40 which sufficed in exceeding the number of free parameters ( $k$ ). The number of free parameters  $k$  denotes the penalty term such that the most parsimonious model is the one in which there are fewer parameters. Thus, the most probable posterior model  $m$  represents beliefs having obtained observer data  $x$ .

The general, unconstrained, model contains 3 free parameters i.e.  $\alpha$ ,  $\beta$  and  $\delta$  for each condition. For example, 3 texture density or 5 inter-element space conditions result in a total of 9 and 15 free parameters respectively. BIC values were used to assess the parsimonious, or least constrained, model in which parameter values were constrained as nested under the unconstrained model. Each model variant was assessed as a significant fit to observer data when each free parameter was in turn, removed. The next consecutive model to the unconstrained is the model for a linear fit of either threshold ( $\alpha$ ), slope ( $\beta$ ) or delta ( $\delta$ ) to observer data. The model for which threshold exposure duration  $\alpha$ , Eq.4, or asymptote  $(1-\delta)$ , Eq.5, is linearly affected by texture density,  $D$ , is an 8 parameter model. For Eq.4,  $a_\alpha D$  is the slope and  $b_\alpha$  is the intercept for a linear fit to observer data for all texture densities and  $\beta$  and  $\delta$  vary freely for each texture density. For Eq.5,  $a_\delta D$  is the slope and  $b_\delta$  is the intercept for a linear fit to observer data for all texture densities and  $\alpha$  and  $\beta$  vary freely for each texture density.

$$\alpha D = a_{\alpha} D + b_{\alpha} \quad (4)$$

$$\delta D = a_{\delta} D + b_{\delta} \quad (5)$$

Furthermore, the model for which threshold exposure duration  $\alpha$ , Eq.6, or asymptote  $(1-\delta)$ , Eq.7, is linearly affected by inter-element space ( $\sigma$ ) is a 12 parameter model. For Eq.6,  $a_{\alpha\sigma}$  is the slope and  $b_{\alpha}$  is the intercept for a linear fit to observer data for all inter-element space conditions and  $\beta$  and  $\delta$  vary freely for each condition. For Eq.7,  $a_{\delta\sigma}$  is the slope and  $b_{\delta}$  is the intercept for a linear fit to observer data for all inter-element space conditions and  $\alpha$  and  $\beta$  vary freely for each condition.

$$\alpha_{\sigma} = a_{\alpha\sigma} + b_{\alpha} \quad (6)$$

$$\delta_{\sigma} = a_{\delta\sigma} + b_{\delta} \quad (7)$$

Removal of another parameter is a model in which threshold ( $\alpha$ ), slope ( $\beta$ ) or delta ( $\delta$ ) are constrained to a single unchanged value. The next consecutive model is the model in which two parameters are a linear fit to observer data and one parameter varies freely. Removal of free parameters continued until the most constrained model was reached for which  $\alpha$ ,  $\beta$  and  $\delta$  are constrained to unchanged values.

For Experiments 1 and 4, a model for a linear fit for slope ( $\beta$ ) was not significant and as such was rejected as a model and not included in results.

### 2.3 Participants

Participants for the studies were recruited via an advertisement on the University notice board or word-of-mouth to academic colleagues, friends and family. Participants were chosen to represent a range of ages and both scientific and non-scientific backgrounds in order to represent as wide a sample of the population as possible. All observers were required to have either normal vision or corrected visual acuity and, other than the author, were naïve to the purpose of each experiment. The most recent visual acuity test and correction, if any, was requested as part of assessment.

Six of the nine recruited observers had no prior experience with dichoptic-overlapping displays. Two observers were females while seven were males; the average age was  $42 \pm 16$  years. A Randot stereo-test (Stereo Optical Co, Chicago) was used as an indication of depth perception (Figure 2.3). One observer with amblyopia was a participant in Experiment 6. Records were maintained for both written consent for observer participation and payment receipts prior to and following experiments respectively.



Figure 2.3. Randot Stereo test and the polarising filters through which each of the random dot stereograms in the right-hand plate were viewed. Observers reported the shape perceived in depth. In the left-hand plate animals or Wirt circles were at different disparities to indicate stereoacuity.

## 2.4 Latin square

Following testing the effect of texture density on inverse cyclopean texture segmentation (Exp. 1), subsequent experiments (Exp. 3, 4 & 5) tested inverse cyclopean texture segmentation for which there were 8 conditions. Blocked trials were used for each condition. The results for each observer were obtained using Latin square order. An example Latin square for conditions 1 through to 8 are shown randomised for two observers In Figure 2.4. The balance-point point found

for each observer in Experiment 2 was used in each of the 8 conditions. The balance-point is the ratio of interocular luminance contrast required to equate differences in effective contrast. The same observers participated in Experiments 2, 3, 4 and 5. The purpose of not changing observers was for results to be comparable between conditions. The retinal eccentricity of the target from fixation changed specifically for the eighth Latin square condition for which an orientation-defined target was viewed with central fixation from a 3 m viewing distance, however, these results were not analysed.

Observer	1				2			
Test sequence	1	2	3	4	1	2	3	4
Condition	3	4	2	8	3	6	7	2
Test sequence	5	6	7	8	5	6	7	8
Condition	6	1	5	7	4	1	8	5

Figure 2.4. Latin square order of 8 conditions for which inverse cyclopean texture segmentation was tested in sequence for each observer.

## 2.5 Task practice

Instructions for the task, the location of the target and use of the keyboard to signal a response were conveyed to observers prior to practice with dichoptic-overlapping stimuli and the task. Observers trained with three consecutive blocks for the condition in which Gabor stimuli were arranged in a dense 12 x 12 grid. A dense texture density was chosen for the practice task since pilot experiments showed segmentation performance was high for this texture density. There were three further blocks for observers inexperienced with dichoptic-overlapping stimuli. Orientation-defined, inverse cyclopean texture segmentation was practiced over a large range of exposure durations between 16 and 1350 ms. Accuracy greater than 75% in identifying the interval containing the target was deemed proficient. Three further observers, two females and one male, were unable to perform above chance and did not participate in the studies. This implies that there are individual differences in the ability to perform a dichoptic-overlapping task.

## 2.6 Feedback

Feedback was present in Experiments 2, 3, 4, 5 and 7 for which an audible tone indicated an observer's correct response to the interval containing the orientation-defined target in the 2-AFC task. Feedback assisted observers in performing the segmentation task. Feedback was not present for Experiments 1 and 6.

## 2.7 Nonius procedure and fixation point

At the start of every trial observers performed a dichoptic nonius procedure to ensure the point of zero horizontal disparity had been achieved in order to control for extraneous cues such as diplopia, fixation disparity and disjunctive fluctuations of vergence. Indeed, vergence instability has been proposed as a potential cue to inverse cyclopean texture segmentation (Howard, 2002). An image showing an example of the nonius procedure is given in Figure 2.5. The task was the lateral alignment of two dichoptic dots (one per eye) and the lateral alignment of two dichoptic vertical lines (one line per eye) that flanked the dots. The dots and lines subtended 0.22 and 0.3 degrees of visual angle respectively and the lines were separated by 0.28 degrees of visual angle. Dichoptic lines were used to increase the accuracy in attaining the point of zero horizontal disparity prior to and during every trial. This type of vernier alignment was shown to have an accuracy of 0.7 arcmin for lines separated by less than 1 degree of visual angle in the centre of the visual field (McKee & Levi, 1987). Observers pressed a key on accomplishing the nonius task and the first interval of texture elements was presented in <5 ms of this response. The text giving the nonius procedure instructions within the display area did not occlude the area for stimuli.

For experiments where the target was in a peripheral retinal location, the nonius dots were present during both the trial and the interstimulus interval, serving both to maintain alignment and as a fixation point. The location of the nonius procedure within the display area was specific to each experiment in order for an orientation-defined target to be an equal visual angle from fixation; examples are given in each experiment. Another purpose for observers performing the nonius procedure prior to each trial for a binocular task was to ensure the observers had no prior knowledge of whether the trial was for a dichoptic or binocular task.

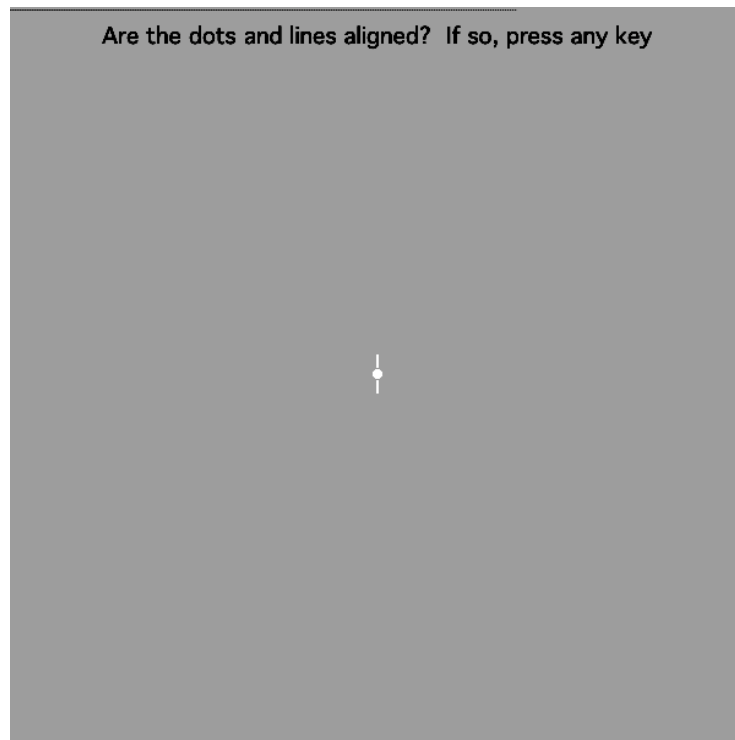


Figure 2.5. Dichoptic nonius procedure showing a dot and a line per eye as horizontally aligned.

### 2.8 Dropped or extra stimulus frames

To prevent the results being affected by the goggle shutters remaining in the open or closed state for more than one video frame, or failing to open, a trial was replaced if this occurred by re-randomising the sequence of that trial and the remaining trials in the block. Psychtoolbox-3 measured the start time and the end time of the interval and the trial was repeated if this measurement differed to the expected time to present the stimuli, calculated from the number of video frames given for the exposure duration.

### 2.9 Stimulus display

For Experiment 1.1, the frame rate of the 37.5 cd/m<sup>2</sup> Sony F520 display was 140 Hz, 70 Hz per eye, and resolution was 13 pixels/degree. For all subsequent experiments, the frame rate of the 34 cd/m<sup>2</sup> Sony 300SF display was 120 Hz, 60 Hz



per eye, and resolution was 36 pixels/degree. The contrast for each Sony display was the maximum attainable. Both displays were gamma corrected with the following procedure.

To reduce luminance artefacts and for finer control of luminance contrast randomisation, Bits# was set to monoPlusPlus mode. The display was calibrated by measuring the output luminance of the display, with a Konica Minolta LS-100 photometer, at 16 increments of the Bits# DAC (digital to analog converter) input voltage and a two parameter equation for Weber contrast was applied to this data to calculate gamma and kappa for gamma correction. Gamma is the gamma characteristic of the display and kappa is the scale factor. The values for gamma and kappa were 2.32 and 0.000021 respectively for the Sony 300SF display. For the Sony F520 display, the values for gamma and kappa were 1.85 and 0.000022 respectively.

## **Experiment 1: Is orientation-defined, inverse cyclopean texture segmentation dependent on texture density?**

### **3.1 Introduction**

Texture segmentation based on the monocular image does occur, even when texture segmentation is impossible in the optically fused image (Kolb & Braun, 1995). Morgan, Mason and Solomon (1997) used a dichoptic-overlapping display to replicate this result and concluded the mechanisms for orientation-defined texture segmentation can access monocular input. However, in the visual search paradigm, when the left eye's target is the right eye's distractor, and vice versa, orientation-defined visual search is impossible (Wolfe & Franzel, 1988). Wolfe and Franzel (1988) concluded monocular input cannot be accessed for visual search. For Kolb and Braun's dichoptic-overlapping stimulus, orientation-defined texture elements occupied positions on a 20 x 20 notional grid; texture elements were dense. On the other hand, for Wolfe and Franzel's dichoptic-overlapping stimulus, 2, 4, or 8 orientation-defined texture elements were spaced evenly on a circle around fixation; texture density was sparse. Therefore, the purpose of the following experiment (Experiment 1.1) is to determine whether the critical variable for the difference between Wolfe and Franzel's and Kolb and Braun's results for texture segmentation is texture density. In Experiment 1.1, orientation-defined, texture segmentation in brief durations was measured when 8 x 8, 10 x 10 and 12 x 12 texture elements covered the same area on a notional grid within each dichoptic stimulus. Figure 3.1 shows the dichoptic-overlapping stimuli (top, third and fifth rows, left and centre panels). The null hypothesis is orientation-defined, dichoptic texture segmentation for grids of 8 x 8, 10 x 10 and 12 x 12 texture elements does not differ. If the outcome for the dichoptic-overlapping displays were that performances for 12 x 12 grids were better than those for sparser grids, then texture density may be the critical variable for the difference between Kolb and Braun's and Wolfe and Franzel's results.

Orientation-defined texture elements within Kolb and Braun's and Wolfe and Franzel's dichoptic-overlapping stimuli competed for the same retinal position; there was competition between the inputs from the two eyes. However, texture segmentation might occur when a large error in vergence rendered dichoptic-

overlapping texture elements effectively nonoverlapping. Therefore, in Experiment 1.1, orientation-defined texture segmentation was measured for dichoptic-nonoverlapping stimuli when texture density was 8 x 8, 10 x 10 and 12 x 12 (second, fourth and sixth rows, left and centre panels). If the outcome for the dichoptic-nonoverlapping displays were that performances for dense 12 x 12 grids were better than performances for sparser grids, then texture density does affect dichoptic orientation-defined, texture segmentation when there is a large error in vergence.

In Experiment 1.1, orientation-defined texture segmentation was measured for two binocular displays. To test Hering's observation that dichoptic-overlapping stimuli were optically fused in brief durations (Hering 1874; Dawson, 1913), performances for the dichoptic-overlapping and binocular-overlapping displays, for which the two images in dichoptic-overlapping stimuli were optically fused (Figure 3.1; top, third and fifth rows, right panel), were compared. The binocular-overlapping task was predicted to be impossible, regardless of texture element density. If performance exceeded chance in brief durations for dichoptic-overlapping displays, orientation-defined, dichoptic-overlapping texture elements cannot be optically fused in brief durations. Texture segmentation was also measured for orientation-defined, nonoverlapping texture elements that were optically fused; a binocular-nonoverlapping stimulus (Figure 3.1; second, fourth and sixth rows, right panel). This stimulus tests the hypothesis that, even if mechanisms for orientation-defined texture segmentation did not have access to monocular input, performance might exceed chance with putative dichoptic-overlapping (inverse cyclopean) texture boundaries if a failure of binocular fusion rendered those textures effectively nonoverlapping (Howard, 2002). Consequently, if, for each texture density, performance with the dichoptic-overlapping display exceeded performance with the binocular-nonoverlapping display, performance for the dichoptic-overlapping display cannot be wholly attributed to a failure of binocular fusion.

We wondered if an effect of texture density on texture segmentation was not specific to dichoptic stimuli. Experiment 1.2 tests if there is an effect of texture density on texture segmentation for a binocular stimulus for which texture density was the same as each dichoptic stimulus used in Experiment 1.1. However, binocular orientation-defined texture segmentation is easy regardless of element density (Nothdurft, 1985; Nothdurft, 1990). Therefore, an effect of texture density on

binocular segmentation was tested when binocular orientation-defined texture segmentation was not trivially easy.

### 3.2 Methods

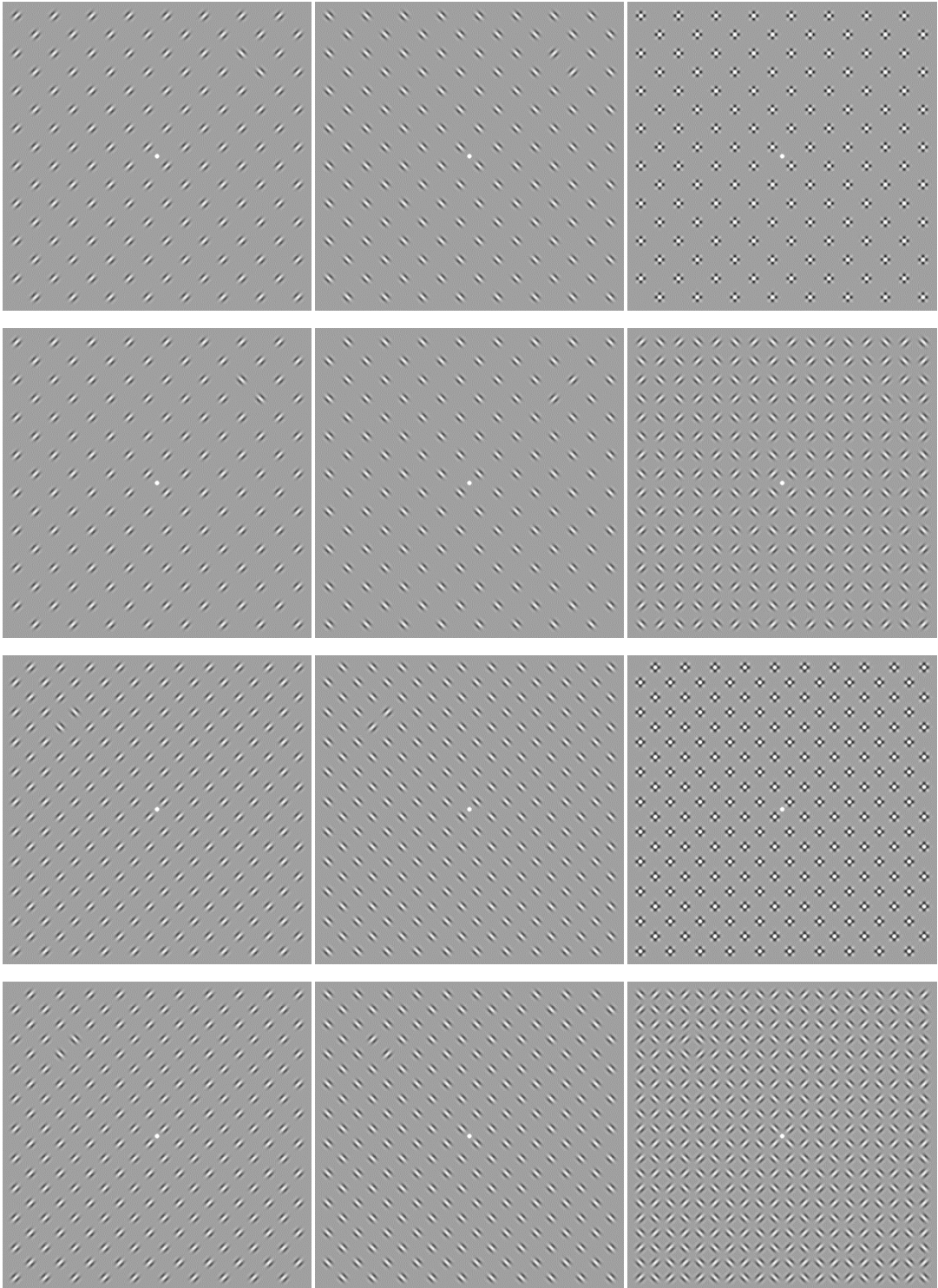
The methods that are applicable to both Experiment 1.1 and Experiment 1.2 are conveyed in this section. The methods specific to each experiment are conveyed in the subsequent sections.

Texture elements occupied alternate positions on 16 x 16, 20 x 20 or 24 x 24 notional checkerboards that covered the same area; the texture density of a dichoptic stimulus was 8 x 8, 10 x 10 or 12 x 12 respectively. Texture density is defined as the number of texture elements per area for a notional checkerboard. The target within each dichoptic stimulus was two Gabor stimuli amongst a background of orthogonal distractors. The target was presented in one quadrant of the display on every trial; the task was 2- and 4-AFC in Experiments 1.1 and 1.2 respectively. The positions of the target within each stimulus were chosen so that the target was approximately an equal visual angle from central fixation across texture densities. For each Gabor stimulus (Eq. 1, Experimental procedure and stimuli, page 45), sigma was 0.14 degrees of visual angle and wavelength was 0.28 degrees; spatial frequency was 3.6 cycles per degree.

Left eye

Right eye

Left & Right (binocular)



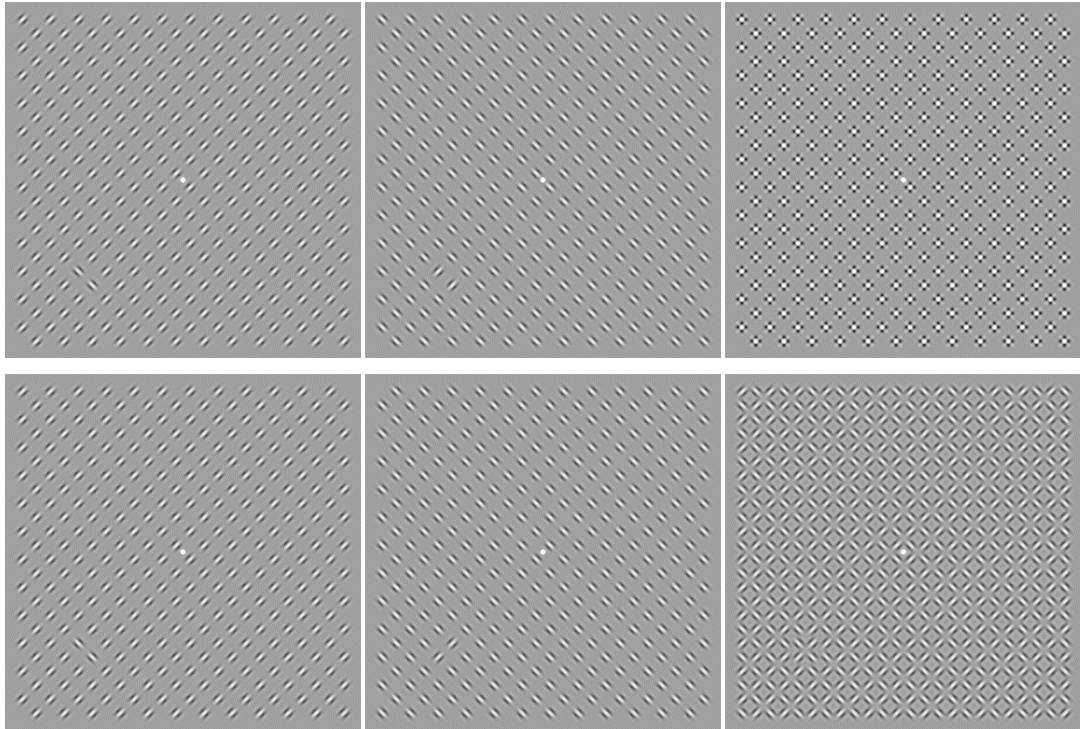


Figure 3.1. 8 x 8, 10 x 10 or 12 x 12 grids of dichoptic-overlapping Gabor stimuli (top, third and fifth rows respectively, left & centre panels) and 8 x 8, 10 x 10 or 12 x 12 grids of dichoptic-nonoverlapping Gabor stimuli (second, fourth and sixth rows respectively, left & centre panels). A binocular-overlapping stimulus is shown in the top, third and fifth rows, right panel, for which the two images in dichoptic-overlapping stimuli were optically fused. A binocular-nonoverlapping stimulus is shown in the second, fourth and sixth rows, right panel, for which the two images in dichoptic-nonoverlapping stimuli were optically fused. Each grid covered an equal unit area.

### 3.2.1 Methods: Experiment 1.1

Orientation-defined texture segmentation was measured for each texture density and observer. There was one block of 400 trials for each texture density. For each block, trials were divided equally between the four segmentation tasks for dichoptic-overlapping stimuli, dichoptic-nonoverlapping stimuli, a binocular-overlapping stimulus and a binocular-nonoverlapping stimulus; for every observer, there were 100 trials for each texture density per task.

A binocular-overlapping stimulus and a binocular-nonoverlapping stimulus were stimuli for which the two images in dichoptic-overlapping and dichoptic-nonoverlapping stimuli respectively were optically fused. This might suggest that

texture density for a binocular-overlapping stimulus and a binocular-nonoverlapping stimulus was 8 x 8, 10 x 10 or 12 x 12 and 16 x 16, 20 x 20 or 24 x 24 respectively, even though the two images in dichoptic-overlapping and dichoptic-nonoverlapping stimuli contained the same number of texture elements. There is a difference in configuration between texture elements within a binocular-overlapping stimulus and a binocular-nonoverlapping stimulus. Therefore, texture density is given for a dichoptic stimulus, but is not given for a binocular stimulus. Binocular orientation-defined texture segmentation was measured when Gabor stimuli were half of the maximum attainable contrast. If binocular and dichoptic stimuli had the same physical contrast, performances with binocular stimuli might be better than those with dichoptic stimuli, simply because binocular summation increases the effective contrast of binocular stimuli. The dichoptic and binocular stimuli are shown in Figure 3.1.

Kolb and Braun's task was 4-AFC for which chance performance was 25%; however, dichoptic-overlapping cues are vaguely visible and rivalrous. To make the dichoptic-overlapping task easier for naive observers, a 2-AFC task was used. For all four segmentation tasks, observers selected one of the four potential quadrants to contain the target by responding 1 for quadrants bounded in the left or 2 for quadrants bounded in the right half of the display on a keypad; chance performance was 50%. Exposure durations ( $x$ ) were between 0.014 and 1.2 seconds.

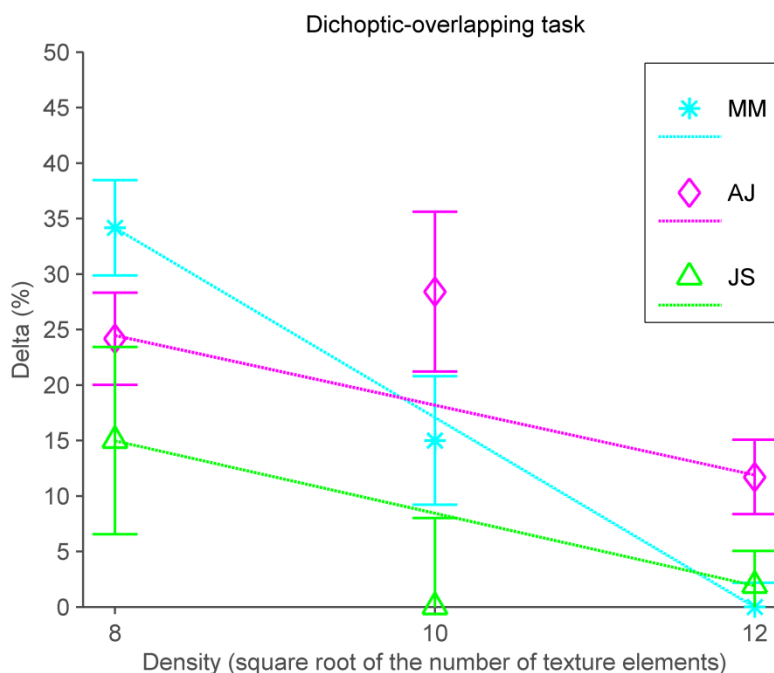
### 3.2.2 Methods: Experiment 1.2

In this experiment, the effect of texture density on segmentation was measured for a binocular orientation-defined stimulus. The stimulus presented to one of the two eyes in Experiment 1.1, for which texture element density was 8 x 8, 10 x 10 or 12 x 12, was viewed without the goggles. To compensate for the reduction in luminance consequent to the shutter goggle method, display luminance was reduced from 34 to 8 cd/m<sup>2</sup>. The observer's task was to state which of four quadrants of the display contained the target by responding on a keypad; chance performance was 25%. This task was trivially easy regardless of texture element density; threshold was less than 100 ms. To increase task difficulty, random noise was interleaved between each video frame for which each pixel was drawn from a uniform distribution of luminance values between 0.15 and 20 cd/m<sup>2</sup>. The purpose of introducing during-stimulus masking was to increase threshold so that threshold was approximately the same as the lowest threshold obtained for dichoptic texture

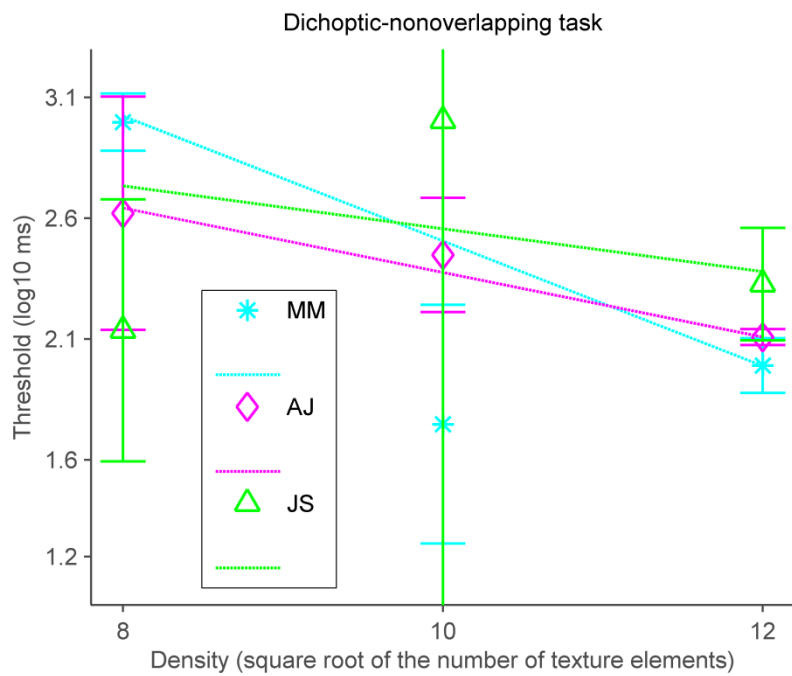
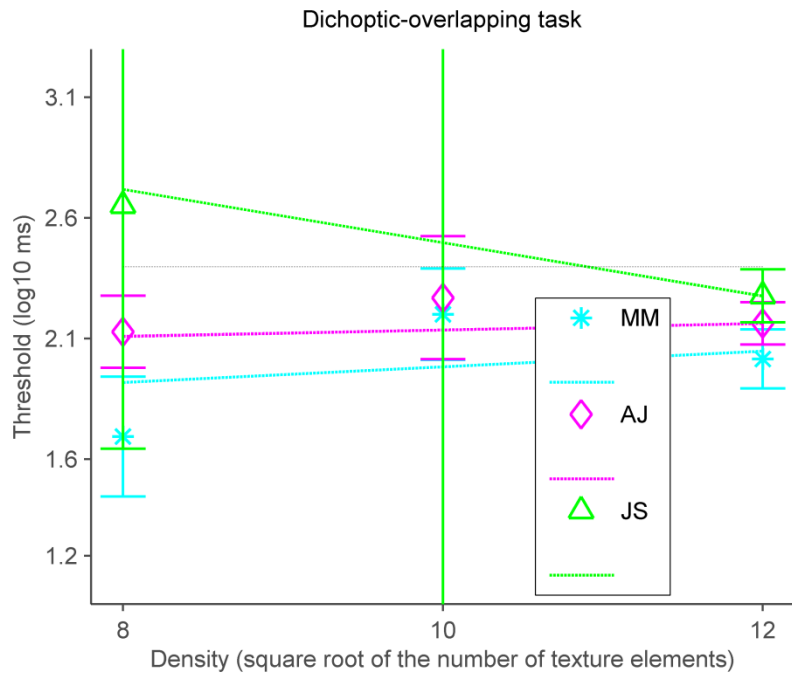
segmentation. Thus, the effect of texture density on binocular and dichoptic orientation-defined texture segmentation was tested when the tasks were of comparable difficulty. Binocular noise-masked orientation-defined, texture segmentation was tested with each texture density for 40 trials. A staircase procedure, Quest (Watson & Pelli, 1983), converged on the exposure duration threshold which corresponded to an accuracy of 62% correct.

### 3.3 Results of Experiment 1.1

The results for the dichoptic-overlapping and dichoptic-nonoverlapping tasks are shown in Figure 3.2. For Figure 3.2 in which there is a linear fit, i.e. straight line, of  $\alpha$  and  $\delta$  to observer data for increasing texture density, the axes are log-lin and lin-lin respectively. The results for all of the observers for both of the dichoptic tasks show that orientation-defined texture segmentation was better for dense texture elements. For the dichoptic-overlapping task, performance was near chance for observer JS when texture density was 10 x 10; the best-fitting value for delta was shown as 0. For the dichoptic-nonoverlapping task, threshold exposure duration ( $\alpha$ ) was 1 second for observers MM and JS when texture density was 8 x 8 and 10 x 10 respectively; although performance for MM and JS was above chance, performance had not improved by the maximum exposure duration of 1.2 seconds for values for  $\delta$  to be determined - the best-fitting values for delta were shown as 0.







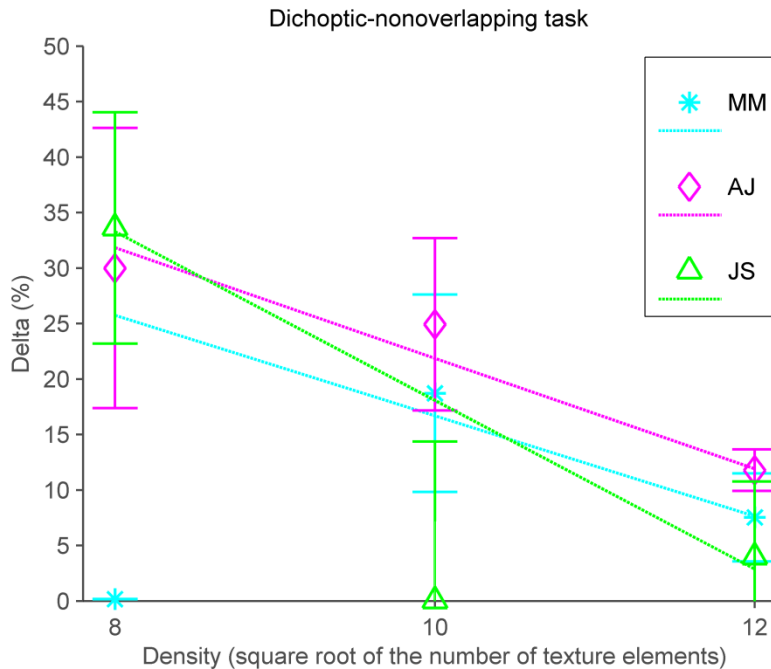


Figure 3.2. The dichoptic-overlapping (top and second rows) and dichoptic-nonoverlapping (third and fourth rows) tasks. For each task, the best-fitting values for threshold exposure duration ( $\alpha$ ) and delta ( $\delta$ ) are shown for each texture density and each observer. For the dichoptic-overlapping task (second row), the gray line corresponds to a threshold exposure duration of 250 ms ( $2.4 \log_{10}$  ms). Error bars show the standard error of the best-fitting parameter values and were determined with a non-parametric bootstrap. Linear fits of  $\alpha$  and  $\delta$  to each observer's data for increasing texture density are shown by the coloured lines.

For the binocular-overlapping task, performance was chance for all observers and all texture densities (i.e. the texture density of a dichoptic-overlapping stimulus).

The results for the binocular-nonoverlapping task are shown in Figure 3.3, in which the best-fitting values for delta ( $\delta$ ) and threshold exposure duration ( $\alpha$ ) are shown for each observer and each texture density (i.e. the texture density of a dichoptic-nonoverlapping stimulus). For all of the observers, performance was poor when texture density was 8 x 8 and 10 x 10 and was chance when texture density was 12 x 12. For observers AJ and JS when texture density was 8 x 8 and 12 x 12 respectively, performance had not improved by the maximum exposure duration of 1.2 seconds for values for  $\delta$  to be determined - the best-fitting values for delta were shown as 0.

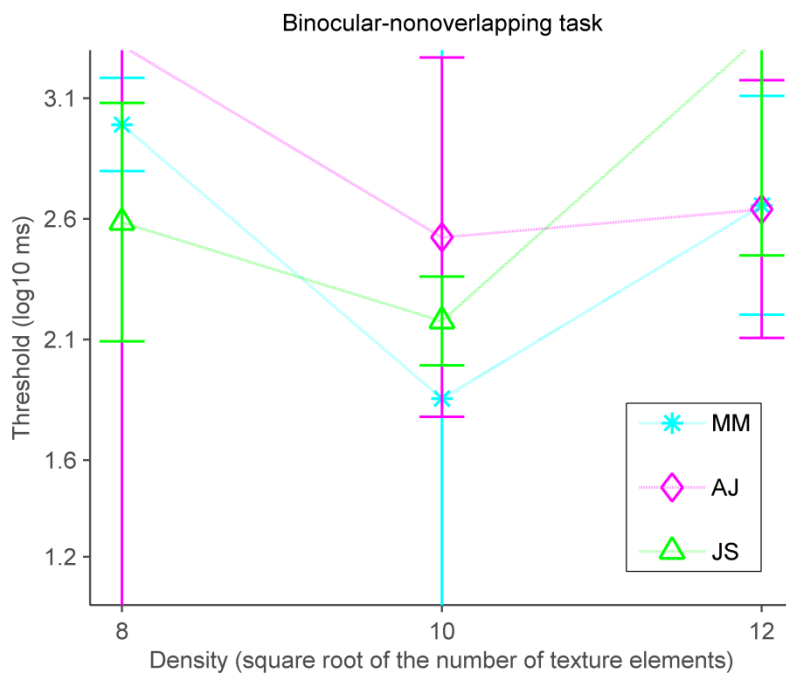
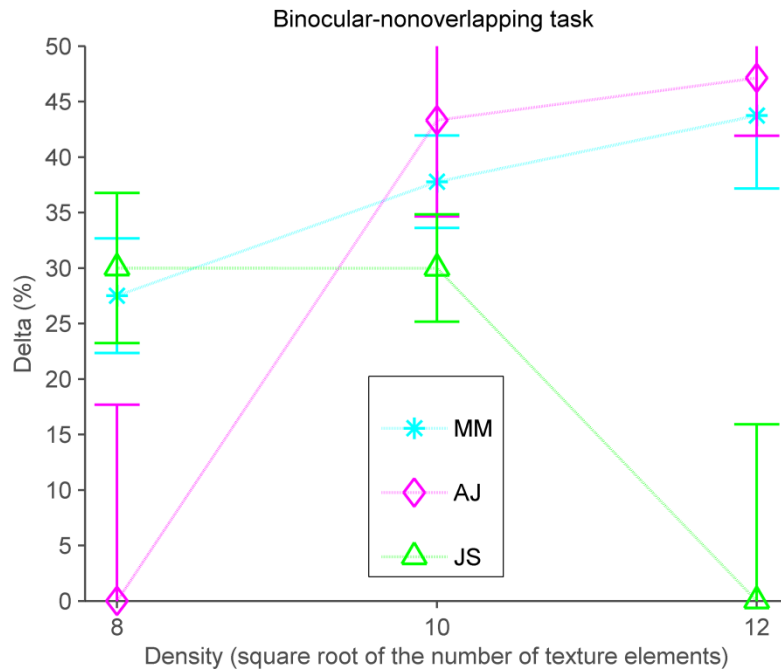


Figure 3.3. The binocular-nonoverlapping task: the best-fitting values for delta ( $\delta$ ) and threshold exposure duration ( $\alpha$ ) are shown for each texture density (i.e. the texture density of a dichoptic-nonoverlapping stimulus) and each observer. Error bars show the standard error of the best-fitting parameter values and were determined with a non-parametric bootstrap.

### 3.3.1 Results of Experiment 1.2

For binocular noise-masked orientation-defined texture segmentation, the best-fitting values for threshold exposure duration ( $\alpha$ ) are shown with a linear fit to observer data in Figure 3.4.

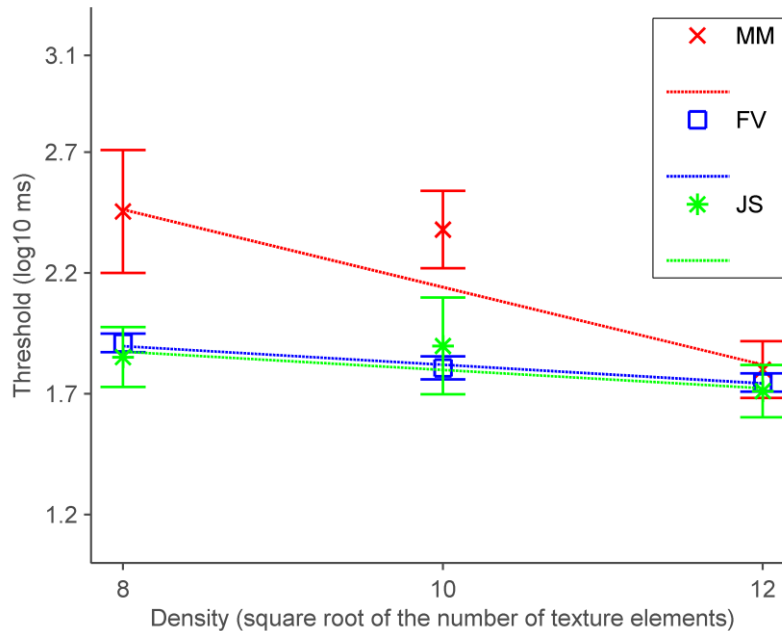


Figure 3.4. Binocular noise-masked orientation-defined texture segmentation: the best-fitting values of threshold exposure duration ( $\alpha$ ) for each texture density are shown for observers MM, FV and JAS. Error bars show the standard error of the best-fitting parameter values and were determined with a parametric bootstrap. Delta ( $\delta$ ) was 2%. Linear fits of  $\alpha$  to each observer's data for increasing texture density are shown by the dotted lines.

### 3.3.2 The effect of texture density on texture segmentation


The effect of texture density on dichoptic orientation-defined texture segmentation (Experiment 1.1) and binocular orientation-defined texture segmentation (Experiment 1.2) were tested with the generalised likelihood ratio. The null hypothesis is the nested model in which the best-fitting parameter values for  $\alpha$ , or  $\delta$ , are equal and unchanged for all texture densities with log-likelihood values  $\ln l_0$  given for each observer in Table 3.1. Log-likelihood values  $\ln l$  are given for the hypothesis texture density linearly affected threshold exposure duration  $\alpha$  (Eq.4, Model variants, page 51) or asymptote  $1-\delta$  (Eq.5, Model variants, page 51).

The critical value for  $2(\ln l - \ln l_0)$  is 8.62, when the critical region of 0.05 is corrected for 15 applications ( $0.05/15 = 0.003$ ) and the nested model has one fewer free parameters. Given a critical value of 8.62, the log-likelihood ratio tests given in Table 3.1 for dichoptic-overlapping stimuli support an effect of texture density on asymptote ( $1-\delta$ ). The results for all of the observers show asymptote improves with denser texture elements (Figure 3.2). Results do not support an effect of texture density on threshold exposure duration ( $\alpha$ ) for dichoptic-overlapping stimuli ( $p > .05$ ; table 3.1). For dichoptic-nonoverlapping stimuli, the log-likelihood ratio tests (Table 3.1) support an effect of texture density on threshold exposure duration ( $\alpha$ ). The results for all of the observers show threshold improves with denser texture elements (Figure 3.2). Results do not support an effect of texture density on asymptote ( $1-\delta$ ) for dichoptic-nonoverlapping stimuli ( $p > .05$ ; table 3.1).

Experiment 1.2: for binocular noise-masked orientation-defined segmentation, the log-likelihood ratio tests (Table 3.1) do not support an effect of texture density on threshold exposure duration ( $\alpha$ ). Prior to correcting the critical region of 0.05 for 15 applications, an effect of texture density on binocular noise-masked orientation-defined segmentation was supported only for observer MM.

Dichoptic-overlapping	Observer	k	LL		LL ratio	P value
Linear fit of alpha ( $\alpha$ ), Beta ( $\beta$ ) & delta ( $\delta$ ) vary freely for each density	MM	8	lnl	-442.3		
	AJ	8	lnl	-723.5		
	JS	8	lnl	-278.5		
Alpha ( $\alpha$ ) is constrained, Beta ( $\beta$ ) & delta ( $\delta$ ) vary freely for each density	MM	7	lnl <sub>0</sub>	-444.1	3.6	0.06
	AJ	7	lnl <sub>0</sub>	-724.4	1.8	0.18
	JS	7	lnl <sub>0</sub>	-280.1	3.1	0.08
Linear fit of delta ( $\delta$ ), Alpha ( $\alpha$ ) & beta ( $\beta$ ) vary freely for each density	MM	8	lnl	-440.6		
	AJ	8	lnl	-724.2		
	JS	8	lnl	-278.5		
Delta ( $\delta$ ) constrained, Alpha ( $\alpha$ ) & beta ( $\beta$ ) vary freely for each density	MM	7	lnl <sub>0</sub>	-455.7	30.1	$p < .001$
	AJ	7	lnl <sub>0</sub>	-736.6	24.9	$p < .001$
	JS	7	lnl <sub>0</sub>	-283.4	9.8	0.002
Dichoptic-nonoverlapping	Observer	k	LL		LL ratio	P value
Linear fit of alpha ( $\alpha$ ), Beta ( $\beta$ ) & delta ( $\delta$ ) vary freely for each density	MM	8	lnl	-447.7		
	AJ	8	lnl	-712.9		
	JS	8	lnl	-493.6		
Alpha ( $\alpha$ ) is constrained, Beta ( $\beta$ ) & delta ( $\delta$ ) vary freely for each density	MM	7	lnl <sub>0</sub>	-457.4	19.4	$p < .001$
	AJ	7	lnl <sub>0</sub>	-719.7	13.7	$p < .001$
	JS	7	lnl <sub>0</sub>	-498.2	9.2	0.002
Linear fit of delta ( $\delta$ ), Alpha ( $\alpha$ ) & beta ( $\beta$ ) vary freely for each density	MM	8	lnl	-447.5		
	AJ	8	lnl	-712.9		
	JS	8	lnl	-493.4		
Delta ( $\delta$ ) constrained, Alpha ( $\alpha$ ) & beta ( $\beta$ ) vary freely for each density	MM	7	lnl <sub>0</sub>	-447.7	0.3	0.61
	AJ	7	lnl <sub>0</sub>	-713.3	0.7	0.39
	JS	7	lnl <sub>0</sub>	-493.7	0.6	0.44
Binocular noise-masked	Observer	k	LL		LL ratio	P value
Linear fit of alpha ( $\alpha$ ), Beta ( $\beta$ ) varies freely for each density. Delta ( $\delta$ ) is fixed 0.02	MM	5	lnl	-360.0		
	FV	5	lnl	-655.3		
	JS	5	lnl	-677.7		
Alpha ( $\alpha$ ) is constrained, Beta ( $\beta$ ) varies freely for each density. Delta ( $\delta$ ) is fixed 0.02	MM	4	lnl <sub>0</sub>	-362.1	4.1	0.04
	FV	4	lnl <sub>0</sub>	-656.6	2.6	0.11
	JS	4	lnl <sub>0</sub>	-678.2	1.0	0.31

Table 3.1. Statistics. The generalised likelihood ratio,  $2(\ln l - \ln l_0)$ , shown as LL ratio, tested the null hypothesis where  $\ln l$  and  $\ln l_0$  are the log-likelihoods (LL) for a maximum likelihood fit to observer data for the model for a linear fit of  $\alpha$ , or  $\delta$ , to all texture densities and the model for which  $\alpha$ , or  $\delta$ , is unchanged for all texture densities respectively.  $k$  is the number of free parameters for each model; models differ in 1 degree of freedom. The critical value from the chi-squared distribution for  $2(\ln l - \ln l_0)$  is 8.62 when the critical region of 0.05 is corrected for 15 applications ( $0.05/15 = 0.003$ ). P values (determined from the chi-squared distribution for LL

ratio values) are also given and are shaded as  =  $p \leq .003$ , or, unshaded =  $p > .05$ .

### 3.4 Discussion

The purpose of Experiment 1.1 was to determine whether the critical variable for the difference between Kolb and Braun's and Wolfe and Franzel's results was the density of orientation-defined, dichoptic-overlapping texture elements. Prior to discussing the effect of texture density on orientation-defined, inverse cyclopean texture segmentation, performances for orientation-defined dichoptic-overlapping and binocular displays are compared. Even if mechanisms for orientation-defined texture segmentation did not have access to monocular input, performance might exceed chance with putative dichoptic-overlapping (inverse cyclopean) texture boundaries if a failure of binocular fusion rendered those textures effectively nonoverlapping (Howard, 2002). Therefore, performance for the dichoptic-overlapping task (Figure 3.2) was compared with performance for the binocular-nonoverlapping task (Figure 3.3) for which orientation-defined, nonoverlapping texture elements were optically fused. For all of the observers, performances for the dichoptic-overlapping task were better than performances for the binocular-nonoverlapping task, for which performances were chance, when texture density was 12 x 12. In brief durations, for observers MM and AJ performances for the dichoptic-overlapping task were better than performances for the the binocular-nonoverlapping task when texture density was 8 x 8; thresholds for the dichoptic-overlapping task (50 and 130 ms respectively) were lower than thresholds for the binocular-nonoverlapping task (980 ms and >1.2 seconds respectively). However, for JS, thresholds for the dichoptic-overlapping and binocular-nonoverlapping tasks were approximately the same (400 ms) when texture density was 8 x 8. Therefore, performances for the dichoptic-overlapping task cannot be wholly attributed to a failure of binocular fusion. Hering observed that dichoptic-overlapping stimuli were optically fused in brief durations (Hering 1874; Dawson, 1913). However, Kolb and Braun (1995) found that orientation-defined texture segmentation based on the monocular image is visible in brief durations. The exposure duration for Kolb and Braun's dichoptic-overlapping display was 250 ms; this exposure duration is shown by the gray line in Figure 3.2 (second row). We found that threshold for the dichoptic-overlapping task was less than 250 ms for all of the observers, regardless

of texture element density; except for JS for which threshold was 400 ms and was undetermined when texture density was 8 x 8 and 10 x 10 respectively. Since performances were chance for the binocular-overlapping task and exceeded chance in brief 250 ms durations for the dichoptic-overlapping task, orientation-defined, dichoptic-overlapping texture elements cannot be optically fused in brief durations.

Texture elements within Kolb and Braun's and Wolfe and Franzel's dichoptic-overlapping stimuli competed for the same retinal position. However, orientation-defined texture segmentation might occur when a large error in vergence rendered dichoptic-overlapping texture elements effectively nonoverlapping. We found that both orientation-defined dichoptic-overlapping and dichoptic-nonoverlapping texture segmentation were better when texture elements were dense (12 x 12); Figure 3.2 and Table 3.1. This implies that orientation-defined, dichoptic texture segmentation does not depend on texture elements that compete for the same retinal position. Whilst threshold improved with denser texture elements when those elements were nonoverlapping, threshold did not improve when texture elements were overlapping. Moreover, whilst asymptote did not improve with denser texture elements when those elements were nonoverlapping, asymptote did improve with denser texture elements when those elements were overlapping. This implies that performances for orientation-defined, inverse cyclopean texture segmentation cannot be wholly attributed to a large error in vergence.

Orientation-defined, inverse cyclopean visual search is impossible (Wolfe & Franzel, 1988). Even though the largest set-size for Wolfe and Franzel's dichoptic-overlapping stimulus was 8 texture elements that were spaced evenly on a circle around fixation, texture density was sparse. We found that when texture density was 8 x 8, performance for the dichoptic-overlapping task was poor for all of the observers; however, the task was possible (Figure 3.2). Orientation-defined texture segmentation based on the monocular image does occur, even when texture segmentation is impossible in the optically fused image (Kolb & Braun, 1995). For Kolb and Braun's dichoptic-overlapping stimulus, texture elements occupied positions on a 20 x 20 notional grid; texture elements were dense. We found that performances for the dichoptic-overlapping task improved when texture elements were denser (12 x 12); Figure 3.2. Orientation-defined, inverse cyclopean texture segmentation was better when texture elements were dense; therefore, the critical



difference between Kolb and Braun's (1995) and Wolfe and Franzel's (1988) experiments may be texture density.

## **Experiment 2: Is orientation-defined, inverse cyclopean texture segmentation affected by an effective contrast imbalance?**

### 4.1 Introduction

An imbalance in the inputs from the two eyes may cause sensory dominance and suppression and, as a result, impede binocular processing (Howard, 2002). A recent paradigm restores binocularity in Amblyopes by balancing the inputs from the two eyes (Baker, Meese & Hess, 2008; Hess, Mansouri & Thompson, 2010; Hess, Mansouri & Thompson, 2011). In this paradigm, interocular suppression from the fellow eye is reduced using a ratio of interocular luminance contrast termed the balance-point. Although observers in Experiment 1.1 were not Amblyopes, it is possible that differences in the effective luminance contrast of the stimuli in the two eyes contributed to detection of the target in a dichoptic-overlapping stimulus. If imperfect binocular integration were to arise from an effective contrast imbalance between the two eyes, the target within a dichoptic-overlapping stimulus might be visible in the optically fused percept and be detected by mechanisms that exist at a binocular stage of processing. Consistent with this possibility was a pilot study in which perfect pop-out was found for a suppressing Amblyope in the absence of a balance point.

In the following experiment, pop-out was measured when luminance contrast was 100%, with no interocular difference, and for different ratios of interocular luminance contrast. The ratio of interocular luminance contrast required to reduce performance to chance, the balance-point, was found for each observer. Very brief exposure durations were used to keep performance below the ceiling of 100%.

### 4.2 Methods: Experiment 2

A sparse 8 x 8 grid of Gabor textures contained an orientation-defined target viewed with central fixation (Figure 4.1). The sparse 8 x 8 grid was tested since this grid was used in Experiment 1.1 and in subsequent experiments. In the following experiment, the viewing distance was increased from 1 m to 3 m. The sparse grid was viewed from an increased distance of 3 m on the grounds that differences in

the two eyes would have a greater effect on target detection, for example, loss of higher spatial frequencies caused by an astigmatism or anisometropia would increase as distance increased. Anisometropia is impaired visual acuity due to unequal refractive errors in the two eyes. For each Gabor stimulus (Eq. 1, Experimental procedure and stimuli, page 45), sigma was 0.07 degrees of visual angle and wavelength was 0.21 degrees; spatial frequency was 4.85 cycles per degree.

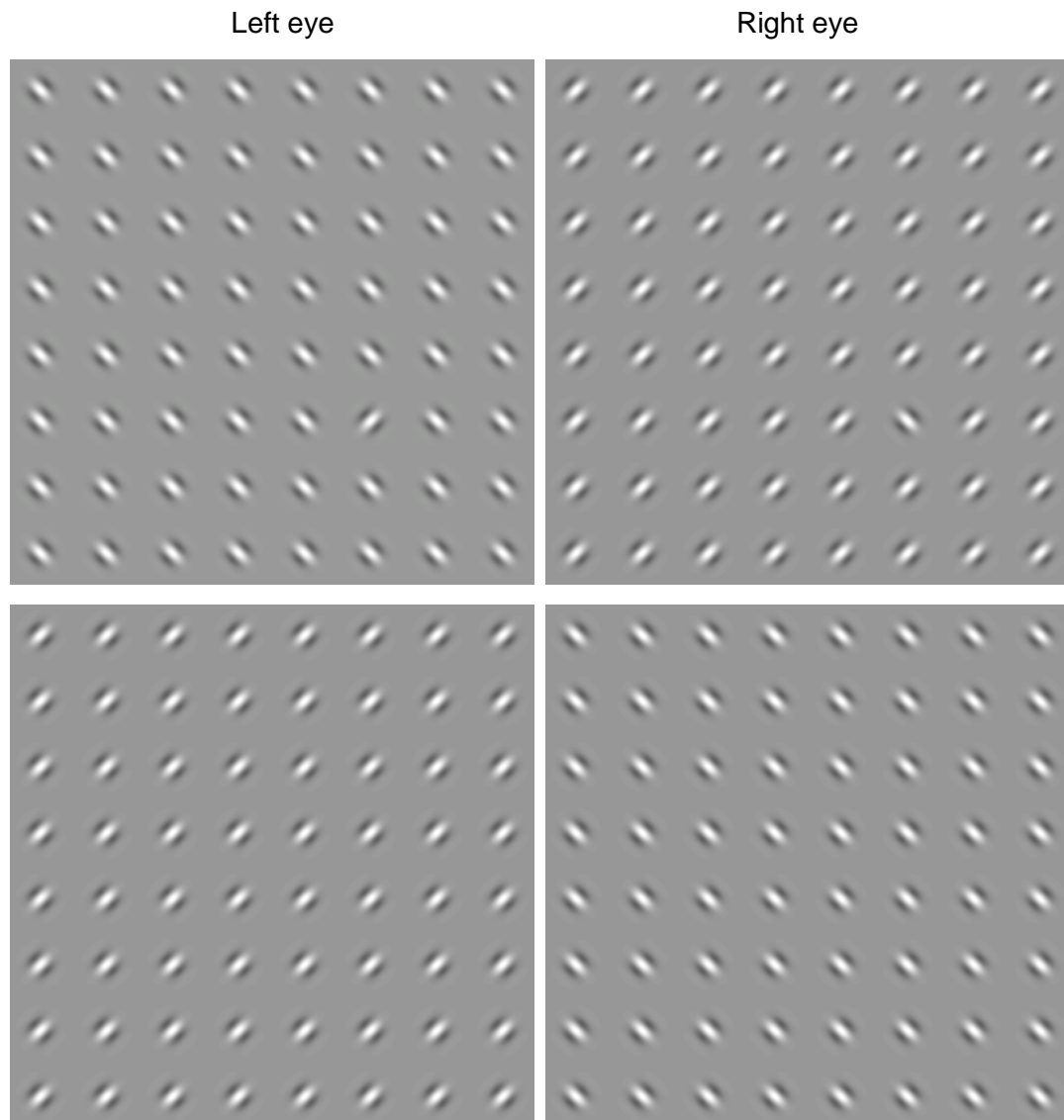


Figure 4.1. Example stimuli: an 8 x 8 grid of Gabor stimuli for each of the two eyes showing an orientation-defined target viewed with central fixation (top row, left and right panels) from a distance of 3m. The other interval of a two alternative forced choice procedure (2-AFC) contained distractors only (second row, left and right panels). The luminance contrast of each image is equal for illustration.

#### 4.2.1 Determining the balance-point

Pop-out performance was initially measured for each observer using a luminance contrast of 100% for which there was no interocular difference. Very brief durations were used for performance to be within a 60% to 65% range, where chance is 50%. The exposure durations for which performance was within this range were 66 ms for observers AJ and KM and 92 ms for JM. To find the balance-point, these exposure durations were used to measure pop-out performance for four ratios of interocular luminance contrast. For each block, luminance contrast was either 80% or 60%, differing in 20% increments, while the contralateral eye had a fixed luminance contrast of 100%. This method ensured that each ratio was tested twice, once for each of the two eyes. The balance-point is the ratio for which observer performance was at chance. To generate stimuli for each ratio, the luminance contrast of each Gabor stimulus within the image for the left or right eye was manipulated while mean image luminance was maintained constant. The sequence of blocks was randomised prior to the experiment in order to control for effects of variables extraneous to luminance contrast.

#### 4.2.2 Dichoptic nonius procedure: Experiment 2

Prior to every trial, observers performed the dichoptic nonius procedure given in Figure 4.2. Since the target was viewed with central fixation, the location of the centre of both the nonius dot and the target was equal within the display. To minimise forward-masking the target, the nonius procedure was absent for 250ms prior to the trial. During the trial the nonius lines and fixation point were absent. Nonius line height and width scaled with viewing distance in order to subtend 0.3 and 0.06 degrees of visual angle respectively and lines were separated by 0.09 degrees of visual angle.

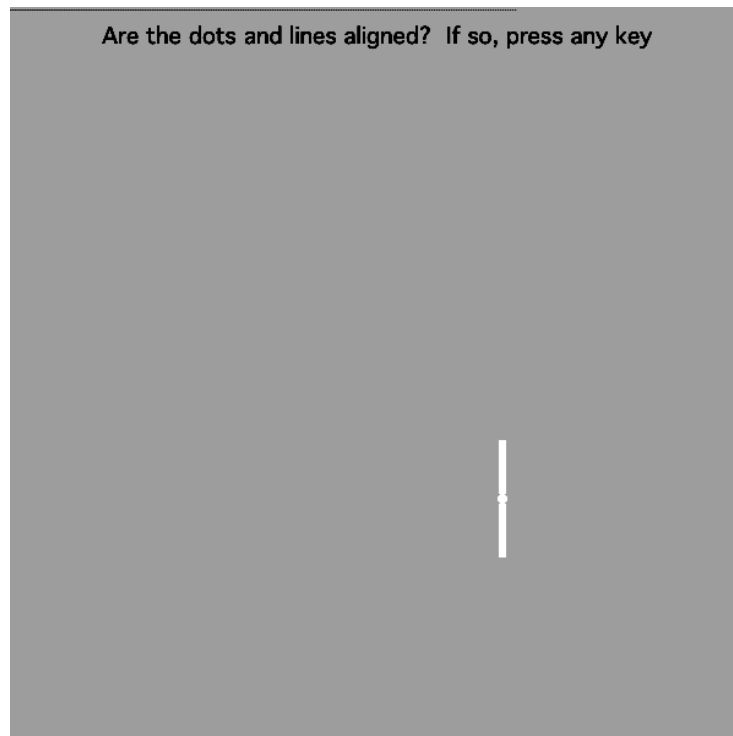
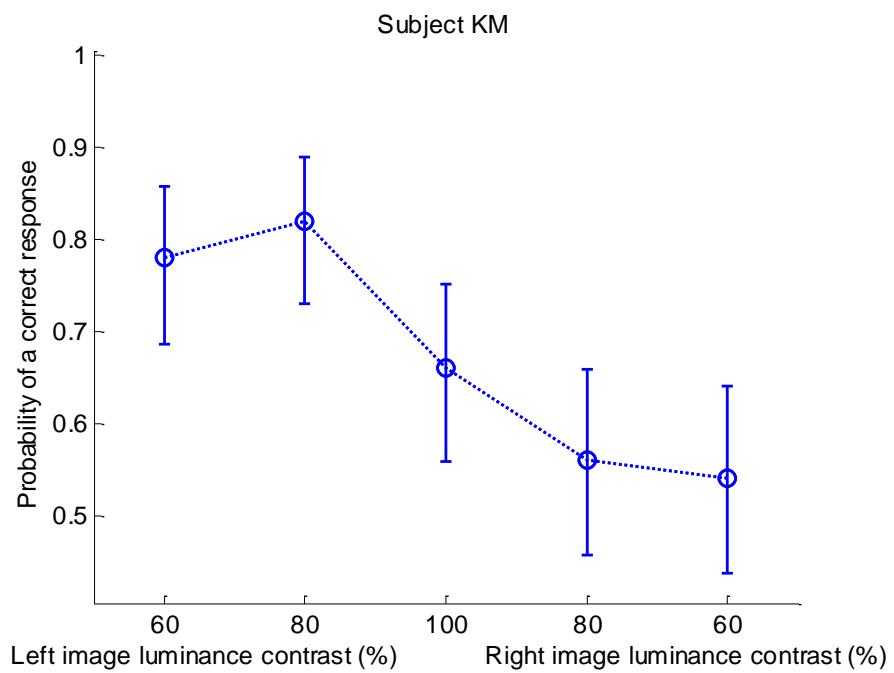
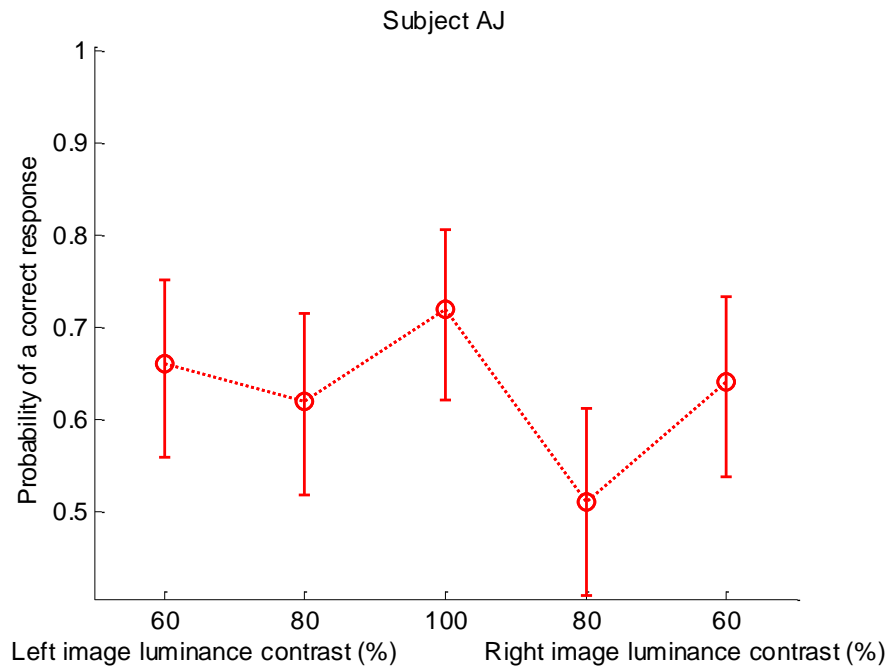


Figure 4.2. Dichoptic nonius procedure showing a dot and a line per eye as horizontally aligned. The location of aligned nonius dots served as the fixation point for a target viewed with central fixation.

#### 4.3 Results of Experiment 2

The results in Figure 4.3 show the performance for each observer with each ratio of interocular luminance contrast. The number of trials was 100 per block for each ratio.



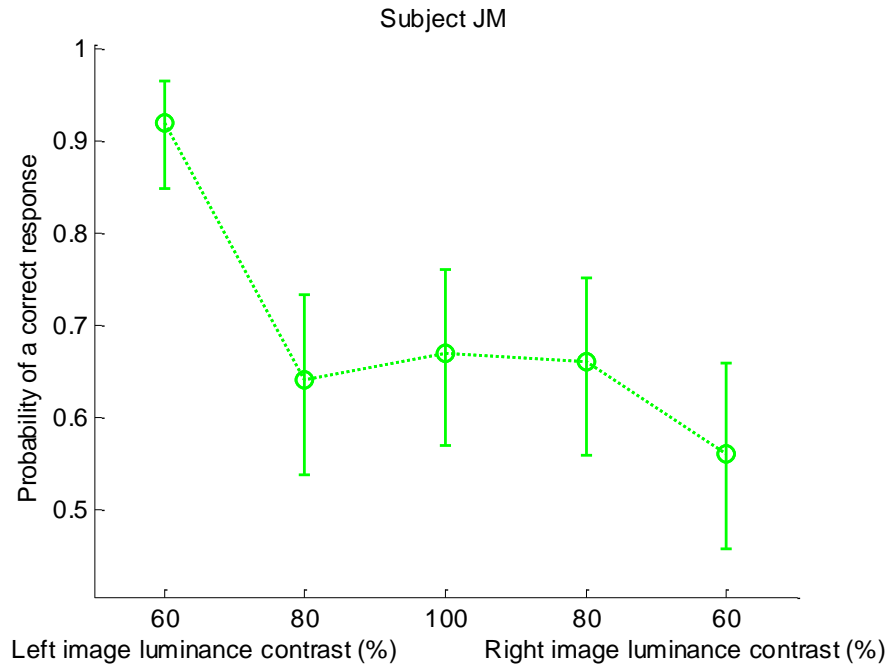


Figure 4.3. Results for observers AJ, KM and JM show the probability of correctly identifying the target with each ratio of interocular luminance contrast when the contralateral eye's image was fixed at 100% luminance contrast. Error bars show 95% confidence intervals.

The results for all three observers suggest that performance was poorest when the luminance contrast of the right eye's image was reduced. For observer AJ, performance was above chance unless the luminance contrast of the right eye's image was reduced to 80% for which performance was chance (51%). Performance decreased with every 20% reduction in luminance contrast of the right eye's image for KM; when the right eye's image was reduced to 70%, pop-out was equated as performance was chance (53%). For observer JM, luminance contrast reduction of the right eye's image had a strong effect on performance; performance was chance (56%) when the right eye's image was reduced to 60%. A fixed luminance contrast of 80%, 70% and 60% for the right eye's image with 100% for the contralateral eye's image for observers AJ, KM and JM respectively was indicative of the ratio required to equate the likelihood of pop-out. These ratios were the balance-points for the observers for which performance was chance.

#### 4.4 Discussion

This experiment investigated whether pop-out in dichoptic-overlapping textures might in part be due to imperfect binocular integration arising from effective contrast differences between the eyes. One source of this may be individual differences between the observer's two eyes. Another might be differences in luminance transmission between the goggle shutters. Each shutter effectively acts a neutral density filter through which dichoptic stimulus frames are viewed. Alternatively, even-numbered alternate frames might be dichoptically masked until the final stimulus frame in which the right image is unmasked. Since performance was above chance at ratios other than the balance-point, the results show an imbalance in luminance contrast input from the two eyes causes the target to be detected at the very brief durations used. This implies that an orientation-defined target within the dichoptic-overlapping stimulus that was used in Experiment 1.1 might pop-out if there were an imbalance in luminance contrast input from the two eyes.

The method of equating effective contrast between the eyes (Baker, Meese & Hess, 2008; Hess, Mansouri & Thompson, 2010; Hess, Mansouri & Thompson, 2011; Huang, Zhou, Lu & Zhou, 2011) was used to balance the inputs from the two eyes. In the context of amblyopia, interocular suppression from the fellow eye has been found for strabismic amblyopia and anisometropic amblyopia. For strabismic amblyopia, in which the two eyes are misaligned, finding the balance-point of interocular luminance contrast sensitivity has been shown to normalise luminance contrast sensitivity of the dominant eye and support binocular visual processing (Baker, Meese & Hess, 2008; Hess, Mansouri & Thompson, 2010; Hess, Mansouri & Thompson, 2011). Also in the context of interocular suppression, increased noise in the amblyopic eye as well as signal attenuation has been shown (Baker, Meese & Hess, 2008). For anisometropic amblyopia both monocular attenuation by the fellow eye and an interocular deficit was found (Huang, Zhou, Lu & Zhou, 2011). However, interocular suppression was later implicated to be an unlikely mechanism for therapeutic recovery in amblyopia (Vedamurthy, Nahum, Bavelier & Levi, 2015). Moreover, perceptual learning for a monocular contrast detection task improved binocular function for anisometropic amblyopia for which both contrast sensitivity and visual acuity improved. Interestingly, both trained and untrained contrast sensitivities at broader band spatial frequencies were improved (Chen, Li, Liu, Cai, Yuan, Deng & Yu, 2016).



The differences in effective contrast between the two eyes found in this experiment and the findings discussed above for Amblyopia suggest that changes in sensitivity are a critical aspect of the underlying sensory processes. Thus, differences in interocular sensitivity exist for observers with normal or with corrected visual acuity and no pre-existing history of amblyopia as well as in anisometropic amblyopia and strabismic amblyopia. The balance-point for each observer equates differences in effective luminance contrast.

In the following experiments (Experiments 3, 4 and 5), attempts were made to equalise a difference in effective contrast between the two eyes using the balance-points determined from this experiment. A limitation of the current study is that the balance-points were measured for a single exposure duration, rather than for each of the durations that were used in the following experiments. Specifically, the balance-points were measured when exposure duration was 66 ms (for observers AJ and KM) or 92 ms (for observer JM). However, the exposure durations in Experiments 3, 4 and 5 were 16, 50, 150, 450 and 1350 ms. Another limitation is that the balance-points were measured for a single spatial frequency (4.85 cycles per degree); observers viewed the texture elements from 3 m. However, the spatial frequency for the texture elements that were used in Experiments 3, 4 and 5 was lower (1.62 cycles per degree); observers viewed the texture elements from 1 m. Furthermore, spatial frequency decreased from 1.62 to 1.08 cycles per degree in Exp. 4. It cannot be assumed that the balance-points found in Exp. 2 were valid for the stimuli in Experiments 3, 4 and 5.

### **Experiment 3: The effect of texture density on inverse cyclopean texture segmentation**

#### **5.1 Introduction**

We found that orientation-defined, inverse cyclopean texture segmentation was poor when texture elements were sparse (8 x 8) and improved when texture elements were dense (12 x 12); Exp. 1.1. However, the target in a dichoptic-overlapping stimulus can pop-out due to interocular differences in effective luminance contrast (Exp. 2). The purpose of the following experiment was to test the effect of texture density on orientation-defined, inverse cyclopean texture segmentation when the balance-points were used to equalise a difference in effective contrast between the two eyes. The balance-points that were determined in Exp. 2 were used in this experiment. However, it cannot be assumed that the balance-points found in Exp. 2 were valid for the stimuli in this experiment (further details are given in Exp. 2; Discussion, page 79).

#### **5.2 Methods: Experiment 3**

In this experiment, the observers viewed dense (12 x 12) and sparse (8 x 8) Gabor stimuli covering an equal unit area. Viewed from 1 m, texture separation was 1.24 and 1.86 degrees of visual angle respectively. The dichoptic-overlapping stimuli are shown in Figure 5.1. The contrasts of the stimuli for the two eyes were the contrasts for the balance-point that was determined for each of the three observers in Exp. 2. Texture segmentation was measured when texture elements were dense (12 x 12) and sparse (8 x 8). Two, of the eight Latin square, conditions were for texture densities of 12 x 12 and 8 x 8. These conditions also served to establish 'benchmark' segmentation performance with respect to performance in subsequent experiments.

For each Gabor stimulus (Eq. 1, Experimental procedure and stimuli, page 45), sigma was 0.21 and wavelength was 0.62 degrees of visual angle; spatial frequency was 1.62 cycles per degree.

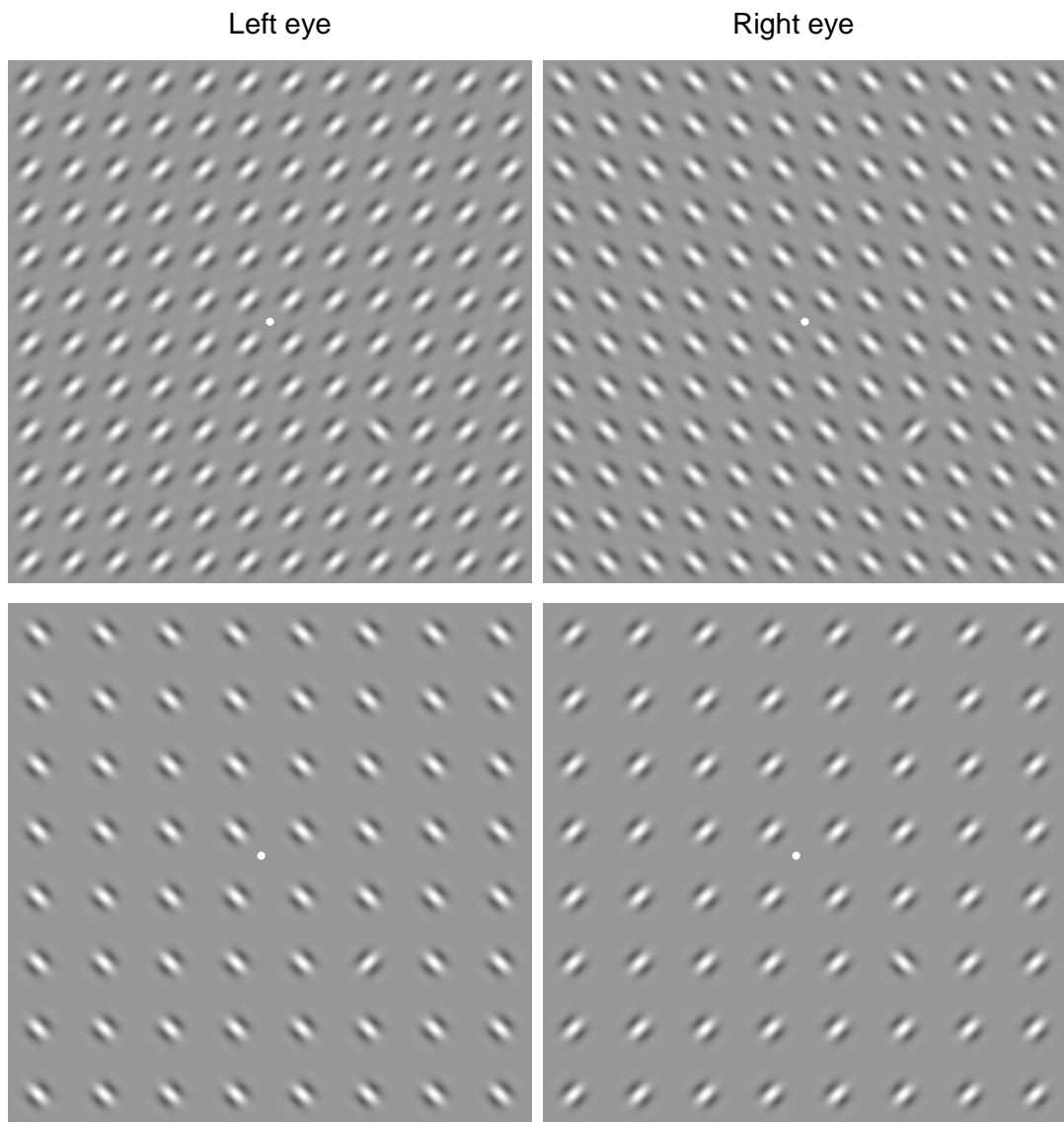


Figure 5.1. 12 x 12 (first row) and 8 x 8 (second row) Gabor textures covered an equal unit area in dense and sparse textures respectively. Each image for the two eyes (left and right panels) is 100% luminance contrast for illustration.

### 5.2.1 Nonius procedure: Experiment 3

The following method maintained the orientation-defined target at 4.3 degrees of visual angle from fixation in Cartesian quadrant IV of the display. The nonius dot was in the centre of the display prior to each trial for dense 12 x 12 stimuli, however, the nonius dot location differed prior to each trial for 8 x 8 stimuli in order for the target to be an equal visual angle from fixation. This method maintained grid scale, alternatively, varying target position would not have conserved texture scale. The nonius procedure for 8 x 8 stimuli is shown in Figure 5.2.

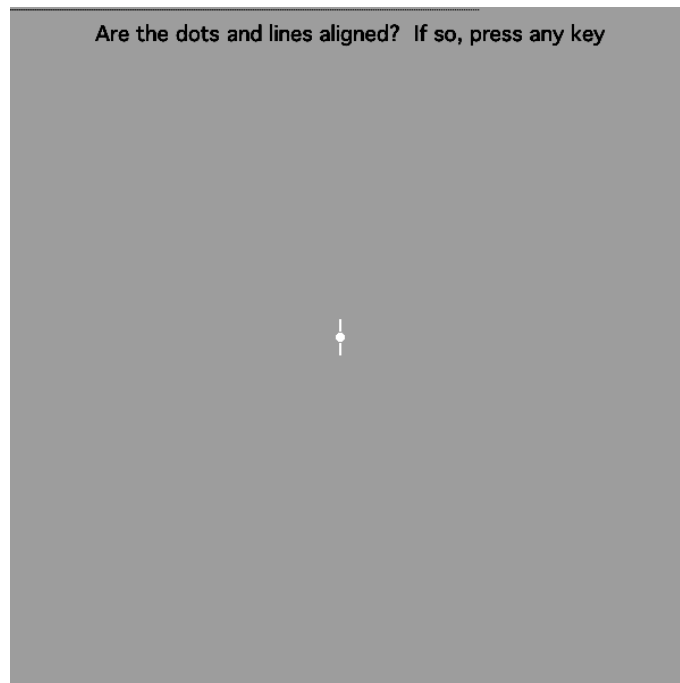


Figure 5.2. Dichoptic nonius procedure for 8 x 8 stimuli showing a dot and a line per eye as horizontally aligned.

### 5.3 Results of Experiment 3

Results for all observers show that performance was poorer when texture elements were sparse (8 x 8). The psychometric functions given in Figure 5.3 illustrate segmentation for sparse 8 x 8 and dense 12 x 12 stimuli. For dense stimuli the number of trials was 550, 400 and 500 while for sparse stimuli the number of trials was 500, 400 and 500 for observers AJ, KM and JM respectively. Asymptote (1- $\delta$ ) and threshold exposure duration ( $\alpha$ ) for each texture density and observer are shown in Figure 5.4.

The effect of texture density on segmentation performance was tested with the generalised likelihood ratio. The null hypothesis is the nested model in which the best-fitting parameter values for delta ( $\delta$ ), or alpha ( $\alpha$ ), are equal and unchanged with texture density. The alternative hypothesis is asymptote (1- $\delta$ ), or threshold exposure duration ( $\alpha$ ), is dependent on texture density.

Given a critical value for  $2(\ln l - \ln l_0)$  of 6.96, where the critical region is 0.05, corrected for 6 applications when the nested model has one fewer free parameters, the log-likelihood ratio tests given for each observer in Table 5.1 support an effect of texture density on asymptote. Results do not support an effect of texture density on threshold exposure duration ( $p > .05$ ; table 5.1).

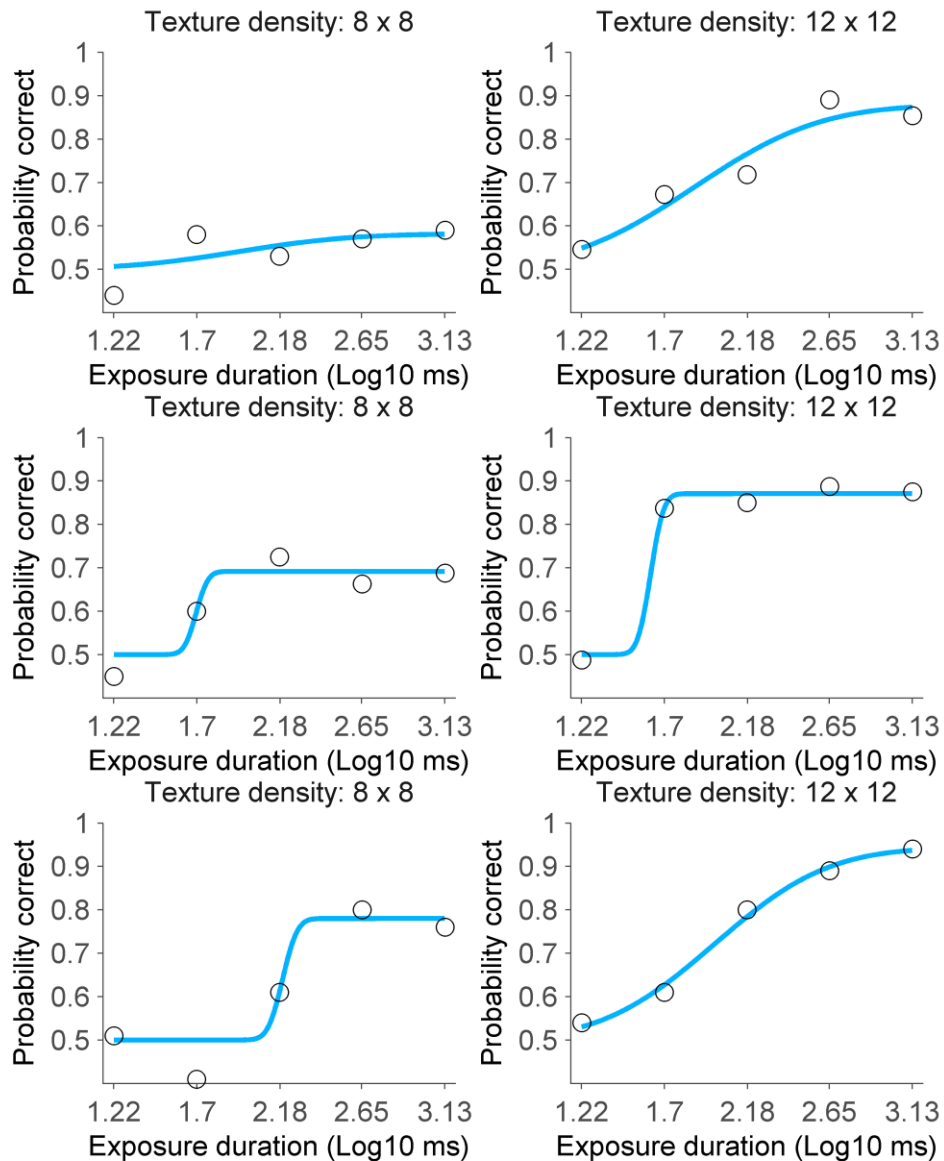


Figure 5.3. Psychometric functions for observers AJ (top row), KM (second row) and JM (third row) show the probability of a correct response at logarithmically spaced exposure durations. The density of texture elements was 8 x 8 (all left panels) and 12 x 12 (all right panels).

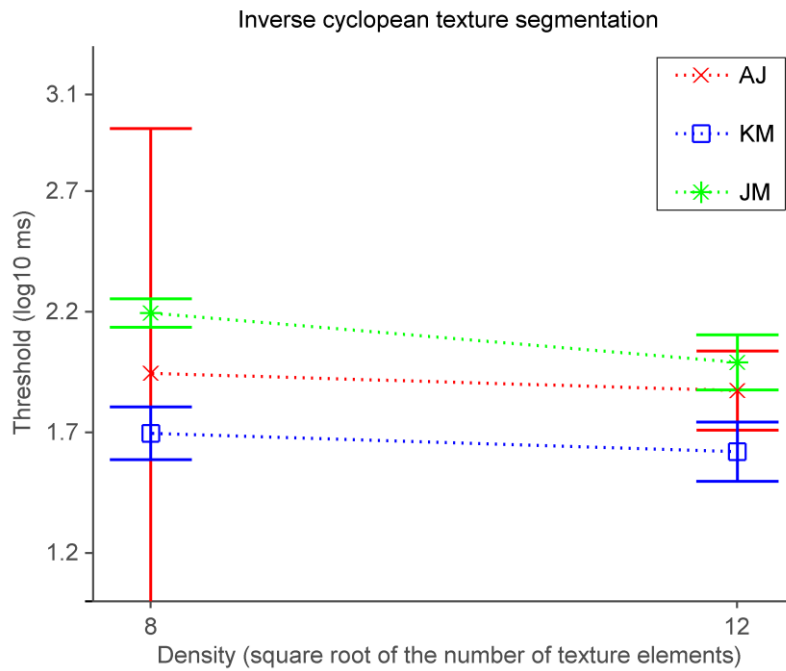
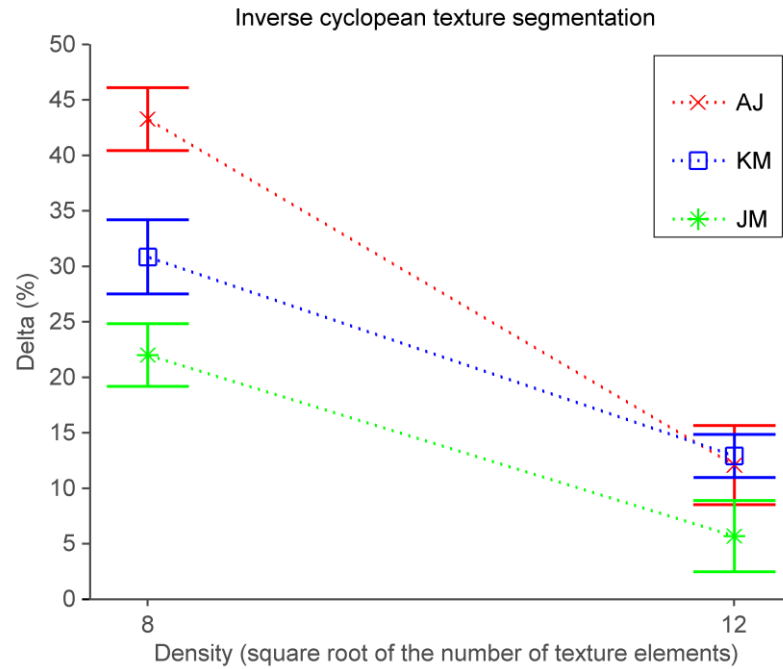


Figure 5.4. The best-fitting values for and delta ( $\delta$ ) and threshold exposure duration ( $\alpha$ ) or each texture density and each observer. Error bars show the standard error of the best-fitting parameter values determined with a non-parametric bootstrap.

Model	Observer	k	LL		LL ratio	P value
Alpha ( $\alpha$ ), Beta ( $\beta$ ) and delta ( $\delta$ ) vary freely for each texture density	AJ	6	lnl	-639.6		
	KM	6	lnl	-440.9		
	JM	6	lnl	-554.4		
Alpha ( $\alpha$ ) is constrained, Beta ( $\beta$ ) & delta ( $\delta$ ) vary freely for each texture density	AJ	5	lnl <sub>0</sub>	-640.4	1.5	0.22
	KM	5	lnl <sub>0</sub>	-440.9	0.0	1.00
	JM	5	lnl <sub>0</sub>	-555.2	1.8	0.18
Delta ( $\delta$ ) is constrained, Alpha ( $\alpha$ ) & beta ( $\beta$ ) vary freely for each texture density	AJ	5	lnl <sub>0</sub>	-668.4	57.4	$p < .001$
	KM	5	lnl <sub>0</sub>	-453.6	25.5	$p < .001$
	JM	5	lnl <sub>0</sub>	-562.5	16.2	$p < .001$

Table 5.1. Statistics. The critical value from the chi-squared distribution for  $2(\ln l - \ln l_0)$  is 6.96 when the critical region of 0.05 is corrected for 6 applications ( $0.05/6 = 0.008$ ). P values:  =  $p \leq .008$ , or, unshaded =  $p > .05$ .

#### 5.4 Discussion

Orientation-defined, inverse cyclopean texture segmentation was better when texture elements were dense (12 x 12) than when texture elements were sparse (8 x 8). It cannot be assumed that the balance-points found in Exp. 2 were valid for the stimuli in this experiment. Furthermore, pop-out was perfect for a suppressing Amblyope in the absence of a balance point when texture elements were dense (12 x 12). These findings imply orientation-defined, inverse cyclopean texture segmentation might depend on a difference in effective contrast between the two eyes. If there were a difference in effective contrast between the two eyes, the target within a dichoptic-overlapping stimulus might be visible in the optically fused percept. Binocular orientation-defined texture segmentation is trivially easy regardless of element density (Nothdurft, 1985; Nothdurft, 1990). However, poorer performances when texture elements were sparse (8 x 8) than when those elements were dense (12 x 12) are inconsistent with trivially easy texture segmentation. Moreover, although performances for observers with no pre-existing history of amblyopia were expected to be imperfect, their reductions in asymptote ( $1-\delta$ ) seem inconsistent with trivially easy texture segmentation. This might suggest that orientation-defined, inverse cyclopean texture segmentation cannot be wholly attributed to an effective contrast difference between the two eyes. Nonetheless, the results suggest that the critical difference between Kolb and Braun's (1995) and Wolfe and Franzel's (1998) results for segmentation might be texture density.

## **Experiment 4: Does a smaller inter-element space affect orientation-defined, inverse cyclopean texture segmentation?**

### **6.1 Introduction**

Inverse cyclopean texture segmentation was better when texture elements were dense (12 x 12) than when those elements were sparse (8 x 8) and covered the same area; Exp 1.1 and Exp. 3. This might suggest that texture segmentation depends on the density of texture elements. Alternatively, texture segmentation might be better because the space between orientation-defined, dichoptic-overlapping boundaries was smaller when texture elements were dense than when those elements were sparse. Specifically, the inter-element space for the Gabor textures that were used in Exp. 3 was 3.03 times smaller when texture elements were dense (12 x 12) than when those elements were sparse (8 x 8). The inter-element space is the difference between the area covered by each notional grid and the area occupied by the texture elements within each grid. The area occupied by the texture elements within each grid was determined by assuming that the luminance of each Gabor texture was zero (i.e. equivalent to the mean luminance of the background) at 3 multiples of sigma ( $\sigma$ ). Further details are given in the methods section (6.2 Methods: Experiment 4). However, the effect of inter-element space on texture segmentation is confounded with the number of texture elements. This is because there were more texture elements within the dense grids (12 x 12) than there were within the sparse grids (8 x 8) that covered the same area. The purpose of the following experiment is to determine whether orientation-defined, inverse cyclopean texture segmentation is affected by a smaller inter-element space when the number of texture elements within the sparse (8 x 8) grid was held constant.

The trials for the sparse (8 x 8) grid of texture elements that were obtained for the observers in Exp. 3 were also used in this experiment. For Exp. 3's Gabor textures, sigma ( $\sigma$ ) and wavelength ( $\lambda$ ) were 0.21 and 0.62 degrees of visual angle respectively. Texture segmentation for these texture elements served as a benchmark for testing an effect of inter-element space on segmentation. In the following experiment, texture segmentation was measured when the inter-element space for the sparse (8 x 8) Gabor textures that were used in Exp. 3 was decreased



by increasing sigma ( $\sigma$ ) in four equal increments of 0.026 degrees. The area covered by the 8 x 8 notional grid remained constant. When sigma was 0.31 degrees, the inter-element space was the same as the inter-element space for the dense (12 x 12) Gabor textures that were used in Exp. 3. Moreover, to conserve the number of cycles per element for each Gabor texture that was used in Exp. 3, wavelength ( $\lambda$ ) was also increased in four equal increments of 0.077 degrees. The null hypothesis is that texture segmentation does not differ when the inter-element space is decreased by increasing sigma in four equal increments. The alternative outcome of the experiment is that texture segmentation is better when the inter-element space is smaller. This would imply that texture segmentation is dependent on orientation-defined texture boundaries that are closer together.

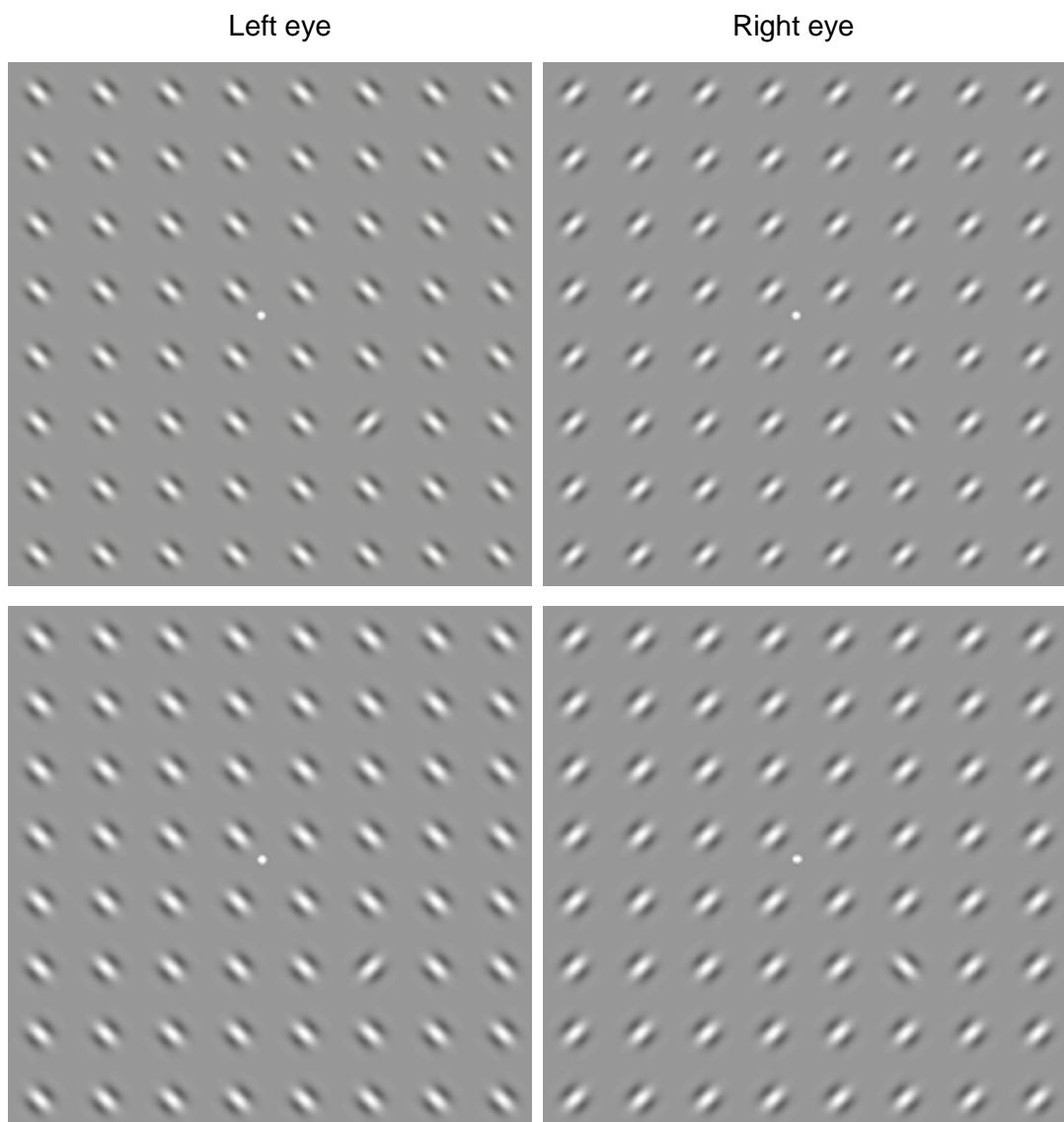
#### 6.2 Methods: Experiment 4

Observers viewed the sparse 8 x 8 grid from 1 m. The standard deviation of the Gaussian envelope, sigma ( $\sigma$ ), was the parameter that was increased to decrease the inter-element space (Eq. 1, Experimental procedure and stimuli, page 45). Moreover, to conserve the number of cycles per element, both sigma ( $\sigma$ ) and wavelength ( $\lambda$ ) were co-varied. For Exp. 3's Gabor textures, sigma ( $\sigma$ ) and wavelength ( $\lambda$ ) were 0.21 and 0.62 degrees of visual angle respectively. Spatial frequency was 1.62 cycles per degree. In the following experiment, texture segmentation was measured when sigma ( $\sigma$ ) and wavelength ( $\lambda$ ) for Exp. 3's Gabor textures were increased in four equal increments of 0.026 and 0.077 degrees of visual angle respectively. There were four conditions; a condition for each increment. Sigma ( $\sigma$ ) and wavelength ( $\lambda$ ) were increased linearly. Sigma was 0.232, 0.258, 0.284 or 0.309 and wavelength was 0.696, 0.773, 0.851 or 0.928 degrees respectively. Spatial frequency was 1.44, 1.29, 1.18 or 1.08 cycles per degree. The stimuli are shown in Figure 6.1.

The inter-element space for the sparse (8 x 8) Gabor textures that were used in Exp. 3 and for the sparse (8 x 8) Gabor textures that were used in the following experiment are given in Table 6.1. The inter-element space for the dense (12 x 12) Gabor textures that were used in Exp. 3 is also given. The area covered by the 8 x 8 and 12 x 12 notional grids was the same; 540 x 540 pixels. To determine the area occupied by all of the texture elements within each grid, the luminance of each

Gabor texture was assumed to be zero (i.e. equivalent to the mean luminance of the background) at 3 multiples of sigma ( $\sigma$ ).

The balance-points that were determined in Exp. 2 were used in this experiment. However, it cannot be assumed that the balance-points found in Exp. 2 were valid for the stimuli in this experiment (further details are given in Exp. 2; Discussion, page 79).



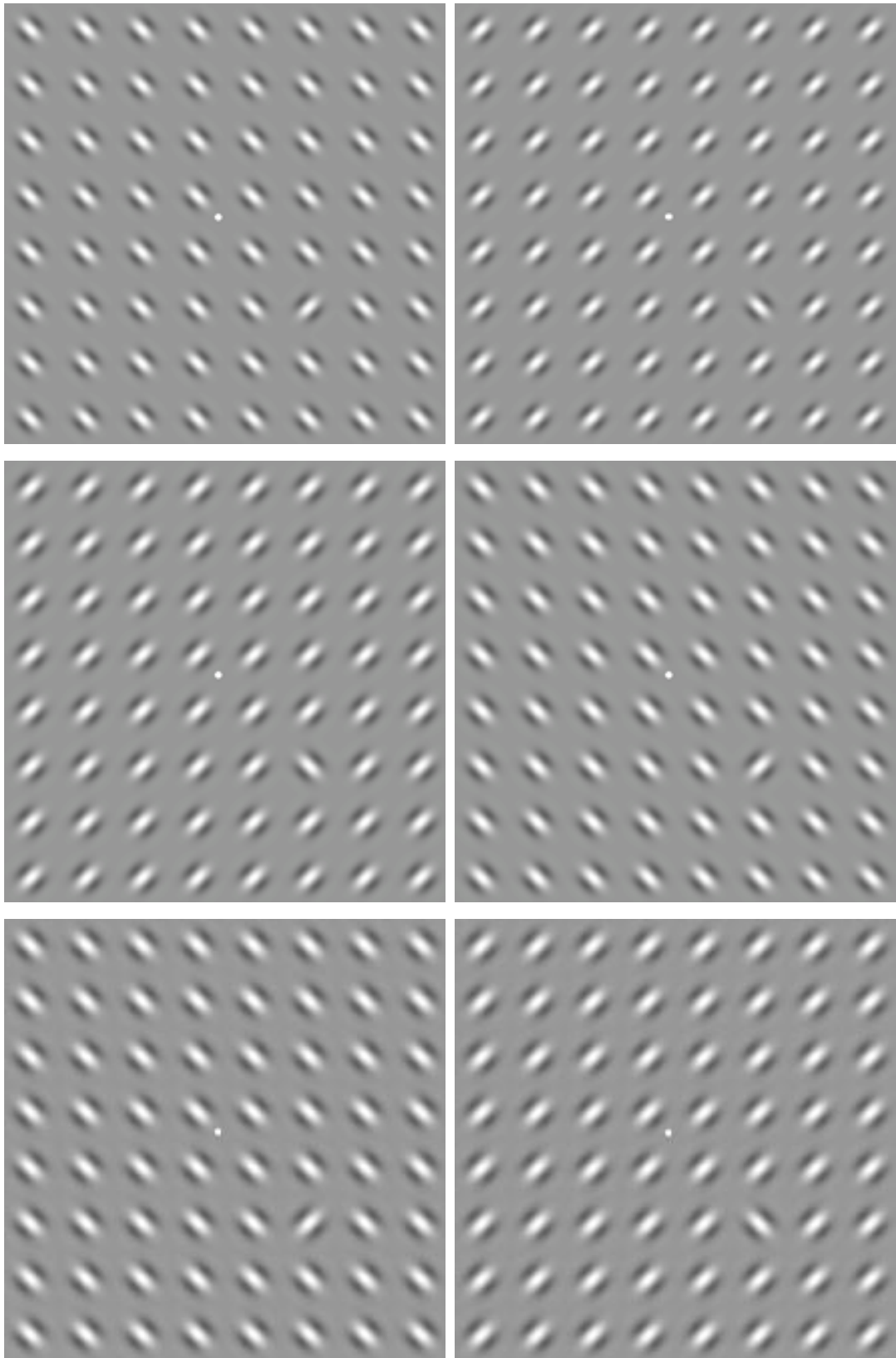


Figure 6.1. A grid of 8 x 8 Gabor textures within each image for the two eyes (left and right panels). Exp. 3's Gabor textures are shown in row 1; four equal increases in sigma ( $\sigma$ ) and wavelength ( $\lambda$ ) for those Gabor textures are shown in rows 2 to 5.

Experiment	3		4			
Texture density	12 x 12	8 x 8	8 x 8			
Sigma (degrees)	0.206	0.206	0.232	0.258	0.284	0.309
Area of Gabor textures (pixels)	229022	101788	128825	159043	192442	229022
Inter-element space (pixels)	62578	189812	162775	132557	99158	62578

Table 6.1. The inter-element space for the sparse (8 x 8) and dense (12 x 12) Gabor textures that were used in each Experiment. The area covered by the 8 x 8 and 12 x 12 notional grids was the same; 291600 pixels. The area occupied by all of the texture elements within each grid is given for each value of sigma.

### 6.3 Results of Experiment 4

The effect of a smaller inter-element space on texture segmentation is illustrated in Figure 6.2 in which the best-fitting values for delta ( $\delta$ ) and threshold exposure duration ( $\alpha$ ) are shown with a linear fit to observer data for each value of sigma. The number of trials was 2500, 1600 and 2500 for observers AJ, KM and JM respectively. The trials for the sparse (8 x 8) grid of Gabor textures that were obtained for these observers in Exp. 3 were also used in this experiment; sigma was 0.21 degrees.

The effect of inter-element space on texture segmentation was tested with the generalised likelihood ratio. The null hypothesis is the nested model in which the best-fitting parameter values for delta ( $\delta$ ), or alpha ( $\alpha$ ), are equal and unchanged with inter-element space. The alternative hypothesis is inter-element space linearly affected asymptote ( $1-\delta$ ), (Eq.7, Model variants, page 51), or threshold exposure duration ( $\alpha$ ), (Eq.6, Model variants, page 51). Given a critical value for  $2(\ln l - \ln l_0)$  of 6.96, where the critical region is 0.05, corrected for 6 applications when the nested model has one fewer free parameters, the log-likelihood ratio tests given in Table 6.2 support an effect of inter-element space on asymptote ( $1-\delta$ ) for all of the observers. An effect of inter-element space on threshold exposure duration ( $\alpha$ ) is supported for observers AJ and JM, but is not supported for observer KM when the critical region of 0.05 is corrected for 6 applications.

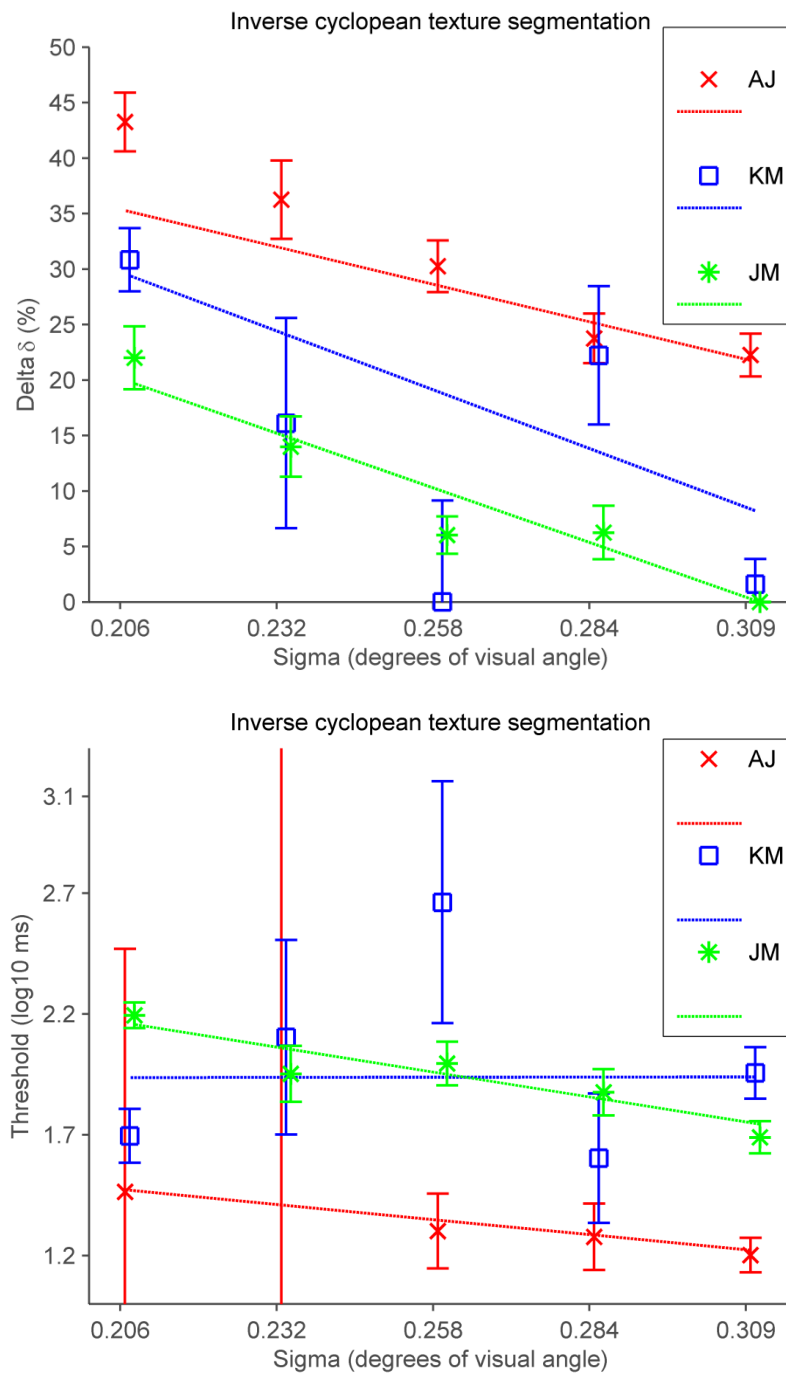


Figure 6.2. The best-fitting values for delta ( $\delta$ ) and threshold exposure duration ( $\alpha$ ) for each value of sigma are shown for each observer. The dotted line is a linear fit of  $\delta$  and  $\alpha$  to each observer's data. Error bars show the standard error of the best-fitting parameter values determined with a non-parametric bootstrap.

Model	Observer	k	LL		LL ratio	P value
			Inl	Inl <sub>0</sub>		
Linear fit of alpha ( $\alpha$ ), Beta ( $\beta$ ) & delta ( $\delta$ ) vary freely for each inter-element space	AJ	12	Inl	-1552.2		
	KM	12	Inl	-920.1		
	JM	12	Inl	-1180.7		
Alpha ( $\alpha$ ) is constrained, Beta ( $\beta$ ) & delta ( $\delta$ ) vary freely for each inter-element space	AJ	11	Inl <sub>0</sub>	-1557.2	10.0	0.002
	KM	11	Inl <sub>0</sub>	-922.3	4.4	0.035
	JM	11	Inl <sub>0</sub>	-1192.6	23.7	$p < .001$
Linear fit of delta ( $\delta$ ), Alpha ( $\alpha$ ) & beta ( $\beta$ ) vary freely for each inter-element space	AJ	12	Inl	-1553.4		
	KM	12	Inl	-923.3		
	JM	12	Inl	-1179.1		
Delta ( $\delta$ ) is constrained, Alpha ( $\alpha$ ) & beta ( $\beta$ ) vary freely for each inter-element space	AJ	11	Inl <sub>0</sub>	-1557.2	7.6	0.006
	KM	11	Inl <sub>0</sub>	-932.1	17.6	$p < .001$
	JM	11	Inl <sub>0</sub>	-1195.6	33.0	$p < .001$

Table 6.2. Statistics. The critical value from the chi-squared distribution for  $2(\ln l - \ln l_0)$  is 6.96 when the critical region of 0.05 is corrected for 6 applications ( $0.05/6 = 0.008$ ). P values:   =  $p \leq .008$  and   =  $p \leq .05$ .

The results for the task when Gabor textures were sparse (8 x 8) and sigma was 0.31 degrees and also the results from Exp. 3 for the task when Gabor textures were dense (12 x 12) are shown in Figure 6.3. The inter-element space was the same for both of these tasks (Table 6.1). Performances were high for both of these tasks (asymptote was > 87%), except for observer AJ when Gabor textures were sparse and sigma was 0.31 degrees (asymptote was 78%). Threshold was less than 100 ms for all of the observers for both of the tasks.

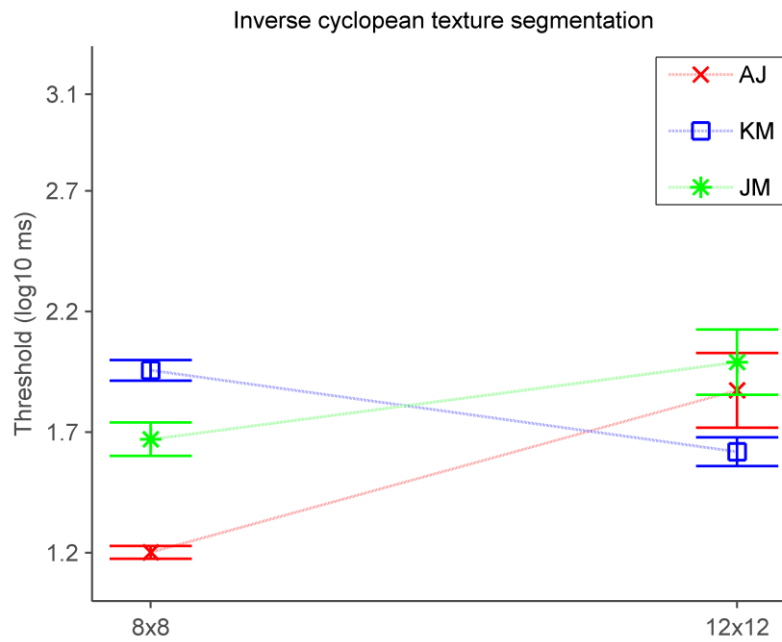
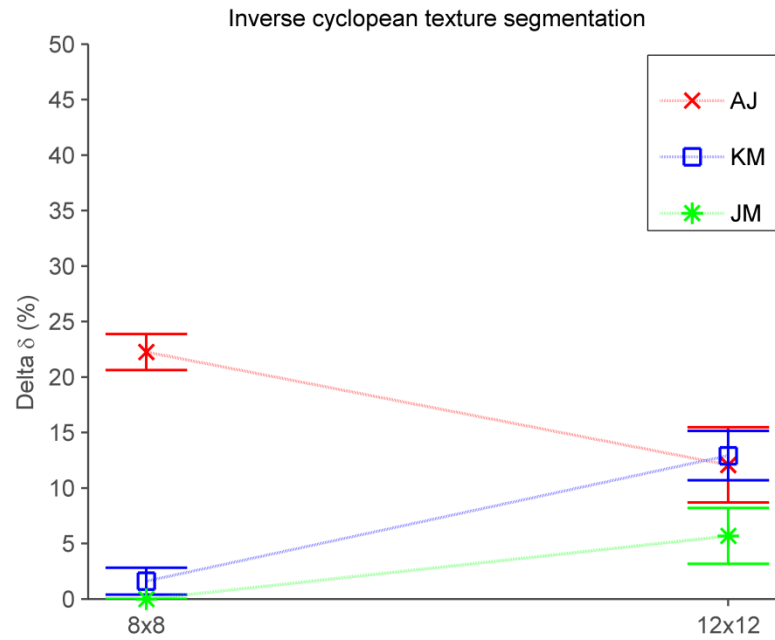


Figure 6.3. The results for the sparse (8 x 8) Gabor textures when sigma was 0.31 degrees and the results for the dense (12 x 12) Gabor textures from Exp. 3. The best-fitting values for delta ( $\delta$ ) and threshold exposure duration ( $\alpha$ ) are shown for each observer. Error bars show the standard error of the best-fitting parameter values determined with a non-parametric bootstrap.

## 6.4 Discussion

This experiment investigated whether orientation-defined, inverse cyclopean texture segmentation was affected by a smaller inter-element space when the number of texture elements within the sparse (8 x 8) grid was held constant. Texture segmentation was better when the inter-element space was decreased by increasing sigma in four equal increments.

The asymptote increased with a smaller inter-element space when the number of texture elements was held constant. This implies that texture segmentation is independent of the number of texture elements. Furthermore, the asymptote was increased when the inter-element space for dense (12 x 12) texture elements was 3.03 times smaller than when those elements were sparse (8 x 8); Exp. 3. Therefore, texture segmentation depends on orientation-defined texture boundaries that are closer together.

Asymptote for observers KM and JM was 98% and 100% respectively when sigma was 0.31 degrees. This might suggest that a dichoptic-overlapping target was visible in the optically fused percept, but only when sigma was 0.31 degrees.

Threshold exposure duration improved for two of the three observers when the inter-element space was smaller. The improvement in threshold seems specific to the increase in the values of sigma and wavelength for the Gabor textures that were used in this experiment. This is because an effect of texture density on threshold is not supported in Experiments 1.1 and 3 when sigma and wavelength were constant. The improvement in threshold might be due to an increase in sensitivity to the coarser spatial frequencies that were used.

Texture segmentation was better when orientation-defined texture boundaries within the sparse (8 x 8) grid were both closer together and occupied a larger area. This might suggest that texture segmentation is sensitive to a local texture gradient (Julesz, 1986). This possibility is consistent with segmentation of both orientation- and luminance-defined line textures depending on the ratio of the line texture length, for which line-texture size is later implicated (Nothdurft, 2000), to the inter-line texture spacing when texture-spacing is unchanged (Nothdurft, 1985).



To conclude, the proximity of orientation-defined texture boundaries is critical for texture segmentation. Texture segmentation was better when orientation-defined texture boundaries were closer together. Putative orientation-defined, inverse cyclopean texture segmentation was independent of the number of texture elements; therefore, texture segmentation is consistent with pre-attentive texture segmentation.

## **Experiment 5: Does inverse cyclopean texture segmentation vary with spatial scale?**

### **7.1 Introduction**

Inverse cyclopean texture segmentation was increased by a smaller inter-element space when the number of texture elements was held constant (Exp. 4). However, in this experiment, inter-element space varied on both the observer's retina and the stimulus display. To test if the effect on segmentation was due to inter-element space on either the retina or the stimulus display, segmentation was measured for an increase in the observer's viewing distance for which a proportional change in spatial scale of a dichoptic-overlapping stimulus was preserved on the retina whilst spatial scale on the stimulus display was unchanged. In the following experiment, observers viewed the sparse 8 x 8 grid that was used in Exp. 3 from an increased distance of 3 m to test if segmentation is dependent on texture spatial scale. This was the same grid that was used to test the effect of inter-element space on segmentation in Exp. 4.

### **7.2 Methods: Experiment 5**

Observers viewed the 8 x 8 grid of Gabor textures that was used in Exp. 3 from 3 m (Figure 7.1). Texture segmentation was measured when the 8 x 8 grid was viewed from 3 m and this was compared with texture segmentation when the grid was viewed from 1 m in Exp. 3.

For each Gabor stimulus (Eq. 1, Experimental procedure and stimuli, page 45), sigma ( $\sigma$ ) was 0.21 and 0.07 and wavelength ( $\lambda$ ) was 0.62 and 0.21 degrees of visual angle for 1 m and 3 m viewing distances respectively; spatial frequency was 1.62 and 4.85 cycles per degree. When observers viewed the nonius procedure from 3 m, nonius line height and width scaled with viewing distance in order to subtend 0.3 and 0.06 degrees of visual angle respectively.

The balance-points that were determined in Exp. 2 were used in this experiment. However, it cannot be assumed that the balance-points found in Exp. 2 were valid

for the stimuli in this experiment (further details are given in Exp. 2; Discussion, page 79).

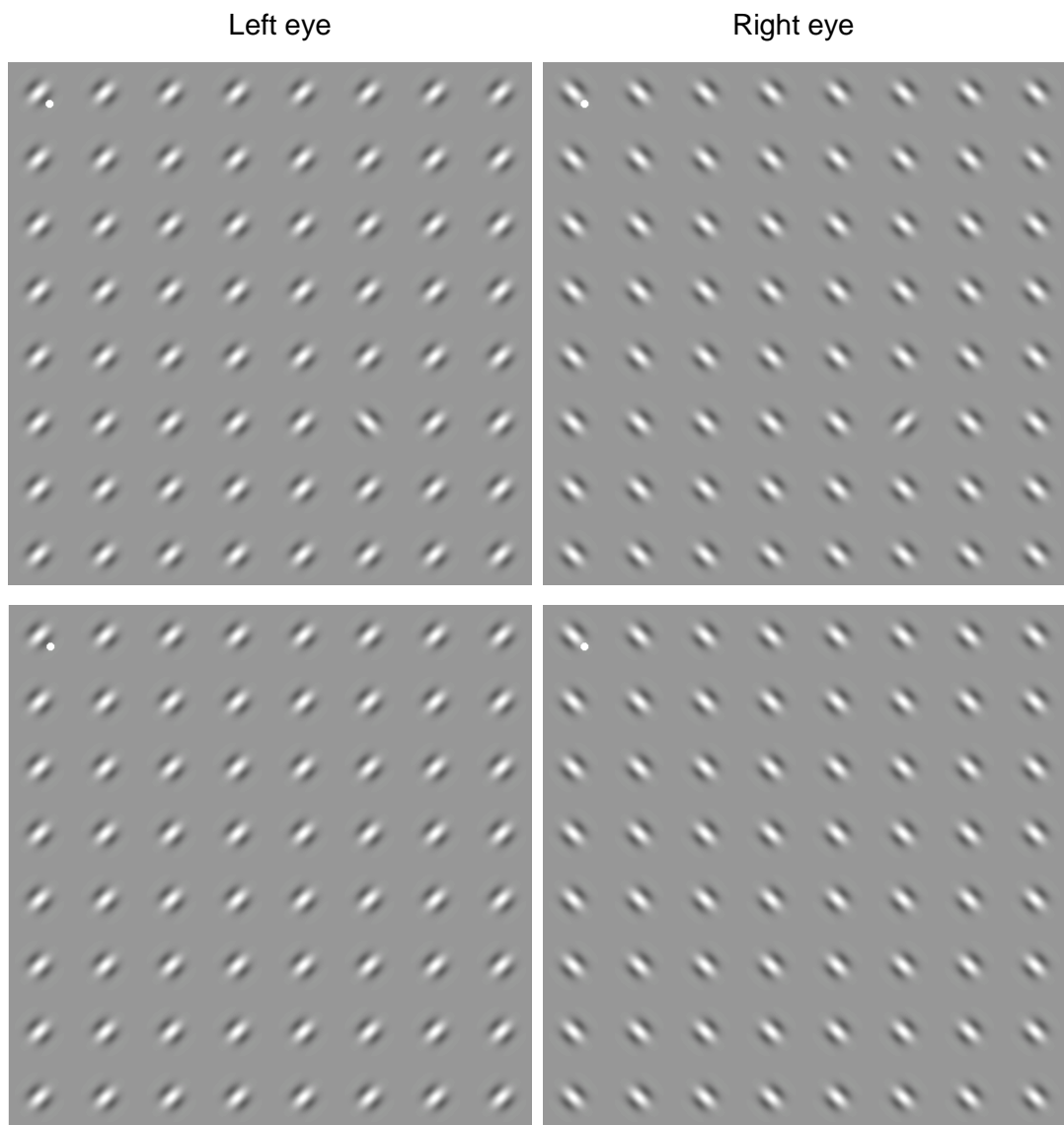


Figure 7.1. The sparse 8 x 8 grid is shown in an image for each of the two eyes (left and right panels). These images show the fixation dot when the viewing distance was 3 m.

### 7.3 Results of Experiment 5

Increased viewing distance affected segmentation asymptote ( $1-\delta$ ) for observers AJ and KM. However, observers AJ and KM found the task impossible for stimuli viewed from 1 m and 3 m respectively. Observer JM performed significantly above chance for both viewing distances. Psychometric functions given in Figure 7.2 illustrate segmentation performance for each observer and the best-fitting values for delta ( $\delta$ ) and threshold exposure duration ( $\alpha$ ) are shown in Figure 7.3.

The effect of texture spatial scale on segmentation performance was tested with the generalised likelihood ratio. The null hypothesis is the nested model in which the best-fitting parameter values for delta ( $\delta$ ), or alpha ( $\alpha$ ), are equal and unchanged with texture spatial scale. The alternative hypothesis is that texture spatial scale affected the asymptote ( $1-\delta$ ), or, threshold exposure duration ( $\alpha$ ).

Given a critical value for  $2(\ln l - \ln l_0)$  of 6.96, where the critical region is 0.05, corrected for 6 applications when the nested model has one fewer free parameters, the log-likelihood ratio tests given in Table 7.1 marginally support an effect of spatial scale on asymptote for observers AJ and KM. The results do not support an effect of spatial scale on threshold exposure duration ( $\alpha$ ).

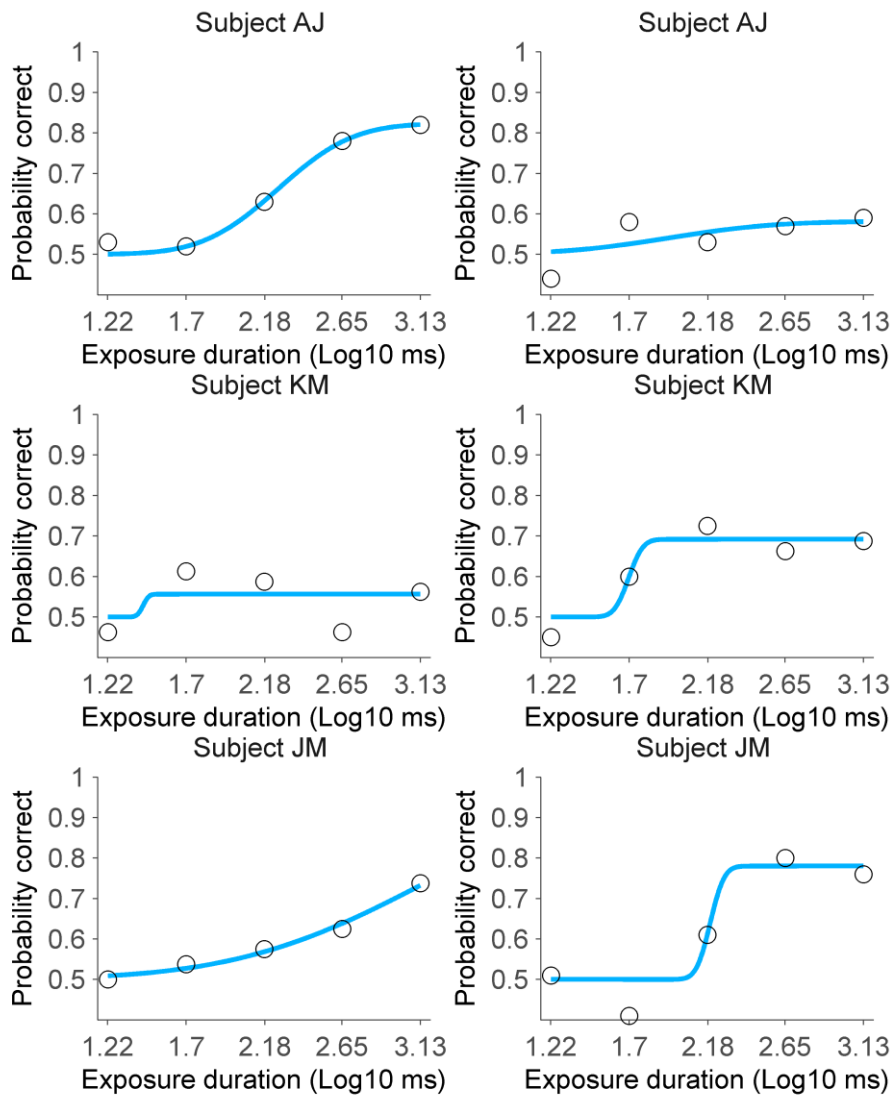


Figure 7.2. Psychometric functions for each observer show the probability of a correct response at logarithmically spaced exposure durations for 3 m (left panels) and 1 m (right panels) viewing distances.

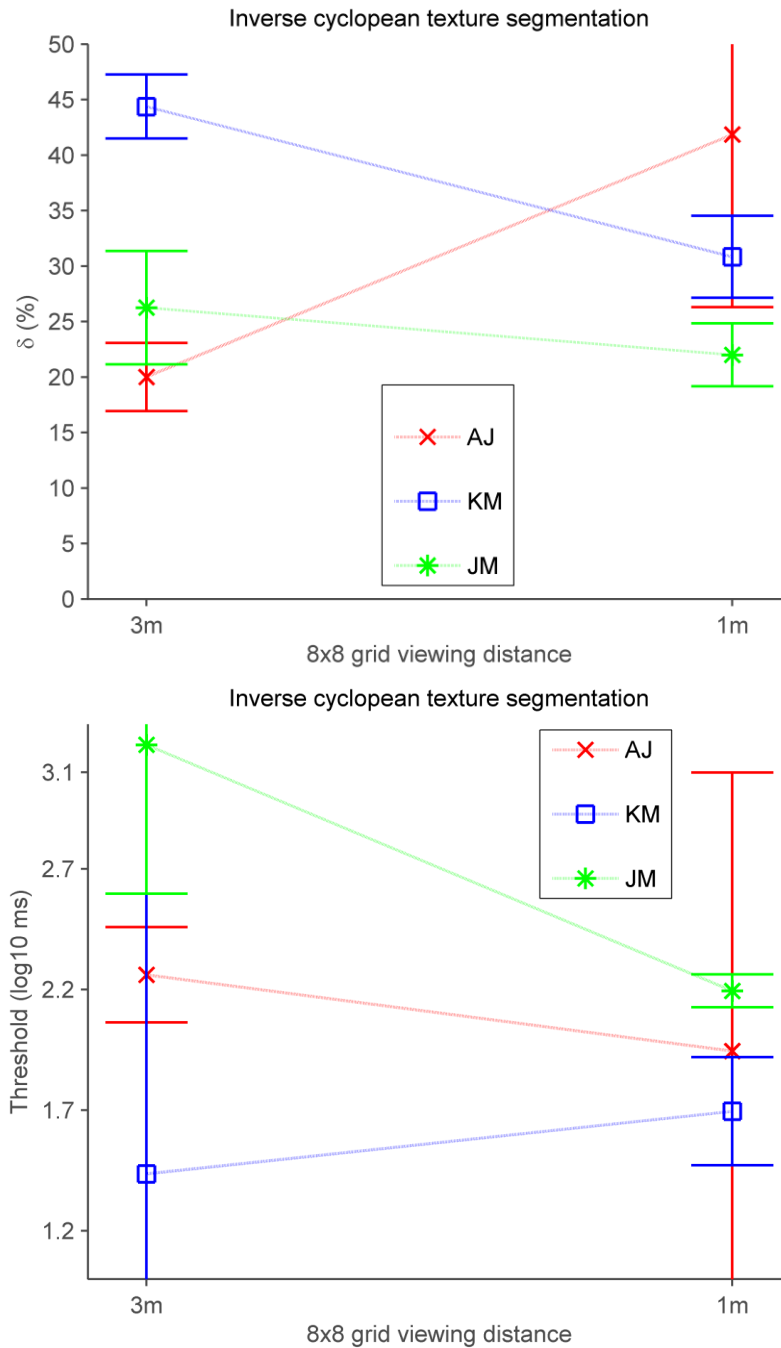


Figure 7.3. The best-fitting values for delta ( $\delta$ ) and threshold exposure duration ( $\alpha$ ) for 3 m and 1 m viewing distances for each observer. Error bars show the standard error of the best-fitting parameter values determined with a non-parametric bootstrap.

Model	Observer	k	LL		LL ratio	P value
Alpha ( $\alpha$ ), Beta ( $\beta$ ) and delta ( $\delta$ ) vary freely for each texture spatial scale	AJ	6	lnl	-647.7		
	KM	6	lnl	-532.8		
	JM	6	lnl	-575.2		
Alpha ( $\alpha$ ) is constrained, Beta ( $\beta$ ) & delta ( $\delta$ ) vary freely for each texture spatial scale	AJ	5	lnl <sub>0</sub>	-647.7	0.03	0.86
	KM	5	lnl <sub>0</sub>	-533.6	1.7	0.19
	JM	5	lnl <sub>0</sub>	-577.8	5.3	0.02
Delta ( $\delta$ ) is constrained, Alpha ( $\alpha$ ) & beta ( $\beta$ ) vary freely for each texture spatial scale	AJ	5	lnl <sub>0</sub>	-655.8	16.2	$p < .001$
	KM	5	lnl <sub>0</sub>	-538.1	10.6	0.0011
	JM	5	lnl <sub>0</sub>	-576.5	2.7	0.10

Table 7.1. Statistics. The critical value from the chi-squared distribution for  $2(\ln l - \ln l_0)$  is 6.96 when the critical region of 0.05 is corrected for 6 applications ( $0.05/6 = 0.008$ ). P values:  =  $p \leq .008$ ,  =  $p \leq .05$  and unshaded P values =  $p > .05$ .

#### 7.4 Discussion

The inverse cyclopean texture segmentation asymptote ( $1-\delta$ ) was spatial scale dependent for observers AJ and KM. Although for observer AJ the task was impossible for stimuli viewed from 1 m, the increase in asymptote for 3 m viewing suggests a retinal effect of texture spatial scale on segmentation. However, the test for scale dependence is valid for a range of viewing distance in which textures can still be resolved. For observer KM, the task was impossible for 3 m viewing, suggesting that stimuli with fine spatial frequency were not resolved. Because threshold exposure duration ( $\alpha$ ) for observer JM was 1.6 seconds for stimuli viewed from 3 m, the task was not possible at the maximum stimulus exposure duration of 1.35 seconds for which the value of asymptote was obtained for this observer. The dependence of orientation-defined, inverse cyclopean texture segmentation on spatial scale is therefore inconclusive. Alternatively, the likelihood of disjunctive vergence fluctuations increases for larger viewing distances for which segmentation may be affected.

## **Experiment 6: Is inverse cyclopean texture segmentation dependent on stereoscopic vision?**

### **8.1 Introduction**

The asymptote for orientation-defined, inverse cyclopean texture segmentation was increased when texture elements were dense (Exp 1.1 & Exp. 3) and when the inter-element space was smaller (Exp.4). Binocular fusion of the images in the two eyes occurs when similar images fall within Panum's fusional area, wherein the fusion range is greater for horizontal than for vertical separations of retinal disparities (Howard, 2002; Panum, 1858). Thus, perceptual fusion of orientation-defined, dichoptic-overlapping texture elements might be formed from the horizontal texture component and occur in parallel with stereopsis or a depth cue. This alternative explanation, the stereo-matching hypothesis, proposes matching of a target Gabor texture with a distractor that has the same orientation in the contralateral eye. A prediction of this hypothesis is that texture segmentation would be impossible, or at least harder, for stimuli arranged in a column since the range of both fusion and stereo vision is less for vertical disparities.

In the following experiment, texture segmentation was measured when 9 Gabor textures were arranged in a column or a row. In Experiments 1.1, 3 and 4, randomisation was used to determine whether the orientation of texture elements within a dichoptic-overlapping stimulus was either 45 or -45 degrees with respect to vertical on every trial. The target was orthogonal to the distractors. However, in the following experiment, randomisation was used to determine whether orientation was either 0 or 90 degrees on every trial. This was because it was thought that there may be stronger matching between same-cardinal stimuli than between same-obliques. If the results with cardinal stimuli had favored the stereo-matching hypothesis, it would have been our intention to repeat using non-cardinal stimuli. The stereo-matching hypothesis is illustrated for the row of texture elements shown in Figure 8.1.



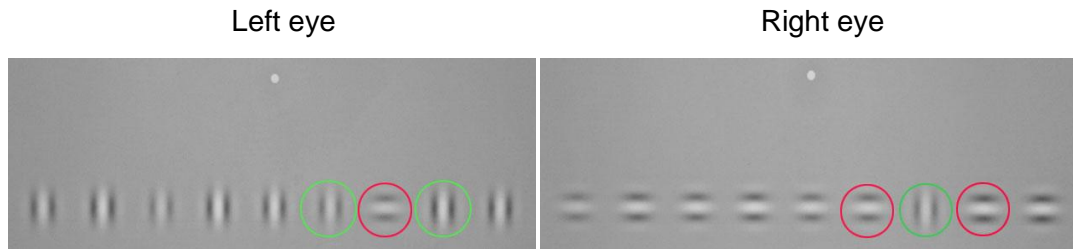


Figure 8.1. The stereo-matching hypothesis. Two matches with a stimulus in the contralateral eye are shown. A 90 degree oriented target presented to the left eye (red circle, left panel) is matched with either of the 90 degree oriented distractors presented to the right eye (red circles, right panel). A 0 degree oriented target presented to the right eye (green circle, right panel) is matched with either of the 0 degree oriented distractors presented to the left eye (green circles, left panel). The fixation point is in the centre of the display.

8.2 Methods: Experiment 6

Orientation-defined, inverse cyclopean texture segmentation was measured when 9 Gabor textures were arranged in a column (Figure 8.2) or a row (Figure 8.3).

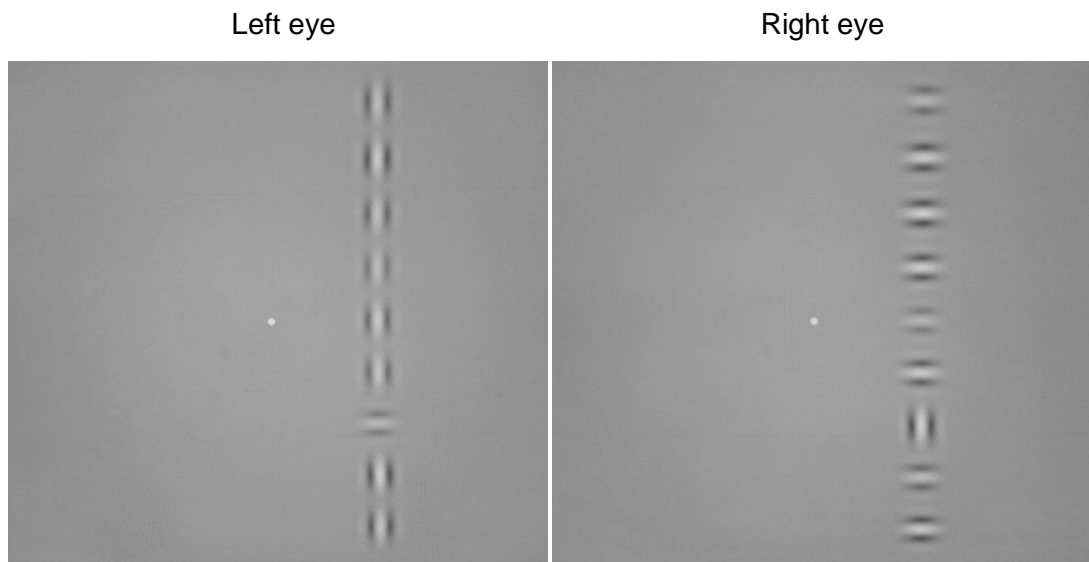


Figure 8.2. A column of Gabor textures with randomised luminance contrast within each image for the two eyes (left and right panels). The target interval is shown; the other interval of a two alternative forced choice procedure (2-AFC) contained distractors.

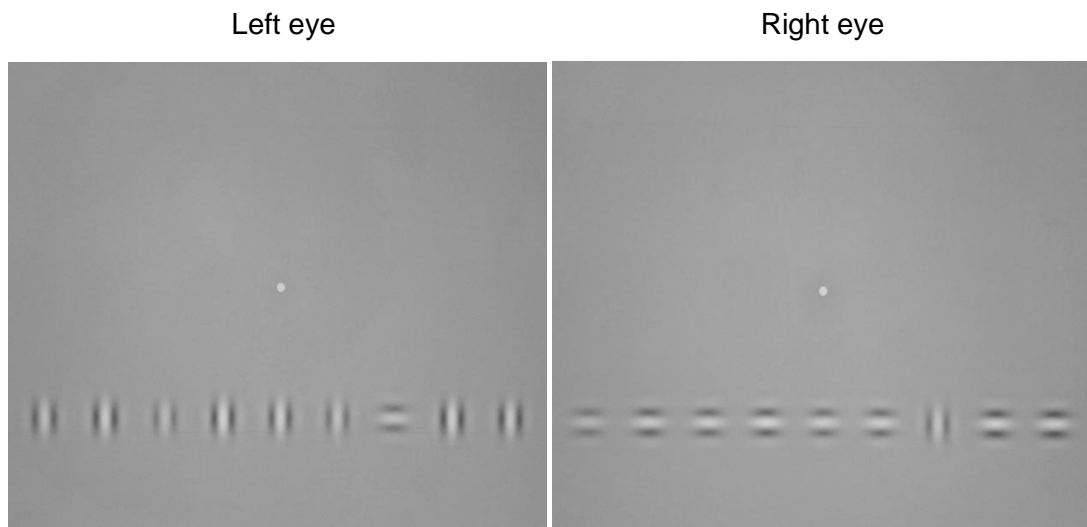


Figure 8.3. A row of Gabor textures within each image for the two eyes (left and right panels). Luminance contrast is randomised. The fixation point is shown in the centre of the display. The target interval is shown; the other interval of a two alternative forced choice procedure (2-AFC) contained distractors.

The luminance contrast of every Gabor texture was randomised to exclude a contrast-defined cue to the target. The range of randomisation was between 40% and 100% of the maximum available luminance contrast which prevented pop-out of the target had the retinally corresponding target been below the contrast threshold.

For each Gabor stimulus (Eq. 1, Experimental procedure and stimuli, page 45), sigma was 0.28 degrees of visual angle and wavelength was 0.55 degrees; spatial frequency was 1.82 cycles per degree. All Gabor textures were separated by 1.65 degrees of visual angle.

The peripheral visual field was used for the spatial location of an orientation-defined target since the target was presented in peripheral locations of the visual field in Experiments 1, 3, 4 and 5. The target was in Cartesian quadrant IV of the display, 4.7 degrees of visual angle from fixation and was in the same retinal position irrespective of the grid, column or row arrangement used. This was achieved by placing a column or a row two positions from fixation in the notional grid and the target occupying the second position from the Gabor texture in the centre of a column and a row.

Although four observer's stereoscopic vision was normal, one observer presented with amblyopia and reported dominance of the right-eye in a Randot stereo-test. Exposure durations were 2 successive video frames for the two observers that were experienced with dichoptic-overlapping displays, or were 16 frames for those inexperienced. The duration for each frame was 8 ms.

Blocked trials were used to test the effect of configuration predicted by the stereo-matching hypothesis. Each block was done consecutively in the order A, B, B and A, where A was a column arrangement and B a row arrangement, to evaluate any effect of practice on the task.

### 8.3 Results of Experiment 6

The stereo-matching hypothesis was tested using an unpaired t-test (two-tailed test) to calculate the probability ( $p$ ) that the means for segmentation for a row and a column differed at a significance level of 0.05. The null hypothesis was that mean segmentation was unchanged, for a row and a column ( $p > .05$ ). This test assumed a symmetric normal distribution for each mean. The results for rows and columns are shown for each observer in Figures 8.4, 8.5 and 8.6 and Table 8.1 shows  $p$  values for the test statistic. The results do not support an effect of texture configuration on texture segmentation, ( $p > .05$ ).

The difference to chance performance was significant ( $p < .05$ ) for both a row and a column. Neither the author nor the naive observers reported an identifiable depth cue. All of the observers reported that the target was vaguely visible and did not pop-out. As trial number increased, four observers reported that there was a contrast-defined cue within the area of the display in which the target was located and that this cue was observed in both of the intervals. However, one of the intervals did not contain a target. One observer advised they were receiving clinical assessment for amblyopia, however, performance poorer than 100% was inconsistent with an effect of amblyopia. The results for a 9 x 9 grid were included for observer AJ since a grid was used in previous experiments; a grid differed significantly to a row and a column ( $p < .0005$ ).

Observer	N (row / column)	P value (i)	P value (ii) (row / column)
AJ	200 / 140	0.67	0.001 / 0.002
JAS	130 / 160	0.62	0.04 / 0.01
BF	130 / 160	0.88	0 / 0
KM	130 / 110	0.11	0 / 0
LE	110 / 180	0.61	0 / 0

Table 8.1. The number of trials (N) and p value (unpaired t-test) for a row and column mean differing (i) or differing to chance (ii). P values:   =  $p \leq .05$  and unshaded P values =  $p > .05$ .

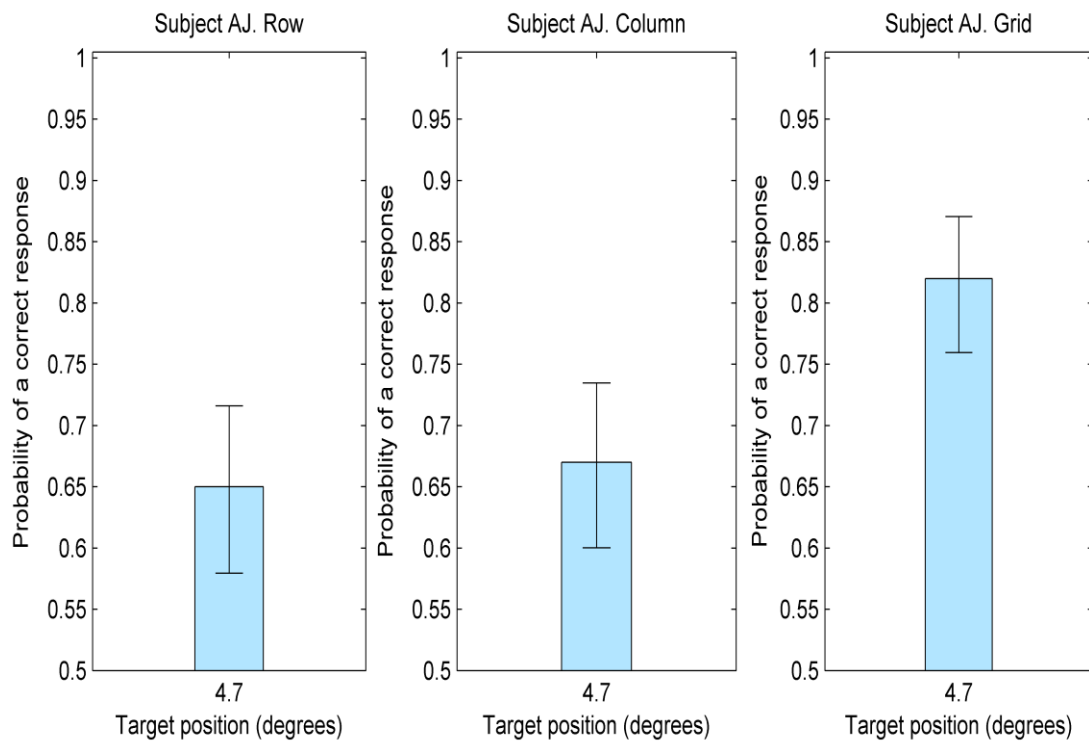


Figure 8.4. Results for observer AJ showing the probability of identifying the target in a row, column or grid. Error bars show 95% confidence intervals.

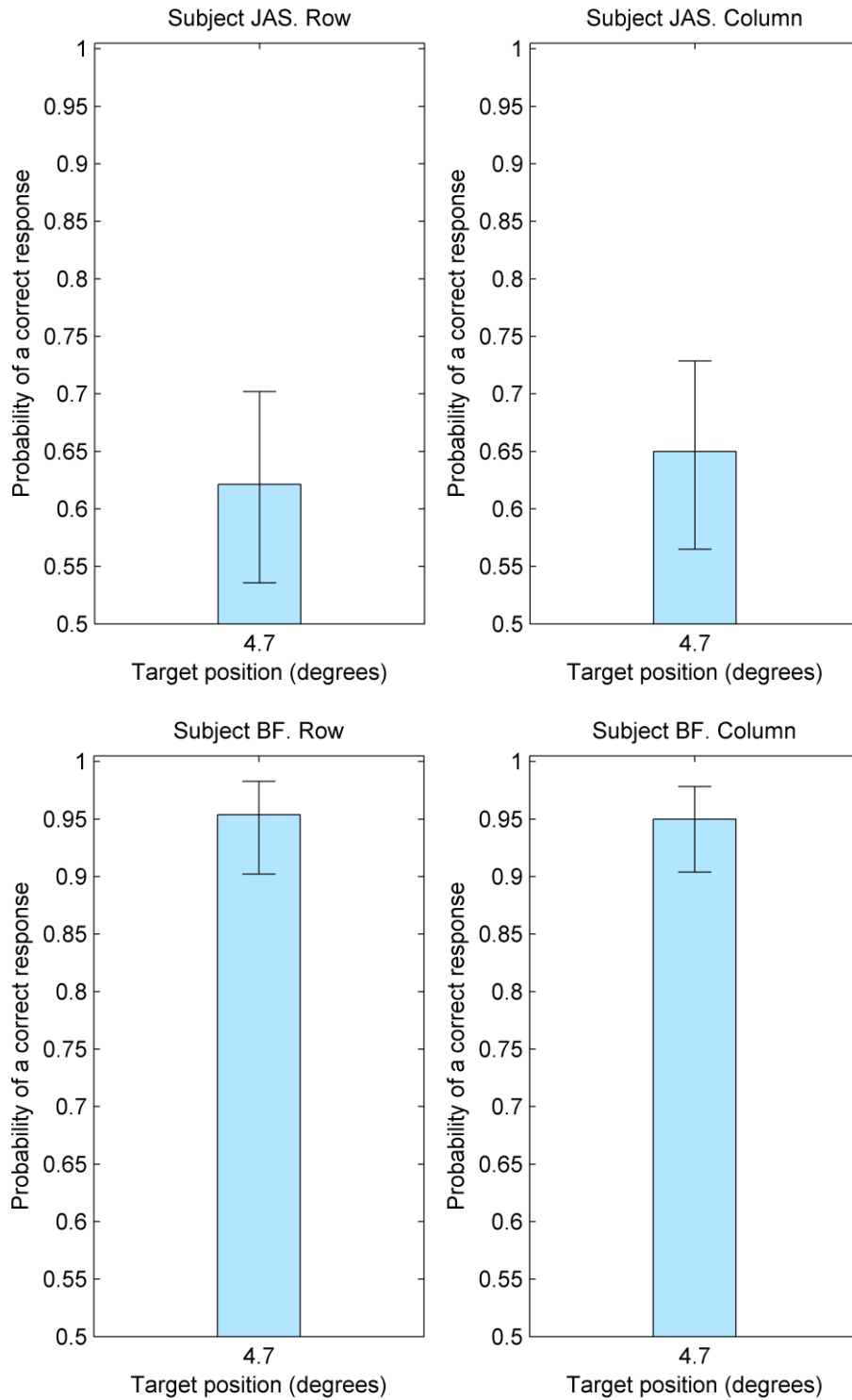


Figure 8.5. Results for observers JAS and BF showing the probability of identifying the target in a row or column. Error bars show 95% confidence intervals.

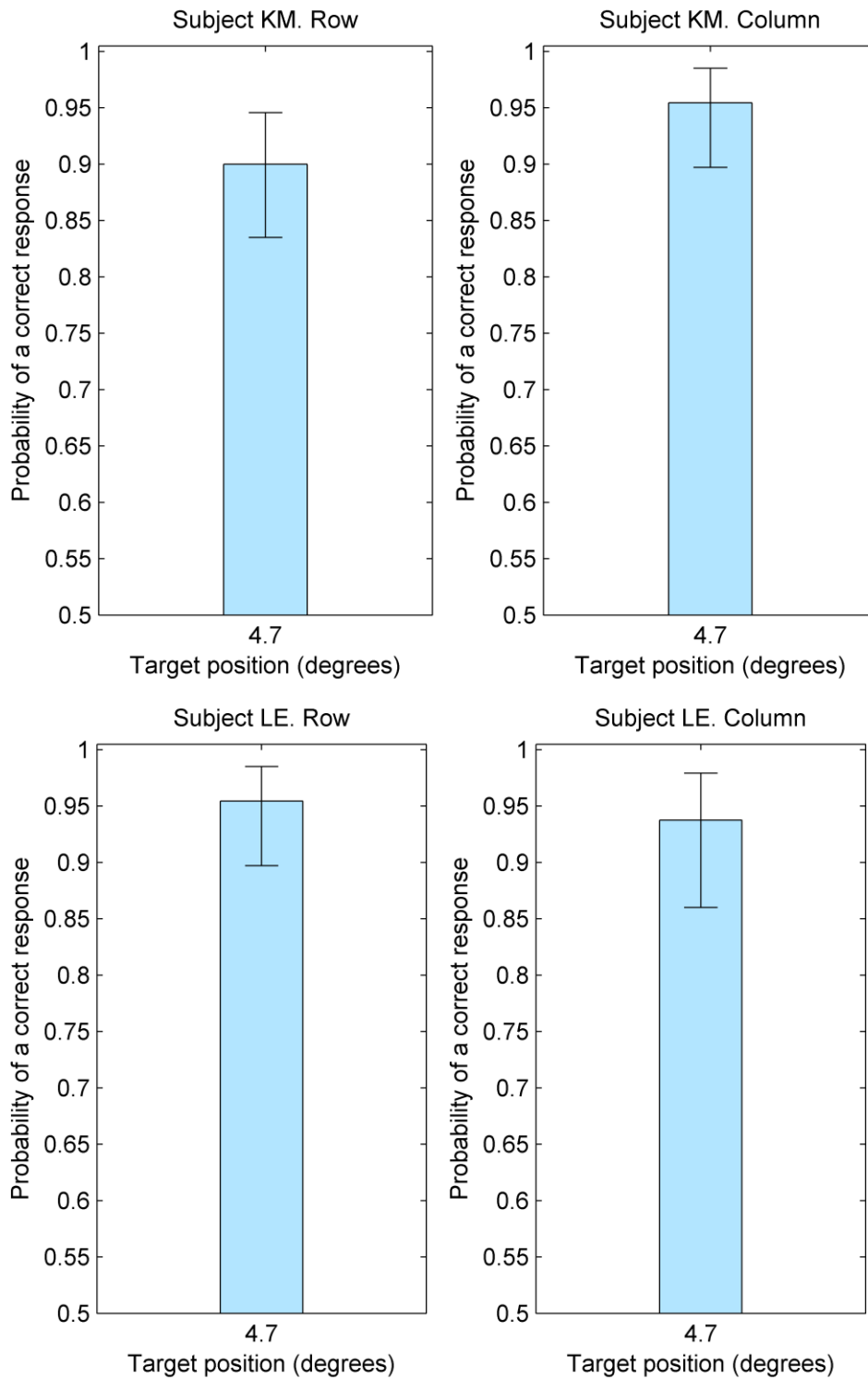


Figure 8.6. Results for observers KM and LE showing the probability of identifying the target in a row or column. Error bars show 95% confidence intervals.

#### 8.4 Discussion

The effect of the configuration of dichoptic-overlapping stimuli that was predicted by the stereo-matching hypothesis, optimal performance in a row and sub-optimal performance in a column, was not supported by the results. The results showed that the difference to chance performance was significant when texture elements were arranged in a column and when texture elements were arranged in a row. The results therefore support vertical as well as horizontal orientation-defined texture segmentation in brief 16 ms or 128 ms exposure durations. The results imply that orientation-defined, inverse cyclopean texture segmentation occurs prior to binocular fusion and stereopsis.

To conclude, inverse cyclopean texture segmentation is independent of stereoscopic vision.

## **Experiment 7: Is effective contrast imbalance the mechanism for the dichoptic advantage for texture segmentation in brief durations?**

### **9.1 Introduction**

An imbalance in sensory input from the two eyes affects orientation-defined, inverse cyclopean texture segmentation (Experiment 2). A dichoptic-overlapping (inverse cyclopean), orientation-defined target was not detected when the effective contrast was balanced between the two eyes. This might suggest that effective contrast imbalance is the only mechanism for detecting an orientation-defined, dichoptic-overlapping (inverse cyclopean) target. However this conclusion is valid only for the stimulus conditions of Experiment 2 and is not necessarily correct for the original stimuli used by Kolb and Braun (1995) and others, for example, Morgan, Mason and Solomon (1997) and Solomon and Morgan (1999). Specifically, in Experiment 2 observers viewed the texture elements from 3 m; spatial frequency was 4.85 cycles per degree. In Experiment 3, an attempt was made to balance the input from the two eyes using the balance-points determined from Experiment 2. However, the spatial frequency for Experiment 3's texture elements was lower, 1.62 cycles per degree, because observers viewed them from 1 m. It cannot be assumed that the balance-point found in Experiment 2 was valid for the stimuli in Experiment 3. Therefore, in the following experiments, both the balance-point and texture segmentation were measured when the spatial frequency of texture elements and the distance from which texture elements were viewed were the same.

The balance-point was measured for each observer in Experiment 7.1 independently of its effect on texture segmentation by a subjective matching method. The balance-point is the ratio of interocular luminance contrast that balanced a difference in effective contrast between the two eyes. In Experiment 7.2, orientation-defined dichoptic texture segmentation was tested when this balance-point was used to equalise the effective contrast difference between the two eyes. In addition, a 'jitter' was added to the contrast of the texture elements by drawing them from a uniform distribution of log contrasts. The purpose of contrast randomisation was to mask any small-to-moderate errors in the balance-point.



The purpose of Experiment 7.2 was to determine whether differences between the effective contrasts of dichoptic stimuli were responsible for a dichoptic advantage for orientation-defined texture segmentation in brief durations. There is a dichoptic advantage for orientation-defined texture segmentation in brief durations if performances for dichoptic texture segmentation were better than performances for binocular texture segmentation. An advantage for dichoptic orientation-defined texture segmentation was revealed by high performance in brief durations (Experiments 1.1, 3, 4, 5 and 6). In brief durations, performances for orientation-defined dichoptic texture segmentation were better than those for binocular texture segmentation, for which performances were chance, when texture elements were dense (12 x 12); Experiment 1.1. To test if effective contrast imbalance was responsible for the dichoptic advantage, texture segmentation in brief 100 ms durations was measured for both dichoptic and binocular orientation-defined texture boundaries. Texture elements within a binocular stimulus were also contrast randomised. The hypotheses are conveyed prior to describing the dichoptic and binocular stimuli that were used to test them.

The null hypothesis is that texture segmentation for orientation-defined dichoptic and binocular texture boundaries does not differ. If there were no dichoptic advantage when the effective contrast difference between the two eyes was equalised, then we can conclude that effective contrast imbalance was the mechanism for the dichoptic advantage revealed by Experiments 1.1, 3, 4, 5 and 6. The alternative outcome of the experiment is orientation-defined, dichoptic and binocular texture segmentation do differ significantly. If segmentation were better for dichoptic texture boundaries, then effective contrast imbalance cannot be the only mechanism for detecting an orientation-defined, dichoptic-overlapping (inverse cyclopean) target. A dichoptic advantage for orientation-defined texture segmentation would confirm that monocular input is available to pre-attentive texture segmentation mechanisms. However, even if mechanisms for orientation-defined texture segmentation did not have access to monocular input, performance might exceed chance with putative dichoptic-overlapping (inverse cyclopean) texture boundaries if a failure of binocular fusion rendered those textures effectively nonoverlapping (Howard, 2002). Texture segmentation was measured for nonoverlapping texture boundaries that were optically fused; the binocular-nonoverlapping stimulus (Figure 9.2; second row, right panel). Consequently, if performance with dichoptic-overlapping (inverse cyclopean) texture boundaries

exceeds performance with binocular-nonoverlapping texture boundaries, performance for the dichoptic-overlapping task cannot be wholly attributed to a failure of binocular fusion. Dichoptic texture segmentation might occur if misalignment of the two eyes rendered dichoptic-overlapping texture boundaries effectively nonoverlapping. Texture segmentation was measured for dichoptic-nonoverlapping texture boundaries (Figure 9.2; second row, left & centre panels). Consequently, if performance with dichoptic-nonoverlapping texture boundaries exceeds performance with binocular-nonoverlapping texture boundaries, performance for dichoptic-nonoverlapping texture boundaries cannot be attributed to differences in effective contrast. Texture segmentation for dichoptic-overlapping and binocular-overlapping texture boundaries, for which the two images in dichoptic-overlapping stimuli were optically fused (Figure 9.2; top row, right panel), was also compared. Segmentation was impossible for binocular-overlapping texture boundaries (Experiment 1.1) that were not contrast randomised. If performance was chance for both dichoptic-overlapping and binocular-overlapping texture boundaries, then effective contrast imbalance might be the mechanism for the dichoptic advantage. However, since chance performance for binocular-overlapping texture boundaries was predicted, it was unlikely that binocular-overlapping texture boundaries were used to test whether contrast imbalance was the mechanism for the dichoptic advantage.

## **9.2 Methods**

The methods which are applicable to both Experiment 7.1 and Experiment 7.2 are conveyed in this section. The methods specific to each experiment are conveyed in the subsequent sections.

The observers viewed the stimulus display from 1 m. For each Gabor stimulus (Eq. 1, Experimental procedure and stimuli, page 45), sigma was 0.17 and wavelength was 0.33 degrees of visual angle; spatial frequency was 3.03 cycles per degree. The exposure duration was 100 ms.

For dichoptic-overlapping stimuli, the luminance contrast of the first and the last stimulus frames were reduced by 50% to minimise forward and backward masking respectively. This method was applied to every stimulus. The balance-point for all

of the observers required a reduction in luminance contrast of the stimulus for the right eye (Exp. 2). One source for this is even-numbered stimulus frames might be dichoptically masked until the last stimulus frame for which the shutter for the right eye opens and backwards masking is absent. The shutter that opened for first stimulus frame was randomised.

### **9.2.1 Methods: Experiment 7.1**

The balance-point for each observer was measured by a subjective matching method, the method of adjustment. Dichoptic-nonoverlapping stimuli were used to find the balance-point; texture elements did not compete for the same retinal position. Texture elements occupied alternate positions on a 12 x 12 notional checkerboard within each dichoptic stimulus; texture density was 6 x 6 (Figure 9.1). The stimuli were viewed repeatedly for 100 ms with an interstimulus interval of 100 ms. A sparse 6 x 6 grid was chosen because rivalry might occur if the texture elements within each stimulus were dense (12 x 12). Although the balance-point for each observer was measured when texture elements were sparse (6 x 6), the balance-point was assumed to be the same when texture elements were dense (12 x 12). An observer may experience difficulty in finding the balance-point for dichoptic-overlapping stimuli as dichoptic-overlapping cues are vaguely visible and rivalrous.

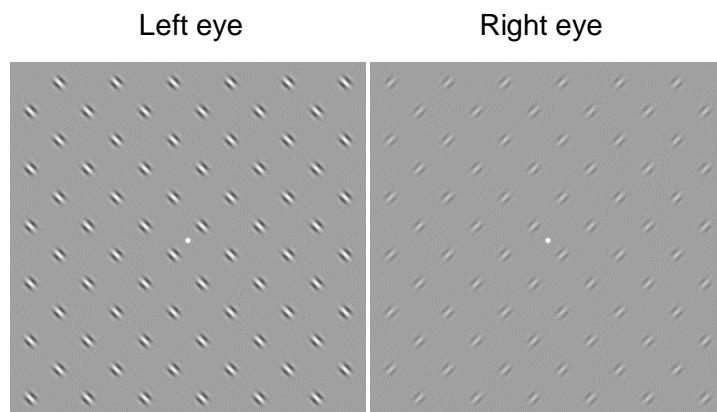


Figure 9.1. A 6 x 6 grid of dichoptic-nonoverlapping Gabor stimuli. In this example, luminance contrast is 80% for -45 degree texture elements (left panel) and is 30% for 45 degree texture elements (right panel).

Observers adjusted the luminance contrast of texture elements within the left or the right eye's stimulus when orientation was – or + 45 degrees from vertical; the contrast of the contralateral eye's stimulus was fixed (30%). The observer's task was to adjust the contrast of -45 or 45 degree elements to match the contrast of 45 or -45 degree texture elements for the other eye respectively. At the start of the task, luminance contrast was 100% until observers signalled decrements and increments in contrast by responding on a keypad. Observers pressed a key when the textures appeared uniform in contrast. The balance-point was measured for 10 blocks for each of the two eyes; 5 blocks when orientation was -45 degrees and 5 blocks when orientation was +45 degrees.

The balance-point for each of the two eyes was measured when orientation was both -45 and +45 degrees because impaired visual acuity for one of the orientations, for example astigmatism, could affect the contrast required for texture elements to appear uniform in contrast. The mean balance-point for each of the two eyes was the mean of the contrasts required for texture elements to appear uniform in contrast when orientation was both -45 and +45 degrees. Thus, a mean balance-point was determined for each of the two eyes. The balance-point for an observer was the mean of these two ratios of interocular contrast; a ratio of interocular luminance contrast termed the ratio. The ratio was 1 when there was no difference in effective contrast between the two eyes and was greater than 1 when there was a difference.

### **9.2.2 Methods: Experiment 7.2**

Texture segmentation was measured for dichoptic and binocular orientation-defined texture boundaries. Orientation-defined texture segmentation was measured for dichoptic-overlapping stimuli and dichoptic-nonoverlapping stimuli when a difference in effective contrast between the two eyes was equalised. Texture elements occupied alternate positions on a 24 x 24 notional checkerboard; the texture density of a dichoptic stimulus was 12 x 12. Orientation-defined texture segmentation was also measured for a binocular-overlapping stimulus and a binocular-nonoverlapping stimulus. A binocular-overlapping stimulus and a binocular-nonoverlapping stimulus were stimuli for which the two images in dichoptic-overlapping and dichoptic-nonoverlapping stimuli respectively were

optically fused; texture density is not given for a binocular stimulus. For a binocular stimulus, the two eyes viewed the same texture elements within the stimulus.

If binocular and dichoptic stimuli had the same physical contrast, performances with binocular stimuli might be greater than those with dichoptic stimuli, simply because binocular summation increases the effective contrast of binocular stimuli. To minimise the gain in texture segmentation due to binocular summation, binocular texture segmentation was measured when the maximum randomised contrast was 50%. However, this reduction in contrast might overestimate the effect that binocular summation has on performance. Binocular-nonoverlapping texture segmentation was also measured when the maximum randomised contrast was 100%.

The ratio found for each observer in Exp. 7.1 was used to equalise the effective contrast difference between dichoptic stimuli for the two eyes. The reciprocal of the ratio specified the reduction in the contrast of texture elements within the dichoptic stimulus for the eye for which the mean balance-point was lowest. 'Jitter' was added to the contrast of the texture elements by drawing their contrast randomly from a 9.5 dB wide uniform distribution of log contrast. The purpose of jitter was to mask any small-to-moderate errors in the ratio, or residual effects of astigmatism, that would cause anisotropies in the fidelity of contrast transduction. This jitter was also added to the contrasts of binocular texture elements; however, the uniform distribution of log contrast was 3.5 dB wide when the maximum contrast was 50%. An imbalance in effective contrast between the two eyes could affect segmentation for binocular texture boundaries; however, the effective contrast difference between the two eyes was not equalised for binocular texture boundaries for which the consequence was improved performance.

Trials for the two dichoptic and the three binocular texture-segmentation tasks were interleaved within each block. The orientation-defined texture boundary was two texture elements within each dichoptic stimulus. Although the aim of the nonius procedure was to achieve the point of zero horizontal disparity prior to every trial for a dichoptic task, the two eyes may become misaligned during the task. Observers were instructed to repeat these trials if the nonius dots were misaligned during the task itself, or, during the interval between the first and second intervals. The sequence of a repeated trial and the remaining trials was randomised.

The dichoptic and binocular stimuli are shown in Figure 9.2.

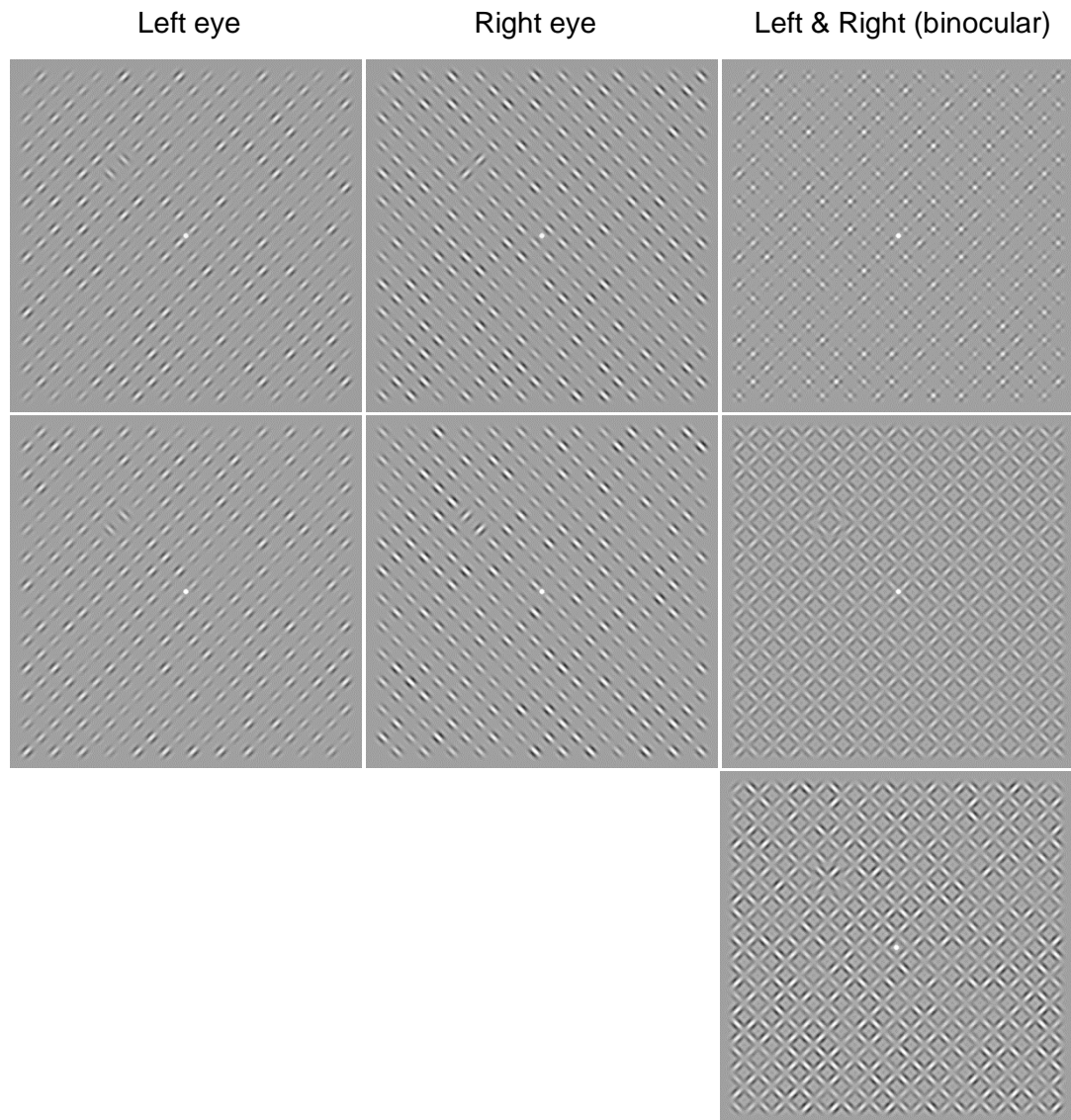


Figure 9.2. 12 x 12 grids of dichoptic-overlapping (top row, left & centre panels) and dichoptic-nonoverlapping Gabor stimuli (second row, left & centre panels). In this example, the contrast of texture elements within the left eye's stimulus was reduced (left panels; the ratio was 1.22). A binocular-overlapping stimulus and a binocular-nonoverlapping stimulus are shown in the right panels of the top and second rows respectively; the maximum randomised contrast was 50%. A binocular-nonoverlapping stimulus for which the maximum randomised contrast was 100% is shown in the right panel, third row. 'Jitter' was added to the contrast of the texture elements by drawing them from a uniform distribution of log contrasts that was 9.5 dB wide (all left, all centre panels & third row, right panel) and 3.5 dB wide (top & second rows, right panels). Each stimulus covered an equal unit area. Texture elements were separated by 0.86 degrees within the 12 x 12 grid. The

target interval is shown; the other interval of a two alternative forced choice procedure (2-AFC) contained distractors.

### **9.3 Results of Experiment 7.1**

The mean contrast for dichoptic texture elements to appear uniform in contrast and the ratio for each observer are given in Table 9.1.

		Contrast of the left eye's stimulus adjusted		Contrast of the right eye's stimulus adjusted		Ratio
		-45	45	-45	45	
AJ	Mean	25.0	28.0	37.0	31.0	1.13
	SD	6.1	6.7	12.0	14.7	
JAS	Mean	40.0	28.3	38.3	25.0	1.04
	SD	0.0	5.8	2.9	0.0	
JM	Mean	66.0	38.0	40.0	30.0	1.22
	SD	12.9	5.7	5.0	5.0	
PL	Mean	28.0	30.0	43.0	35.0	1.17
	SD	4.1	4.8	9.7	4.1	

Table 9.1. The mean contrast (%) for dichoptic texture elements to appear uniform in contrast, the standard deviation (SD) for each mean and the ratio are given for each observer. Observers adjusted the contrast of texture elements within the left or the right eye's stimulus when orientation was – or + 45 degrees from vertical; the contrast of the contralateral eye's stimulus was fixed (30%).

The ratio was greater than 1 for all of the observers (Table 9.1); a difference in effective contrast between the two eyes is supported. The highest ratio was 1.22 for observer JM and the lowest was 1.04 for JAS.

Table 9.1 shows the mean contrast for dichoptic-nonoverlapping texture elements to appear uniform in contrast was affected by the orientation of texture elements. There were individual differences in the magnitude of this effect. For JM, the mean contrast for -45 degrees (66%) was higher than the mean contrast for 45 degrees when the contrast of the left eye's stimulus was adjusted and this mean contrast (66%) was also higher than the means for both – and + 45 degrees when the contrast of the right eye's stimulus was adjusted. For JAS, the mean contrast for -

45 degrees was higher than the mean contrast for 45 degrees for each of the two eyes. The effect of orientation on dichoptic textures appearing uniform in contrast was smaller for AJ and PL.

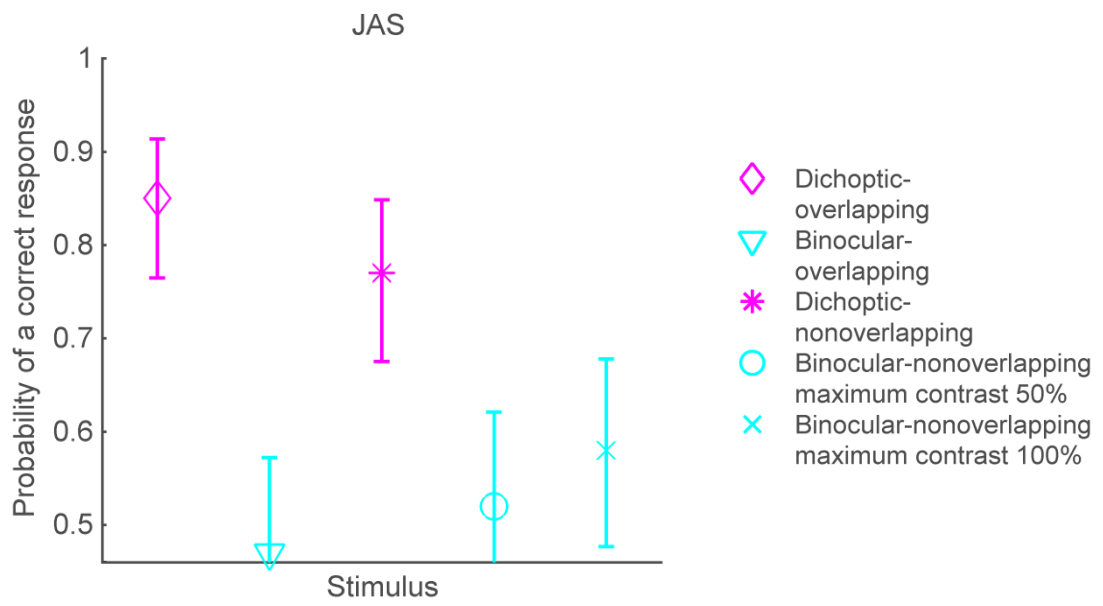
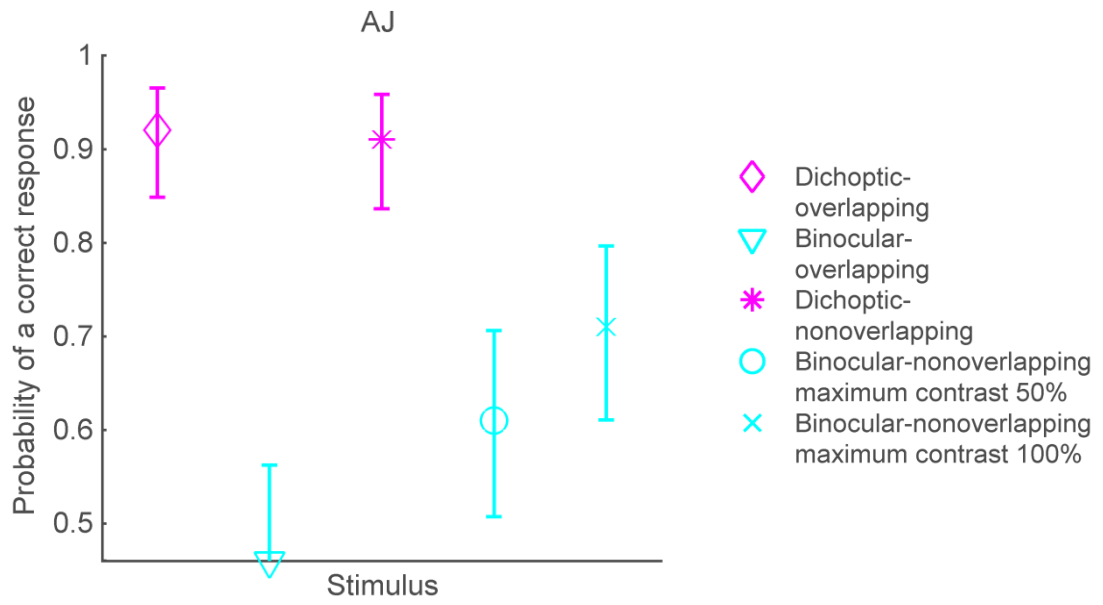
The mean balance-point for each of the two eyes was lowest when the contrast of the left eye's stimulus was adjusted for observers AJ ( $M = 26.5$ ,  $SD = 6.3$ ) and PL ( $M = 29$ ,  $SD = 5.2$ ) and was lowest when the contrast of the right eye's stimulus was adjusted for observers JAS ( $M = 31.7$ ,  $SD = 7.5$ ) and JM ( $M = 35$ ,  $SD = 7.1$ ).

### **9.3.1 Results of Experiment 7.2**

The effective contrast difference between the two eyes was equalised for dichoptic texture boundaries by reducing the contrast of the left eye's stimulus for observers AJ and PL and the right eye's stimulus for JAS and JM by the reciprocal of the ratio for these observers. The results for the two dichoptic tasks show the proportion of correct responses to the interval containing the texture boundary was lower, albeit only slightly, for dichoptic-nonoverlapping stimuli than for dichoptic-overlapping stimuli for all of the observers (Figure 9.3). For dichoptic-nonoverlapping stimuli, the probability of a correct response  $p = .91$ ,  $.77$ ,  $.75$  and  $.89$  for AJ, JAS, JM and PL respectively. For dichoptic-overlapping stimuli,  $p = .92$ ,  $.85$ ,  $.80$  and  $.90$  for AJ, JAS, JM and PL respectively.

For the three binocular tasks, for all of the observers the proportion of correct responses was highest for a binocular-nonoverlapping stimulus for which the maximum randomised contrast was 100% (Figure 9.3). For a binocular-nonoverlapping stimulus (the maximum contrast was 100%),  $p = .71$ ,  $.58$ ,  $.54$  and  $.68$  for AJ, JAS, JM and PL respectively. When the maximum randomised contrast for a binocular-nonoverlapping stimulus was 50%, performance was near chance for AJ and PL and was chance for JAS and JM. For a binocular-overlapping stimulus, performance for all of the observers was chance (Figure 9.3).





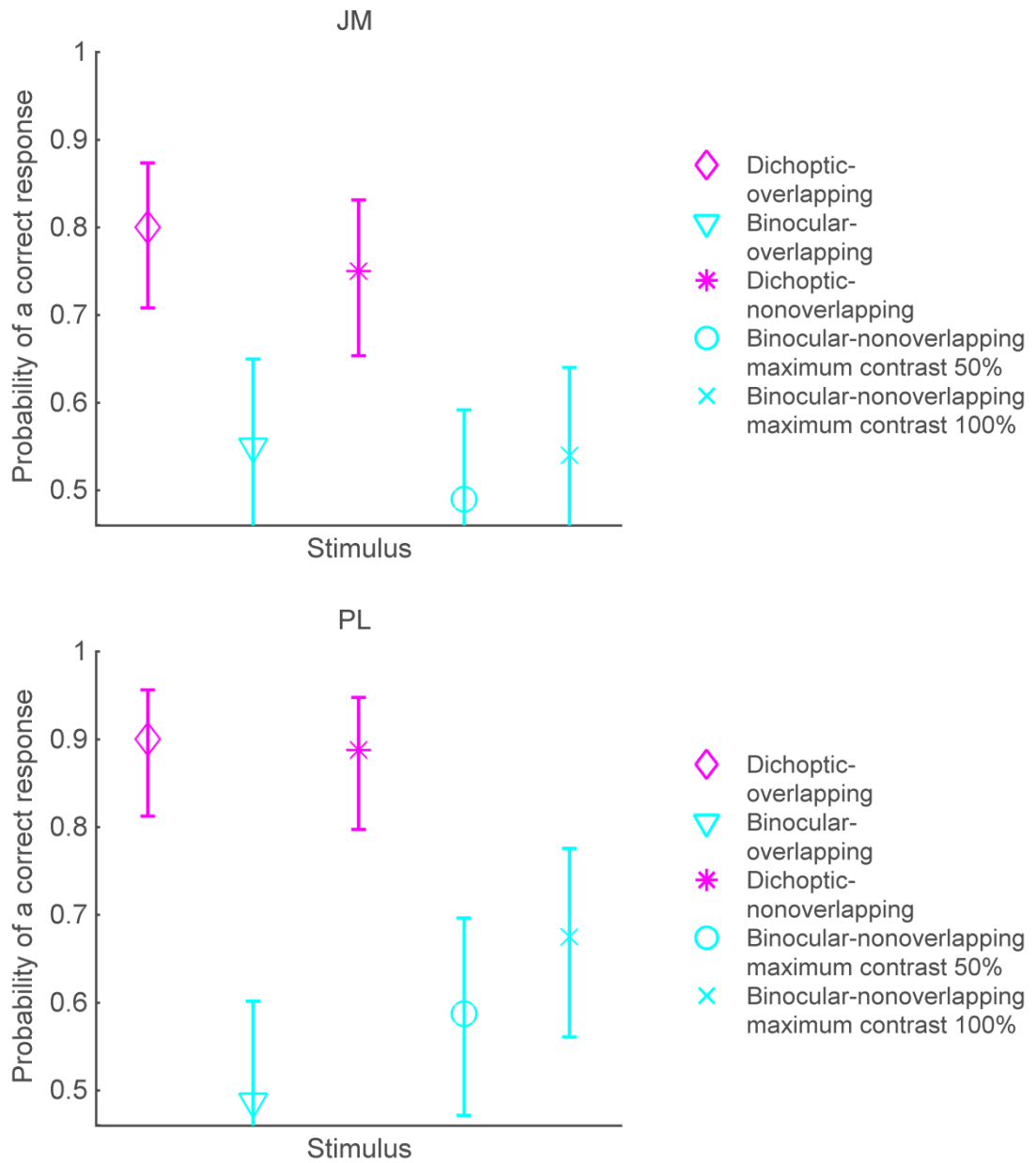


Figure 9.3. Results show the probability of a correct response to the interval containing an orientation-defined texture boundary for the two dichoptic tasks (shown in magenta) and the three binocular tasks (shown in cyan) for each observer. Error bars show 95% confidence intervals.

The null hypothesis that segmentation for dichoptic and binocular texture boundaries does not differ was tested with the Pearson's chi-square ( $\chi^2$ ) test. The critical value for the chi-square distribution is 6.63, where the critical region = .01, with one degree of freedom. The following assumptions for this test were met. The proportion of correct and incorrect responses to the interval containing a texture boundary for a dichoptic task and a binocular task each formed a cell in a 2 x 2 contingency table. The proportion of responses for the null hypothesis was also > 5. The null hypothesis was tested with the dichoptic-nonoverlapping (Figure 9.3; \*) and binocular-nonoverlapping (Figure 9.3; X, the maximum randomised contrast was 100%) tasks. Table 9.2 shows the number of trials for each task and p values for the chi-square statistic.

Observer	Number of trials for each task	Chi-square value	P value
AJ	100	13.00	0.0003
JAS	100	8.23	0.0041
JM	100	9.63	0.0019
PL	80	10.57	0.0011

Table 9.2. Statistics. The null hypothesis was tested with the dichoptic-nonoverlapping (Figure 9.3; \*) and binocular-nonoverlapping (Figure 9.3; X, the maximum contrast was 100%) tasks. The number of trials for each task and p values for the chi-square statistic are given for each observer. The critical value for the chi-square distribution is 6.63, where the critical region = .01, with one degree of freedom. P values: ■ =  $p \leq .01$ .

Dichoptic-nonoverlapping (Figure 9.3; \*) and binocular-nonoverlapping (Figure 9.3; X, the maximum randomised contrast was 100%) texture segmentation differed significantly for all of the observers,  $\chi^2(1, N = \text{see Table 9.2}) = \text{see Table 9.2}$ ,  $p < .01$ . Since dichoptic-overlapping texture segmentation (Figure 9.3; ◇) was better than dichoptic-nonoverlapping texture segmentation (Figure 9.3; \*), dichoptic-overlapping and binocular-nonoverlapping texture segmentation (Figure 9.3; X) differed significantly. The results show texture segmentation for dichoptic texture boundaries was better than segmentation for binocular texture boundaries for all of the observers (Figure 9.3).

## **9.4 Discussion**

The difference in interocular gain putatively responsible for a difference in effective contrast between the two eyes was measured in Experiment 7.1. Interocular gain was higher for the left eye for two of the observers (AJ and PL) and was higher for the right eye for two observers (JAS and JM). Inconsistencies in luminance transmission between the goggle shutters cannot explain this result; however, an effect of the apparatus for displaying dichoptic stimuli cannot be ruled-out entirely. The contrast of the first and last stimulus frames were reduced by 50% to minimise an effect of forward and backward masking respectively on the balance points. That is, for the stimuli shown in Figure 9.1, were the shutter for the left eye to open first, the contrast of the first frame for the left eye was reduced from 80% to 40% and the contrast of the last frame for the right eye was reduced from 30% to 15%. A further method to minimise an effect of masking on the balance-points was randomising the shutter that opened for first stimulus frame. A difference in gain between the two eyes is consistent with this result. A difference in gain could arise from changes in the sensitivity of the underlying sensory processes. Alternatively, impaired visual acuity, for example astigmatism, may explain these differences. Gain differing between the two eyes suggests that there is a different contrast sensitivity function (CSF) for each eye.

In Experiment 7.2, a dichoptic advantage for texture segmentation was tested by comparing segmentation for dichoptic and binocular texture boundaries. In brief durations, texture segmentation for dichoptic and binocular texture boundaries differed significantly. For the binocular-nonoverlapping task, texture segmentation was poor even when the maximum randomised contrast was 100%. Texture segmentation for dichoptic-overlapping texture boundaries was better than segmentation for binocular-nonoverlapping texture boundaries; therefore, a dichoptic advantage for orientation-defined, inverse cyclopean texture segmentation cannot be explained by a failure of binocular fusion. Texture segmentation for dichoptic-nonoverlapping texture boundaries was also better than segmentation for binocular-nonoverlapping texture boundaries; thus, segmentation for dichoptic texture boundaries can occur when the two are misaligned. Binocular-nonoverlapping texture segmentation might be poor because the inter-element space is too small in the optically fused percept. Nonetheless, a dichoptic advantage for texture segmentation in brief durations was supported by the results

for all of the observers. Chance performance for the binocular-overlapping task shows that a dichoptic-overlapping texture boundary is invisible in the optically fused percept.

Texture segmentation for dichoptic texture boundaries was better than segmentation for binocular texture boundaries, even when, for dichoptic texture boundaries, the balance-point was used to equalise a difference in effective contrast between the two eyes. Moreover, 'jitter' was used to mask any small-to-moderate errors in the balance-point. This implies that the dichoptic advantage cannot be attributed to an effective contrast difference between the two eyes. Effective contrast imbalance cannot be the only mechanism for detecting orientation-defined dichoptic texture boundaries. Thus, the dichoptic advantage is consistent with monocular input being available to texture segmentation mechanisms.

## **General Discussion**

Texture segmentation based on the monocular image does occur, even when texture segmentation is impossible in the optically fused image (Kolb & Braun, 1995). On the other hand, in the visual search paradigm, when the left eye's target is the right eye's distractor, and vice versa, orientation-defined visual search is impossible (Wolfe & Franzel, 1988). The research question for the experiments reported in this thesis is: what difference in experimental procedures is responsible for these different results?

The purpose of Experiment 1.1 was to determine whether the critical variable for the difference between Kolb and Braun's and Wolfe and Franzel's results was the density of orientation-defined, dichoptic-overlapping (inverse cyclopean) texture elements. In Experiment 1.1, orientation-defined texture segmentation in brief durations was measured when the texture density of a dichoptic stimulus was 8 x 8, 10 x 10 and 12 x 12. For Wolfe and Franzel's dichoptic-overlapping stimulus, 2, 4, or 8 orientation-defined texture elements were spaced evenly on a circle around fixation. Even though the largest set-size for Wolfe and Franzel's dichoptic-overlapping stimulus was 8 texture elements, texture density was sparse. We found that when texture density was 8 x 8, performances for the dichoptic-overlapping task were poor; however, the task was possible. On the other hand, for Kolb and Braun's dichoptic-overlapping stimulus, orientation-defined texture elements occupied positions on a 20 x 20 notional grid; texture elements were dense. We found that performances for the dichoptic-overlapping task improved when texture elements were denser (12 x 12).

Performances for our dichoptic-overlapping task cannot be wholly attributed to a failure of binocular fusion. This is because, in brief durations, performances for the dichoptic-overlapping task were better than performances for the binocular-nonoverlapping task when texture elements were dense (12 x 12) and, for two of the three observers, when texture elements were sparse (8 x 8). Texture elements within Kolb and Braun's and Wolfe and Franzel's dichoptic-overlapping stimuli competed for the same retinal position. However, texture segmentation might occur when a large error in vergence rendered dichoptic-overlapping texture elements effectively nonoverlapping. In Experiment 1.1, orientation-defined texture segmentation was measured for dichoptic-nonoverlapping stimuli when texture

density was 8 x 8, 10 x 10 and 12 x 12. The results for Experiment 1.1 show that both orientation-defined dichoptic-overlapping and dichoptic-nonoverlapping texture segmentation were better when texture elements were dense (12 x 12). However, performances for orientation-defined, inverse cyclopean texture segmentation cannot be wholly attributed to a large error in vergence. This is because, whilst asymptote for orientation-defined dichoptic texture segmentation did not improve with denser texture elements when those elements were nonoverlapping, asymptote did improve with denser texture elements when those elements were overlapping. Furthermore, whilst threshold for orientation-defined dichoptic texture segmentation improved with denser texture elements when those elements were nonoverlapping, threshold did not improve when texture elements were overlapping. Putative inverse cyclopean texture segmentation in brief durations was better when texture elements were dense; therefore, the critical difference between Kolb and Braun's (1995) and Wolfe and Franzel's (1988) experiments may be texture density.

We found that inverse cyclopean texture segmentation was better when texture elements were dense (12 x 12) than when those elements were sparse (8 x 8) and covered the same area; Exp 1.1 and Exp. 3. In each of these Experiments, there were more texture elements within the dense grids (12 x 12) than there were within the sparse grids (8 x 8) that covered the same area. This might suggest that texture segmentation depends on the density of texture elements. However, texture segmentation improved when the number of Gabor textures within the sparse grid (8 x 8) was held constant and orientation-defined texture boundaries were closer together (Exp. 4). In Exp. 4, sigma ( $\sigma$ ) for the sparse (8 x 8) Gabor textures that were used in Exp. 3 was increased linearly so that the texture boundaries were closer together and the inter-element space was smaller. This implies that texture segmentation depends on orientation-defined, dichoptic-overlapping texture boundaries that are closer together. Orientation-defined texture boundaries within Kolb and Braun's dichoptic-overlapping stimulus were closer together than those within Wolfe and Franzel's stimulus, even when there were 8 texture elements within Wolfe and Franzel's stimulus. Therefore, the results for Exp. 4 imply that the critical difference between Kolb and Braun's (1995) and Wolfe and Franzel's (1988) experiments is the proximity of orientation-defined, dichoptic-overlapping texture boundaries. The results for Exp. 4 suggest that putative orientation-defined, inverse cyclopean texture segmentation was independent of the number of texture

elements; thus, texture segmentation is consistent with pre-attentive texture segmentation.

The experiments reported in this thesis used the inverse cyclopean paradigm to investigate the visual processing that occurs prior to integration of the inputs from the two eyes. An orientation-defined, dichoptic-overlapping (inverse cyclopean) target is invisible in the optically fused percept; thus, an orientation-defined, dichoptic-overlapping (inverse cyclopean) target can only be detected by a mechanism that exists at a monocular stage of processing. It would be impossible for an orientation-defined, dichoptic-overlapping (inverse cyclopean) target to be detected after the inputs from the two eyes are integrated. However, if imperfect binocular integration were to arise from an effective contrast imbalance between the two eyes, the target within a dichoptic-overlapping stimulus might be visible in the optically fused percept and be detected by mechanisms that exist at a binocular stage of processing. Orientation-defined, inverse cyclopean visual search is impossible (Wolfe & Franzel, 1988). This led Wolfe and Franzel to conclude that monocular input cannot be accessed for visual search. On the other hand, Kolb and Braun (1995) showed that texture segmentation based on the monocular image does occur, even when texture segmentation is impossible in the optically fused image. This implies that orientation-defined, dichoptic-overlapping (inverse cyclopean) texture boundaries were detected by a monocular process, prior to integration of the inputs from the two eyes.

A dichoptic advantage for orientation-defined texture segmentation was revealed by high performance in brief durations when texture elements were dense (12 x 12); Exp. 1.1. That is, performances for orientation-defined, inverse cyclopean texture segmentation were better than those for binocular-nonoverlapping texture segmentation, for which performances were chance. Furthermore, high performance for orientation-defined, inverse cyclopean texture segmentation in brief durations was reported when texture elements were dense (12 x 12; Exp. 3) and when texture boundaries were closer together (Exp. 4). However, an imbalance in sensory input from the two eyes affects orientation-defined, inverse cyclopean texture segmentation (Exp. 2). A dichoptic-overlapping (inverse cyclopean), orientation-defined target was not detected when the effective contrast was balanced between the two eyes. This might suggest that effective contrast imbalance is the only mechanism for the dichoptic advantage for orientation-defined



texture segmentation in brief durations. If effective contrast imbalance were the only mechanism for the dichoptic advantage for texture segmentation, an orientation-defined, dichoptic-overlapping target might be visible in the optically fused percept and be detected by mechanisms that exist at a binocular stage of processing. Whilst an orientation-defined target within Exp. 1's dichoptic-overlapping stimulus might be detected by binocular mechanisms when texture elements were dense (12 x 12), an orientation-defined target within Exp. 1's binocular-nonoverlapping stimulus might be harder to detect because the inter-element space is too small in the optically fused percept.

In Experiments 3, 4 and 5 an attempt was made to balance the input from the two eyes using the balance-points determined from Exp. 2. However, it cannot be assumed that the balance-points found in Exp. 2 were valid for the stimuli in these experiments. Specifically, whilst in Exp. 2 observers viewed the texture elements from 3 m (spatial frequency was 4.85 cycles per degree), in Experiments 3, 4 and 5 observers viewed the texture elements from 1 m (spatial frequency was lower; 1.62 cycles per degree). Also, spatial frequency decreased from 1.62 to 1.08 cycles per degree in Exp. 4. Furthermore, in Exp. 2 the balance-points were measured for a single exposure duration that was different from each of the durations that were used in Experiments 3, 4 and 5. Therefore, in Exp. 7, both the balance-point and texture segmentation were measured when the spatial frequency of texture elements and the distance from which texture elements were viewed were the same. Both the balance-point and texture segmentation were measured when exposure duration was 100 ms. The purpose of Exp. 7.2 was to determine whether differences between the effective contrasts of dichoptic stimuli were responsible for the dichoptic advantage for orientation-defined texture segmentation in brief durations.

In Exp. 7.2, texture segmentation was measured for dichoptic-overlapping and dichoptic-nonoverlapping stimuli when the balance-point was used to equalise the effective contrast difference between the two eyes. Texture elements occupied alternate positions on a 24 x 24 notional checkerboard; the texture density of a dichoptic stimulus was 12 x 12. 'Jitter' was added to the contrast of the texture elements by drawing them from a uniform distribution of log contrasts. The purpose of 'jitter' was to mask any small-to-moderate errors in the balance-point. Texture segmentation was also measured for nonoverlapping texture boundaries that were

optically fused; the binocular-nonoverlapping stimulus. Texture elements within this stimulus were also contrast randomised. This stimulus tests the hypothesis that, even if mechanisms for orientation-defined texture segmentation did not have access to monocular input, performance might exceed chance with putative dichoptic-overlapping (inverse cyclopean) texture boundaries if a failure of binocular fusion rendered those textures effectively nonoverlapping (Howard, 2002). Orientation-defined texture segmentation for dichoptic texture boundaries was better than segmentation for binocular texture boundaries, even when, for dichoptic texture boundaries, the balance-point was used to equalise a difference in effective contrast between the two eyes (Exp. 7.2). Moreover, 'jitter' was used to mask any small-to-moderate errors in the balance-point, or residual effects of astigmatism, that would cause anisotropies in the fidelity of contrast transduction. This implies that the dichoptic advantage cannot be wholly attributed to an effective contrast difference between the two eyes. Therefore, orientation-defined, dichoptic texture boundaries are detected by a monocular process, prior to integration of the inputs from the two eyes. The dichoptic advantage for texture segmentation is consistent with monocular input being available to pre-attentive texture segmentation mechanisms (Morgan, Mason & Solomon, 1997; Solomon & Morgan, 1999).

Orientation-defined texture segmentation based on the monocular image occurs in brief 250 ms durations, even though texture segmentation is impossible in the optically fused image (Kolb & Braun, 1995; Morgan, Mason & Solomon, 1997; Solomon & Morgan, 1999). We confirmed that performances for orientation-defined, inverse cyclopean texture segmentation exceeded chance in brief 250 ms durations (Exp. 1). Moreover, threshold was approximately 100 ms regardless of the density of the texture elements; except for observer JS for which threshold was 400 ms and was undetermined when texture density was 8 x 8 and 10 x 10 respectively; Exp. 1. Furthermore, performances for orientation-defined, inverse cyclopean texture segmentation were significantly different from chance when very brief durations were used; the durations were 16 ms and 128 ms for two and three of the observers respectively (Exp. 6). The texture elements that were used in Exp. 6 were contrast randomised. The purpose of contrast randomisation was to eliminate effective contrast imbalance between the two eyes. In brief 100 ms durations, performances for orientation-defined, inverse cyclopean texture segmentation were high (> 80%) when the balance-point was used to equalise a difference in effective contrast between the two eyes (Exp. 7.2). Thus, the results

for the experiments reported in this thesis show that inverse cyclopean texture segmentation does occur in brief durations.

We found that performance for a dichoptic-overlapping display was perfect for a suppressing Amblyope in the absence of a balance point. Texture elements were dense (12 x 12). Observer SG is a 'stereoblind' observer for which a Randot stereo-test confirmed stereo vision was poor. For observers with normal stereo vision, performances for orientation-defined, inverse cyclopean texture segmentation were imperfect when texture elements were dense (12 x 12; Exp 1.1 & Exp. 3). This reduction in asymptote might be attributed to stimulus-independent errors (Wichmann & Hill, 2001a). However, the reduction in asymptote for sparse texture elements (8 x 8; Exp 1.1 & Exp. 3) is inconsistent with stimulus-independent errors. Performances for sparse texture elements (8 x 8) were poor and did not improve with prolonged inspection of dichoptic-overlapping displays.

Any model for orientation-defined dichoptic texture segmentation would explain that the signal-to-noise ratio is higher when there is more information for neural mechanisms to collect. There were less texture elements within the sparse grid (8 x 8) than there were within the dense grid (12 x 12) that covered the same area. The signal-to-noise ratio is lower when texture elements are sparse (Exp. 1.1 & Exp. 3) than when texture elements are dense (Exp 1.1, Exp. 3 & Exp. 7.2) because there is less information. Both orientation-defined inverse cyclopean and dichoptic-nonoverlapping texture segmentation were better when texture elements were dense (12 x 12) than when those elements were sparse (8 x 8); Exp. 1.1. Performances improved as exposure duration increased for both of these dichoptic tasks; however, the improvement in performances for orientation-defined inverse cyclopean texture segmentation was better when texture elements were dense (12 x 12) than when those elements were sparse (8 x 8). Therefore, texture density affects asymptote for orientation-defined, inverse cyclopean texture segmentation because the signal-to-noise ratio is higher when the information is densely distributed and is lower when the information is sparsely distributed. Whilst threshold for orientation-defined, inverse cyclopean texture segmentation did not improve with denser texture elements, threshold for dichoptic-nonoverlapping texture segmentation did improve (Exp. 1.1). Therefore, texture density affects threshold for orientation-defined, dichoptic-nonoverlapping texture segmentation

because the signal-to-noise ratio is higher when the information is densely distributed and is lower when the information is sparsely distributed.

Orientation-defined, inverse cyclopean texture segmentation is consistent with two models; the filter-based model of texture segmentation (Chubb & Landy, 1991) and the V1 salience model (Li, 1999).

For the bottom-up V1 salience model (Li, 1999), a dichoptic-overlapping, orientation-defined target was more salient than the distractors. This is because the maximum responses of V1 neurons to the target are not suppressed by neurons outside the classical RF due to iso-orientation suppression (Knierim & van Essen, 1992; Levitt & Lund, 1997; Zipser, Lamme & Schiller, 1996) of neuronal responses to the distractors. Although neuronal connections between layers of cortex extend over short distances, some intra-cortical connections extend to 4 or 5 mm (Ramon y Cajal, 1995). This means within-layer sensory processing is limited as spatially local and is piecemeal (Hubel & Wick, 1995). The salience of an orientation-defined target is modulated via intra-cortical connections with ocular dominance columns (Li, 1999). However, high performances for a dichoptic-overlapping display in which dense texture elements (12 x 12) were separated by 0.86 degrees of visual angle (Exp. 7.2) are inconsistent with the diminished salience of orientation-defined line textures that were separated by 2 degrees of visual angle or less (Nothdurft, 2000). In both of these experiments, the orientation-defined targets were presented at a similar retinal eccentricity from fixation. This suggests that the texture elements used in Exp. 7.2 were too dense for the orientation-defined target to be salient. Moreover, the salience of an orientation-defined target is affected when the separation of surrounding orientation-defined texture is smaller than 1.8 degrees (Zipser, Lamme & Schiller, 1996).

Texture elements within Wolfe and Franzel's dichoptic-overlapping stimuli were contrast randomised. The purpose of contrast randomisation was to eliminate a difference in effective contrast between the two eyes. Solomon and Morgan (2004) reported orientation-defined, inverse cyclopean texture segmentation following randomised luminance contrast of each Gabor stimulus within a dichoptic-overlapping stimulus. Since salience is based on one sensory dimension, randomised luminance contrast produced variations in salience across the entire image to mask the local salience difference that might be produced by an

interocular contrast difference interacting with the local orientation-defined target. Their results were consistent with channels tuned to orientation differences. In Experiment 7.2, performances for orientation-defined, inverse cyclopean texture segmentation were >80% when the balance-point was used to equalise a difference in effective contrast between the two eyes. Performances for orientation-defined, inverse cyclopean texture segmentation were consistent with monocular input being available to pre-attentive texture segmentation mechanisms. In this experiment, contrast randomisation was used to mask any small-to-moderate errors in the balance-point. Another purpose of contrast randomisation was to eliminate the salience of an orientation-defined, dichoptic-overlapping target. The results for Exp. 7.2 confirm that orientation-defined, inverse cyclopean texture segmentation does occur, even when texture elements are contrast randomised. The V1 salience model cannot explain these results. Therefore, orientation-defined, inverse cyclopean texture segmentation is consistent with channels tuned to orientation differences. This implies that 2<sup>nd</sup> order filtering can occur prior to integration of the inputs from the two eyes. Thus, a pre-attentive texture segmentation mechanism can access monocular signals.

High performances for orientation-defined, inverse cyclopean texture segmentation when dense (12 x 12) texture elements are separated by a small visual angle (0.86 degrees; Exp. 7.2) are consistent with the filter-based model of texture segmentation (Chubb & Landy, 1991). Specifically, orientation-defined, inverse cyclopean texture segmentation can be explained by an increase in the responses of orientation-selective neurons when texture elements are close together.

Alternatively, vergence instability of the two eyes could reveal dichoptic-overlapping texture boundaries (Howard, 2002). Vergence movements manoeuvre each eye laterally to achieve binocular fusion. Both fluctuations in vergence and high velocity vergence movements such as microsaccades (Ko, Snodderly & Poletti, 2016) were tested using binocular jitter of orientation-defined texture elements to simulate the eyes moving in different directions, thereby disrupting binocular fusion. The performance with 30 Hz and 1.2 degree fluctuations was perfect for 250 ms displays; however, performance was at chance after 1 s of (a) 0.12 degree fluctuations at 30 Hz and (b) 1.2 degree fluctuations at 2 Hz. Thus, large high velocity vergence movements remain a potential cue.

## **10.1 Conclusion**

Conventional wisdom ordains perceptual fusion for brief durations of orthogonal dichoptic stimuli (Hering 1874; Dawson, 1913). If perceptual fusion did occur for brief presentations, then performances for orientation-defined, inverse cyclopean texture segmentation would be comparable to those for binocular-overlapping texture segmentation for which performances were chance (Exp. 1.1 & Exp. 7). However, the experiments reported in this thesis and elsewhere confirm that texture segmentation invisible in the fused image is nonetheless visible in 250 ms exposure durations (Kolb & Braun, 1995; Morgan, Mason & Solomon, 1997; Solomon & Morgan, 1999). Thus, rather than perceptual fusion prior to the onset of binocular rivalry, monocular access is available to pre-attentive texture segmentation mechanisms. Orientation-defined, inverse cyclopean texture segmentation is consistent with the filter-based model of texture segmentation (Chubb & Landy, 1991).

The inputs from the two eyes remain segregated in ocular dominance columns within V1 which coexist with binocularly driven cells (Hubel & Wick, 1995) implying that binocular processing is incomplete in V1. The most likely site of orientation-defined, inverse cyclopean texture segmentation is V1, in agreement with the V1 salience model (Li, 1999); however, monocular neurons are not absent from pre-striate and extrastriate areas (Baker, Grigg & von Noorden, 1974; Burkhalter & Van Essen, 1986).

Orientation-defined, inverse cyclopean segmentation is independent of stereoscopic vision (Exp. 6). Therefore, the possibility remains that simultaneous perceptions of rivalry, stereopsis and fusion (Julesz & Miller, 1975; Marr & Poggio, 1979; Georgeson & Wallis, 2014) are occurring with orientation-defined, inverse cyclopean texture segmentation.

## References

Alais, D., O'Shea, R. P., Mesana-Alais, C., & Wilson, I. G. (2000). On binocular alternation. *Perception*, 29(12), 1437-1445.

Anderson, J. D., Bechtoldt, H. P., & Dunlap, G. L. (1978). Binocular integration in line rivalry. *Bulletin of the Psychonomic Society*, 11(6), 399-402.

Baker, F. H., Grigg, P., & von Noorden, G. K. (1974). Effects of visual deprivation and strabismus on the response of neurons in the visual cortex of the monkey, including studies on the striate and prestriate cortex in the normal animal. *Brain Research*, 66(2), 185-208.

Baker, D. H., Meese, T. S., & Hess, R. F. (2008). Contrast masking in strabismic amblyopia: attenuation, noise, interocular suppression and binocular summation. *Vision research*, 48(15), 1625-1640.

Bergen, J. R., & Adelson, E. H. (1988). Early vision and texture perception. *Nature*, 333, 363–364.

Bergen, J. R., & Landy, M. S. (1991). Computational modeling of visual texture segregation. In M. S. Landy & J. A. Movshon (Eds.), *Computational models of visual processing* (pp. 253-271). Cambridge, MA: MIT Press.

Blake, R., O'Shea, R. P. & Mueller, T. J. Spatial zones of binocular rivalry in central and peripheral vision. *Vis. Neurosci.* 8, 469–478 (1992).

Burkhalter, A., & Van Essen, D. C. (1986). Processing of color, form and disparity information in visual areas VP and V2 of ventral extrastriate cortex in the macaque monkey. *Journal of Neuroscience*, 6(8), 2327-2351.

Caelli, T., & Julesz, B. (1978). On perceptual analyzers underlying visual texture discrimination: Part I. *Biological Cybernetics*, 28(3), 167-175.

- Chen, Z., Li, J., Liu, J., Cai, X., Yuan, J., Deng, D., & Yu, M. (2016). Monocular perceptual learning of contrast detection facilitates binocular combination in adults with anisometropic amblyopia. *Scientific reports*, 6.
- Chubb, C., & Landy, M. S. (1991). Orthogonal distribution analysis: A new approach to the study of texture perception. In M. S. Landy & J. A. Movshon (Eds.), *Computational models of visual processing* (pp. 291–301). Cambridge, MA: MIT Press.
- Dakin, S. C., & Mareschal, I. (2000). Sensitivity to contrast modulation depends on carrier spatial frequency and orientation. *Vision research*, 40(3), 311-329.
- Dawson, S. (1913). Binocular and unocular discrimination of brightness. *British Journal of Psychology*, 6(1), 78-108.
- Diaz-Caneja, E. (1928). On binocular alternation. *Ann. Ocul*, 721-731.
- Georgeson, M. A., & Wallis, S. A. (2014). Binocular fusion, suppression and diplopia for blurred edges. *Ophthalmic and Physiological Optics*, 34(2), 163-185.
- Gilbert, C. D., & Wiesel, T. N. (1983). Clustered intrinsic connections in cat visual cortex. *The Journal of Neuroscience*, 3(5), 1116-1133.
- Graham, N. (1991). Complex channels, early local nonlinearities, and normalization in texture segregation. In M. S. Landy & J. A. Movshon (Eds.), *Computational models of visual processing* (pp. 273-290). Cambridge, MA: MIT Press.
- Hering, E. (1874). *Outlines of a theory of the light sense*. Cambridge, MA 1964, Harvard University Press.
- Hess, R. F., Mansouri, B., & Thompson, B. (2010). A new binocular approach to the treatment of amblyopia in adults well beyond the critical period of visual development. *Restorative neurology and neuroscience*, 28(6), 793-802.



Hess, R. F., Mansouri, B., & Thompson, B. (2011). Restoration of binocular vision in amblyopia. *Strabismus*, 19(3), 110-118.

Howard, I. P., & Rogers, B. J. (2002). *Seeing in depth, volume 2: Depth perception*. Ontario: I. Porteous.

Huang, C. B., Zhou, J., Lu, Z. L., & Zhou, Y. (2011). Deficient binocular combination reveals mechanisms of anisometropic amblyopia: Signal attenuation and interocular inhibition. *Journal of vision*, 11(6), 4-4.

Hubel, D. H., Wensveen, J., & Wick, B. (1995). *Eye, brain, and vision* (pp. 191-219). New York: Scientific American Library.

Julesz, B. (1971). *Foundations of cyclopean perception*. Chicago: The University of Chicago Press.

Julesz, B. (1984). A brief outline of the texton theory of human vision. *Trends in Neurosciences*, 7(2), 41-45.

Julesz, B. (1986). Texton gradients: The texton theory revisited. *Biological cybernetics*, 54(4-5), 245-251.

Julesz, B. (1995). *Dialogues on perception*. MIT Press.

Julesz, B., & Bergen, J. R. (1983). Human factors and behavioral science: Textons, the fundamental elements in preattentive vision and perception of textures. *Bell System Technical Journal*, The, 62(6), 1619-1645.

Julesz, B., Gilbert, E. N., Shepp, L. A., & Frisch, H. L. (1973). Inability of humans to discriminate between visual textures that agree in second-order statistics—revisited. *Perception*, 2(4), 391-405.

Julesz, B., Gilbert, E. N., & Victor, J. D. (1978). Visual discrimination of textures with identical third-order statistics. *Biological cybernetics*, 31(3), 137-140.

- Julesz, B. & Miller, J. E. (1975). Independent spatial-frequency-tuned channels in binocular fusion and rivalry. *Perception*, 4(2), 125-143.
- Julesz, B., & Schumer, R. A. (1981). Early visual perception. *Annual review of psychology*, 32(1), 575-627.
- Keeble, D. R. T., Kingdom, F. A. A., Moulden, B., & Morgan, M. J. (1995). Detection of orientationally multimodal textures. *Vision research*, 35(14), 1991-2005.
- Kingdom, F. A., & Keeble, D. R. (1999). On the mechanism for scale invariance in orientation-defined textures. *Vision research*, 39(8), 1477-1489.
- Kleiner, M., Brainard, D., & Pelli, D. (2007). What's new in Psychtoolbox-3? *Perception*, 36 ECVF Abstract Supplement.
- Knierim, J. J., & Van Essen, D. C. (1992). Neuronal responses to static texture patterns in area V1 of the alert macaque monkey. *Journal of Neurophysiology*, 67(4), 961-980.
- Ko, H. K., Snodderly, D. M., & Poletti, M. (2016). Eye movements between saccades: Measuring ocular drift and tremor. *Vision research*, 122, 93-104.
- Kolb, F. C., & Braun, J. (1995). Blindsight in normal observers. *Nature*, 377(6547), 336-338.
- Landy, M. S. (2013). *Texture analysis and perception. The new visual neurosciences*, MIT Press, Cambridge, Mass, 639-652.
- Landy, M. S., & Oruç, İ. (2002). Properties of second-order spatial frequency channels. *Vision research*, 42(19), 2311-2329.
- Levitt, J. B., & Lund, J. S. (1997). Contrast dependence of contextual effects in primate visual cortex. *Nature*, 387(6628), 73-76.

- Li, Z. (1999). Visual segmentation by contextual influences via intra-cortical interactions in the primary visual cortex. *Network: computation in neural systems*, 10(2), 187-212.
- Livingstone, M. S., & Hubel, D. H. (1984). Anatomy and physiology of a color system in the primate visual cortex. *J Neurosci*, 4(1), 309-356.
- Marr, D. & Poggio, T. (1979). A computational theory of human stereo vision. *Proceedings of the Royal Society of London Biological Sciences*, 204, 301-328.
- McKee, S. P., & Levi, D. M. (1987). Dichoptic hyperacuity: the precision of nonius alignment. *JOSA A*, 4(6), 1104-1108.
- Morgan, M. J., Mason, A. J. S., & Solomon, J. A. (1997). Blindsight in normal subjects. *Nature*, 385(6615), 401-402.
- Morgan, M. J., Ross, J., & Hayes, A. (1991). The relative importance of local phase and local amplitude in patchwise image reconstruction. *Biological Cybernetics*, 65(2), 113-119.
- Nothdurft, H. C. (1985). Sensitivity for structure gradient in texture discrimination tasks. *Vision research*, 25(12), 1957-1968.
- Nothdurft, H. C. (1990). Texton segregation by associated differences in global and local luminance distribution. *Proceedings of the Royal Society of London. B. Biological Sciences*, 239(1296), 295-320.
- Nothdurft, H. C. (2000). Saliency from feature contrast: variations with texture density. *Vision research*, 40(23), 3181-3200.
- Prins, N & Kingdom, F. A. A. (2009) Palamedes: Matlab routines for analyzing psychophysical data.
- Rainville, S. J., & Kingdom, F. A. (2002). Scale invariance is driven by stimulus density. *Vision research*, 42(3), 351-367.

- Ramon y Cajal, S. R. (1995). *Histology of the nervous system of man and vertebrates* (Vol. 1). Oxford University Press, USA.
- Sagi, D. (1988). The combination of spatial frequency and orientation is effortlessly perceived. *Attention, Perception, & Psychophysics*, 43(6), 601-603.
- Schwarz, G. (1978). Estimating the dimension of a model. *The annals of statistics*, 6(2), 461-464.
- Solomon, J. A., & Morgan, M. J. (1999). Dichoptically cancelled motion. *Vision research*, 39(14), 2293-2297.
- Solomon, J. A., & Morgan, M. J. (2004). Inverse cyclopean texture segregation survives contrast randomisation. *Perception*, 33 ECVF Abstract Supplement.
- Sutter, A., Beck, J., & Graham, N. (1989). Contrast and spatial variables in texture segregation: Testing a simple spatial-frequency channels model. *Perception & Psychophysics*, 46(4), 312-332.
- Sutter, A., Sperling, G., & Chubb, C. (1995). Measuring the spatial frequency selectivity of second order texture mechanisms. *Vision Research*, 35(7), 915-924.
- Treisman, A. M., & Gelade, G. (1980). A feature-integration theory of attention. *Cognitive psychology*, 12(1), 97-136.
- Treisman, A., & Gormican, S. (1988). Feature analysis in early vision: evidence from search asymmetries. *Psychological review*, 95(1), 15.
- Treutwein, B., & Strasburger, H. (1999). Fitting the psychometric function. *Perception & psychophysics*, 61(1), 87-106.
- Tyler, C. W. (2004). Theory of texture discrimination of based on higher-order perturbations in individual texture samples. *Vision Research*, 44(18), 2179-2186.

Vedamurthy, I., Nahum, M., Bavelier, D., & Levi, D. M. (2015). Mechanisms of recovery of visual function in adult amblyopia through a tailored action video game. *Scientific reports*, 5, 8482.

Wade, N. J. (1998). Early studies of eye dominances. *Laterality: Asymmetries of body, brain and cognition*, 3(2), 97-108.

Watson, A. B., & Pelli, D. G. (1983). QUEST: A Bayesian adaptive psychometric method. *Perception & psychophysics*, 33(2), 113-120.

Weiskrantz, L., Barbur, J. L., & Sahraie, A. (1995). Parameters affecting conscious versus unconscious visual discrimination with damage to the visual cortex (V1). *Proceedings of the National Academy of Sciences*, 92(13), 6122-6126.

Wichmann, F. A., & Hill, N. J. (2001a). The psychometric function: I. Fitting, sampling, and goodness of fit. *Perception and Psychophysics*, 63(8), 1293–1313.

Wilson, H. R. (2010). Binocular Rivalry: Neurons Unwire When They Can't Simultaneously Fire. *Current Biology*, 20(17), R715-R717.

Wolfe, J. M. (1983). Influence of spatial frequency, luminance, and duration on binocular rivalry and abnormal fusion of briefly presented dichoptic stimuli. *Perception*, 12(4), 447-456.

Wolfe, J. M., Cave, K. R., & Franzel, S. L. (1989). Guided search: an alternative to the feature integration model for visual search. *Journal of Experimental Psychology: Human perception and performance*, 15(3), 419.

Wolfe, J. M., & Franzel, S. L. (1988). Binocularity and visual search. *Perception and Psychophysics*, 44(1), 81-93.

Wolfe, J. M., & Horowitz, T. S. (2004). What attributes guide the deployment of visual attention and how do they do it? *Nature Reviews Neuroscience*, 5(6), 495-501.

Yeshurun, Y., & Carrasco, M. (2000). The locus of attentional effects in texture segmentation. *Nature Neuroscience*, 3(6), 622.

Zeki, S., Watson, J. D., Lueck, C. J., Friston, K. J., Kennard, C., & Frackowiak, R. S. (1991). A direct demonstration of functional specialization in human visual cortex. *Journal of neuroscience*, 11(3), 641-649.

Zhaoping, L. (2008). Attention capture by eye of origin singletons even without awareness—a hallmark of a bottom-up saliency map in the primary visual cortex. *Journal of Vision*, 8(5), 1.

Zhaoping, L., & May, K. A. (2007). Psychophysical tests of the hypothesis of a bottom-up saliency map in primary visual cortex. *PLoS Computational Biology*, 3(4), e62.

Zipser, K., Lamme, V. A., & Schiller, P. H. (1996). Contextual modulation in primary visual cortex. *The Journal of Neuroscience*, 16(22), 7376-7389.